

“Physical Chemistry of Mechanisms for Low Salinity Waterflood”

Christer Llano Andresen

Master Thesis

Physical Chemistry – Reservoir Chemistry



***Department of Chemistry
Centre of Integrated Petroleum Research (Uni CIPR)
University of Bergen
October 2013***

Acknowledgement

The majority of the experimental work presented in this thesis has been carried out at the Centre of Integrated Petroleum Research (CIPR), at the University of Bergen. A small part of the research was performed at SINTEF in Bergen, in cooperation with the Department of Chemistry at the University of Bergen and CIPR.

First of all, I would like to express my highest gratitude to Professor Arne Skauge for all the guidance, advice and support throughout this experience.

Also, I am grateful for all the discussion of topics I had with Kristine Spildo, Bartek Vik, Edin Alagic, Anette Johannessen, Kjetil Djurhuus, Tore Skodvin and Tanja Barth.

Furthermore, this experience would not have been the same without all the students at CIPR. Thank you all for all the help, especially Tom Gilje and Daniel Sævland for all the discussions and counseling.

I wish to thank my parents who inspired me throughout my life to always aim high and never give up. Finally, a special appreciation goes to my best friend Dan Christian Stein for letting me live at his apartment while studying and my partner Susanne Økland Wembstad for all support and motivation.

Christer Llano Andresen

Bergen, October 2013.

Abstract

Low salinity injection as an alternative EOR method to enhance the production of reserves has for decades been investigated. Increasing evidence that reduction in brine salinity can cause a significant impact on the oil recovery has led to a greater worldwide interest among scientists and industry. Despite all the attention, the prevailing mechanism responsible for the favorable contribution is up to date an unsettled issue due to the complex in-situ crude oil/brine/rock interactions.

The physical chemistry of mechanisms occurring between crude oil and brine has been investigated in this thesis. For a comprehensive study, adhesion maps were performed to examine the wettability behavior in different three phase systems.

The two different crude oils used in this thesis came from the Heidrum field, located in the North Sea.

Crude oil/brine interactions were investigated through electrophoretic and interfacial tension studies. These interactions were examined as a function of pH and brine composition. The composition of brine was modified with respect to ionic strength, ion type and ion-valence.

Through the electrophoretic studies it was proven that brine composition and pH impacted the charge between crude oil/brine significantly. Higher pH caused more acidic constituents in the oil phase to ionize and thus increased the net negative charge at the oil/brine interfaces.

Reduced salinity, especially from multivalent to monovalent cations, lowered the screening potential and caused a higher negative charge at the oil/brine interfaces.

Interfacial tension between crude oil/brine was only partially affected by reduction in brine salinity, but pH at high alkaline environment resulted in dramatic reduction in the interfacial tension due to ionized acidic species granting the oil phase a hydrophilic character.

The adhesion map results revealed that wettability alteration from water-wet towards oil-wet was not affected by brine salinity, but was rather highly dependent on pH where adhesion was mainly observed at intermediate acidic conditions.

Nomenclature

Variables

A	Cross-section area, m ²
C	Concentration, M, mole/L or mole/Kg
Eq	Molar equivalence, eq/L
F	Force, N (1 N = 1 Kg·m/s ²)
g	Gravitational constant, 9.80665 m/s ²)
G	Gibs free energy, J
I	Ionic strength, mmole/L
m	Mass, Kg
Mm	Molar mass, g/mole
N _{vc}	Capillary number, dimensionless
P	Pressure, Pa (1 Pa = 10 ⁻⁵ bar)
P _c	Capillary pressure, Pa
pH	<i>Pondus hydrogenii</i> (lation), dimensionless
R	Radius, m
T	Temperature, °C
T	Period, s ⁻¹
U _e	Electrophoretic mobility, μ·mc·m·Vs ⁻¹
V	Volume, m ³
Z	Charge number if the ion, dimentionless
ϑ	Contact angle, °
μ/η	Viscosity, Pa·s (1 Pa·s = 10 ³ cP)
ρ	Density, g/m ³
σ	Interfacial tension, mN/m
e	Standard deviation
u	Darcy velocity, m ³ ·s ⁻¹
Z	Zeta-potential, mV
ε	Permeability of medium, C2·N ⁻¹ ·m ⁻²

A Cross-section area, m²

Subscript

A	Areal
aq	Aqueous
c	Capillary
i	Initial
l	Liquid
o	Oil
r	Residual
s	Solid
w	Water
ow	Oil/Water
os	Oil/Solid
ws	Water/Solid

Abbreviations

Δ	Difference between final and start point
AIM SM	Advanced Ion Management
AN	Acid number of oil
BN	Base number of oil
BP	British petroleum
CDC	Capillary Desaturation Curve
COBR	Crude oil/brine/rock system
DCM	Dichloromethane

DLVO	Deryaguin, Landau, Verwey and Overbeek
e.g.	For example (<i>exempli gratiā</i> , latin)
EOR	Enhanced oil recovery
<i>et al.</i>	And others (<i>et alii</i> , latin)
FW	Fractional water
HS	High salinity
i.e.	In other words (<i>id est</i> , latin)
IEP	Isoelectric point
IFT	Interfacial tension
ISFET	Ion-sensitive field-effect transistor
KOH	Potassium hydroxide
LDV	Laser Doppler Velocimetry
LS	Low salinity (0,3 wt% NaCl)
LSE	Low salinity effect
LSW	Low salinity water flooding
MI	Miscible injectant
MWL	Mixed wet, large pores are oil-wet
MWS	Mixed wet, small pores are oil-wet
NSO atoms	Nitrogen, Sulfur and Oxygen atoms
OOIP	Original oil in place
ppm	Parts per million
SAS	Small Angle Scattering
SB	Synthetic brine
SD	Standard deviation
S_o	Oil saturation
SOP	Standard operational procedure
S_{orw}	residual oil saturation
SSW	Synthetic sea water
SW	Sea water
S_w	Water saturation
SWCTT	Single well chemical tracer tests

TAN	Total acid number
TDS	Total dissolved solid
TOW	Towards oil-wet
W/o	Without
x&i	20% xylene and 20% iododecane

Table of Content

Acknowledgment	iii
Abstract	v
Nomenclature	vii
1. Introduction	1
2. Wettability Theory and Definitions	4
2.1. Interfacial Tension	4
2.2. Wettability and Different Wetting Properties	6
2.2.1. Wettability	6
2.2.2. Rock Wettability	8
2.2.3. Wettability Alteration	10
2.3. Capillary Pressure	12
3. Electrokinetic Interactions	14
3.1. Fundamentals of Electrokinetic	14
3.1.1. Van der Waals Interactions	14
3.1.2. Electrostatic Interactions between Electrical Double Layers	15
3.1.3. Zeta-Potential	18
3.1.4. Structural Forces	19
3.1.5. Summary – Electrostatic Interactions	20
3.2. The oil, Brine, and Solid Phase	21
3.2.1. The Oil Phase	21
3.2.2. The Aqueous Phase	23
3.2.3. The Solid Phase	24
3.3. Crude oil/Brine Interactions	25
4. Enhanced Oil Recovery (EOR)	28

4.1.	Low Salinity Waterflooding	29
4.2.	Field Scale LSW	39
4.3.	Suggested Mechanisms for Low Salinity Effects	41
4.3.1.	Wettability Alteration	41
4.3.2.	Fine Migration	44
4.3.3.	pH Variation	47
4.3.4.	Multicomponent Ionic Exchange (MIE)	49
4.3.5.	Double Layer Expansion	52
4.4.	Perception of LSW as an EOR Method	54
5.	Experimental Equipment and Procedures	55
5.1.	Chemicals and Fluids	56
5.1.1.	Brines	56
5.1.2.	Crude Oils	57
5.2.	Equipment for Sample Preparation	58
5.2.1.	Ultrasonic Bath	58
5.2.2.	Centrifuge	60
5.3.	Equipment for Fluid Analysis	61
5.3.1.	pH-Meter	61
5.3.2.	Densitometer	63
5.4.	Experimental Apparatus and Equipment	66
5.4.1.	Drop Volume Method	66
5.4.2.	Nanosizer	71
5.4.3.	Adhesion Map	76
5.4.4.	SARA-Analysis and Determination of TAN	79
6.	Main Results and Discussion	82
6.1.	SARA-Analysis	82
6.2.	Electrophoresis	85

6.2.1.	Dispersed Crude Oil A-12 in Diluted SSW, HS Water and LS Water	86
6.2.2.	Dispersed Crude Oil Exp-12 _{x&i} in LS Water Containing Different Ions	89
6.2.3.	Dispersed Crude Oil Exp-12 _{x&i} in LS Water with Constant Electrolyte Concentration	92
6.3.	Interfacial Tension (IFT)	95
6.3.1.	IFT between Crude Oil A-12 and SSW, HS Water and LS Water	96
6.3.2.	IFT between Crude Oil Exp-12 _{x&i} and LS Water Containing Different	98
	Ions	
6.3.3.	IFT as a Function of Time in Contact between Crude Oil Exp-12 _{x&i} and	102
	Brines	
6.4.	Adhesion Map (Wettability Alteration)	106
7.	Parameters Influence on the Results and Previous Work	110
8.	Summary and Conclusions	114
9.	Further Work	116
10.	References	118
	Appendix	124
A.1.	Brines	125
A.2.	Density Data	128
A.3.	SARA-Analysis and TAN	131
A.3.1.	Saturated, Aromatic and Resins Content	131
A.3.2.	Asphaltene Precipitation	133
A.3.3.	Total Acid Number	133
A.4.	Zeta-Potential and Electrophoretic Mobility Measurements	137
A.4.1.	Crude Oil A-12/Brine Emulsions	137
A.4.2.	Crude Oil Exp-12 _{x&i} /Brine Emulsions	142
A.4.3.	Crude Oil Exp-12 _{x&i} /Brine Emulsions at Constant Brine Molality	146
A.5.	Interfacial Tension Measurements	150

A.5.1.	IFT between Crude Oil A-12 and SSW, HS Water and LS Water	150
A.5.2.	IFT between Crude Oil Exp-12 _{x&i} and LS Water Containing Different ... Ions	151
A.5.3.	IFT as a Function of Time in Contact between Crude Oil Exp-12 _{x&i} and Brines	155
A.6.	Diverging pH in the Aqueous Phase	158

1 Introduction

Petroleum is the world leading energy source compared to other sources like coal, gas, nuclear energy, etc. The demand of energy around the world is rising as the global population is growing, and more people are gaining access to modern energy.

One way to meet this demand is through innovative technology and research to optimize the production of hydrocarbons.

The recovery process is distinguished through three categories, respectively, primary, secondary and tertiary recovery.

Through primary recovery the hydrocarbons are produced by pressure depletion, such as natural production from a gas-drive reservoir. The differential pressure between bottomhole and wellbore drives the hydrocarbons towards the well until its limit is reached, when the pressure is so low that the production is no longer economical. Typically this is around 10% of the initial hydrocarbons in place.

One way to keep the pressure up and sweep the oil towards the wellbore is through secondary recovery where an external fluid such as water or gas is injected. The secondary recovery is limited when the injected fluid is produced from the production wells and the production is no longer economical. The production often reaches its limit between 15-40% of the original oil in place.

Tertiary oil recovery which is often referred to as enhanced oil recovery (EOR), is applied to unconventional methods used to increase or accelerate the production of the reserves by comprising recovery methods that follow waterflooding and pressure maintenance. By the use of these methods, up to 60% or more of the reservoir's original oil can be extracted.

To understand in more detail the proven positive effects of EOR, it is important to investigate the interactions between crude oil/brine/rock (COBR).

The focus of this study was to investigate the interfacial interactions between crude oil and brine through experimental work based on physical chemistry principles.

This thesis is structured by first presenting an introduction of the characteristics of the interactions between crude oil, brine and rock encountered in a reservoir in chapter 2.

The interactions between COBR are strongly dependent on the surface charges at their interfaces. Chapter 3 provides basic fundamentals of electrokinetic to describe how different parameters such as pH of the aqueous phase, composition to the brine and oil phase, and the mineralogy of the reservoir rock affects the mechanisms encountered in this three phase system (CORB).

Study of the positive effects of enhanced oil recovery has been investigated for many decades by many scientists. Chapter 4 summarizes a part of this diverse literature to introduce the research obtained up to date. This includes laboratory and field studies, and the proposed mechanisms causing the enhanced increase in oil recovery.

Chapter 5 presents the experimental equipment and procedures. In addition, fluid properties of the crude oils and brines used in this project is listed.

Results and discussion of the experimental work in this thesis is presented in Chapter 6.

Finally, chapter 7 summarizes previous research in the literature in relationship to the results presented in this chapter. In addition, the influence of the parameters on the results is explained. Chapter 8 and 9 presents the conclusion and further work.

2 Wettability Theory and Definitions

2.1 Interfacial Tension

When two immiscible fluids meet and form an interface, then the molecules of each bulk phase will experience an attraction force to their bulk rather than mix [1]. This magnitude of work, or energy, which is required to keep the two fluids apart at constant pressure, P , temperature, T , and mass, M , in an equilibrium state is called interfacial tension (IFT), and is defined by equation 2.1 [2].

$$\sigma = \left(\frac{\partial G}{\partial A} \right)_{T,P,M_{1,2}} \quad (2.1)$$

Where G is the Gibbs free energy and A is the interface area. The interfacial tension, σ , is expressed as N/m or J/m^2 .

The IFT is also described by the free energy cost of increasing the interfacial area between two phases. If the interfacial tension is large, the two media will tend to minimize their interfacial contact area [3].

The minimization of the fluids surface area is explained by the anisotropy of intermolecular attractions and dynamic interactions between the molecules at the fluid phase's surface and bulk. A molecule at the surface has a higher potential energy than the bulk, which means that a greater energy, or work, is required to move a molecule from the fluids phase's interior to the surface and to increase the surface area. The surface area is proportional to the potential energy, minimum Gibbs free energy, consequently that the surface area of the fluid phase will always be minimized [2], see figure 2.1.

The IFT between crude oil/brine will in most cases decrease as the temperature is increased [4], because the water solubility in oil increases exponentially with the temperature which reduces the free energy between these two immiscible fluids [5].

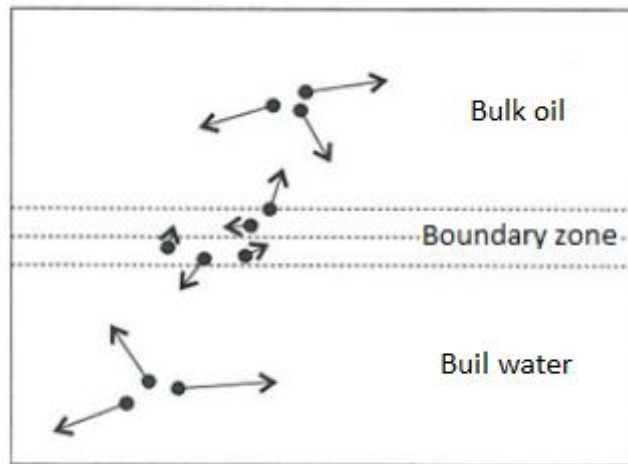


Figure 2.1 Schematic illustration of two immiscible fluids (i.e. water and oil) in contact, showing that the motion of molecules in the boundary zone is much more limited than the bulk [2].

2.2 Wettability and Different Wetting Properties

2.2.1 Wettability

Wettability is defined as “the tendency one fluid has to spread on, or adhere to, a solid surface in the presence of other immiscible fluids.” [6].

When two immiscible fluids, liquid/liquid or liquid/gas, are simultaneously present near a solid surface, there exist cohesive forces between the fluid molecules and their respective interactions to the surface. However, when equilibrium is reached, one of the fluids will experience a greater interactional force to the surface than the other. This fluid is then defined as the wetting fluid, and the other as non-wetting fluid [7].

The wettability of a surface is defined through the contact angle derived from a force balance between the interfacial tensions that act in a three phase system [8].

For an oil/water/solid system which is in static equilibrium, the contact angle is expressed through Young's equation, equation 2.2, [1, 7]:

$$\sigma_{ow} \cdot \cos\theta + \sigma_{ws} = \sigma_{os} \quad (2.2)$$

Where:

σ_{ow} is the interfacial tension between oil and water, N/m.

σ_{ws} is the interfacial tension between water and the solid surface, N/m.

σ_{os} is the interfacial tension between oil and the solid surface, N/m.

The contact angle, θ , is measured through the densest fluid, as shown in figure 2.2.

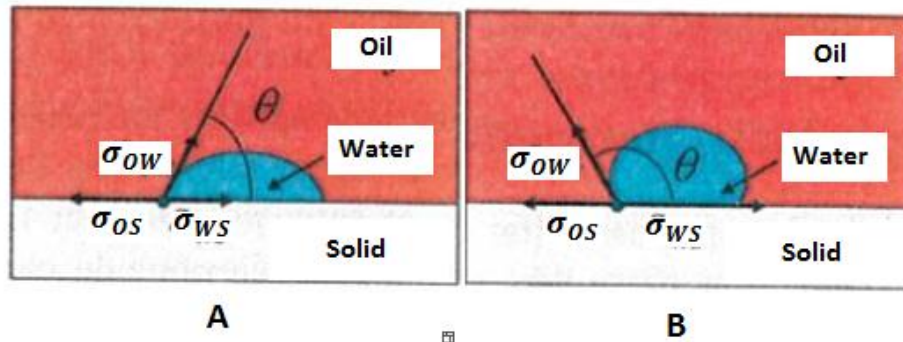


Figure 2.2 Illustration of the contact angle, θ , in a water/oil/solid system [7].
 a) $\theta < 90^\circ$, which gives a water-wet surface.
 b) $\theta > 90^\circ$, which gives an Oil-wet surface.

The contact angle is irreproducible, this phenomenon is called the contact angle hysteresis. The hysteresis is a consequence of two categories of reasons. The first refers to the uppermost layer of the surface which is relevant to determining the contact angle. This surface layer often has coating or traces of contamination that bears little or no resemblance to the bulk material. The second category refers to the method of measurement, *i.e.* to the difference between the contact angle measured when the liquid is being advanced, θ_A , over the solid surface as opposed to when it is being receded, θ_R , from the surface, as shown in figure 2.3 [1]. The magnitude of the difference between θ_A and θ_R is referred to as contact angle hysteresis.

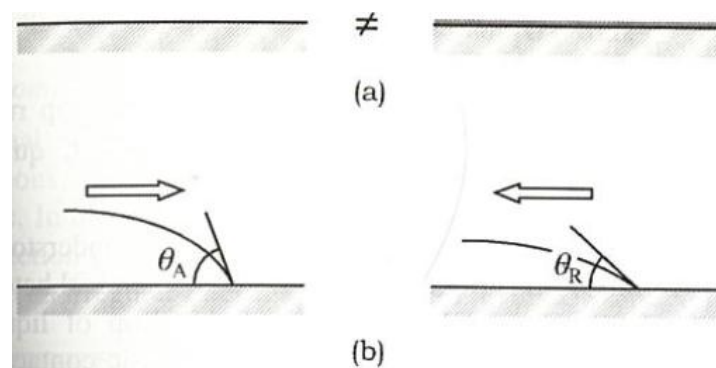


Figure 2.3 Irreproducible contact angles [1].
 a) Surface composition is different between nominally identical bulk solid, b) Contact angle depends on whether liquid is advancing or receding across solid surface: hysteresis.

2.2.2 Rock Wettability

The wettability of a reservoir rock can be estimated quantitatively by the wetting angle, which reflects when the interfacial tension of the fluid phases and their individual adhesive attraction to the solid is in equilibrium.

The wettability of rock's surface is also dependent upon the chemical composition of the oil and the rock's mineral composition [2].

Table 2.1 reflects the wettability classes for an oil/water system:

2.1 Arbitrary wettability classes for an oil/water system [2]

Wetting angle θ (degree)	Wettability preference
0-30	Strongly water-wet
30-90	Preferentially water-wet
90	Neutral wettability
90-150	Preferentially oil-wet
150-180	Strongly oil-wet

Wettability can be classified as homogenous or heterogeneous.

Homogenous is the extreme case where the rock is strongly water-wet, oil-wet or intermediate-wet (equal wetted by both water and oil) which is illustrated in figure 2.4.

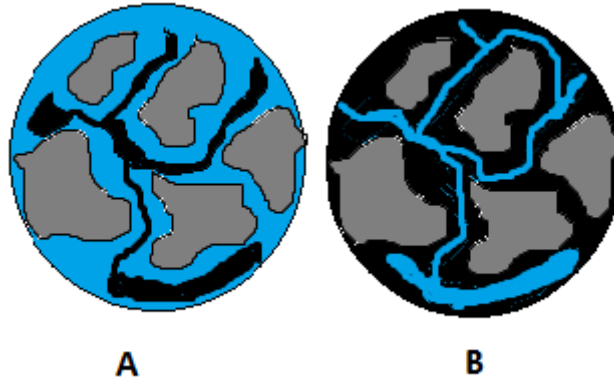


Figure 2.4 Illustration of strongly water-wet and oil-wet pores. Gray color represents grains, blue the water and black the oil. In a) the water is wetting the grains which gives strongly water-wet conditions, and b) the oil is wetting the grain surface which leads to strongly oil-wet conditions.

In reality, the wettability can be non-uniform and is then classified as heterogeneous. Heterogeneous pores have either fractional or mixed wettability's, as shown in figure 2.5.

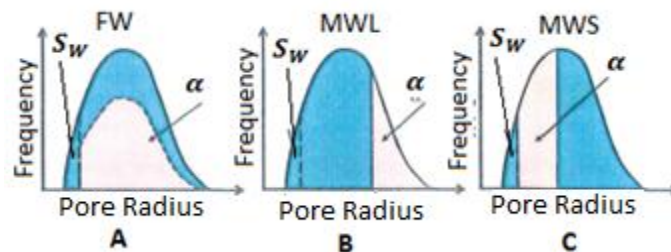


Figure 2.5 Three types of non-uniform wettability [7]. α is the proportion of the oil-wet pores. In a) FW, both small and large pores is oil-wet; b) MWL, only the largest pores is oil-wet; c) MWS, only the smallest pores is oil-wet.

In fractional wet (FW) pores, there exists scattered zones which are strongly water-wet and the rest has wetting affinity to oil. This may occur if the chemistry of the mineral surface of the rock varies (not homogeneous) so the wetting properties are altered. There is also no correlation between the pore size and the wetting properties [7, 9].

Mixed wettability can be divided into two subclasses, i) mixed wet large (MWL) and ii) mixed wet small (MWS).

In situation i, the largest pores are completely saturated by oil and the aqueous phase occupies the small pores, while in ii) the smallest pores are saturated by oil and the largest by the aqueous phase.

2.2.3 Wettability Alteration

The wettability of a reservoir is affected by several factors, such as the crude oil and brine composition initially present, in-situ brine pH, composition and pH of the injected brine, and the mineralogy of the rock.

Buckley *et al.* [10-12] have studied several mechanisms affecting the COBR interactions, which up to date is believed to be the main factors causing wettability alteration.

In their approach, Buckley *et al.* emphasized considerable attention to the oil composition and how it affects the interactions between crude oil/brine/rock interactions.

The mechanisms describing the COBR interactions were:

- *Polar interactions (predominate in the absence of a water film between oil and solid).*

Adsorption of asphaltenes directly from crude oil onto mineral surfaces (clay mineral).

Some important factors affecting the adsorption onto mineral surface, and thus alter the wettability, are the type of clay, nitrogen content in the crude oil surface and the oils ability to solubilize surface active compounds. Figure 2.6 (a).

- *Surface precipitation.*

Crude oils vary widely in their ability to act as solvents for their asphaltenes and other high molecular weight, polar constituents. If the oil is a poor solvent, the tendency for wetting alteration may be enhanced. Indications have shown that more adsorption and

less water-wet conditions are achieved as the oil becomes a poorer solvent. Figure 2.6 (b).

- *Acid/base interactions.*

In the presence of water, both the solid and crude oil interface becomes charged. The rock mineral and crude oil can behave as acids and bases, depending on their polar functional groups. Figure 2.6 (c).

- *Ion-binding or interactions between charged sites and higher valency ions.*

When Ca^{2+} is present, the acid/base interactions are reduced. Some possible interactions are:

- 1) oil-Ca-oil
- 2) mineral-Ca-mineral
- 3) Oil-Ca-minera

The first two can limit wettability alteration, whereas the last can promote it. Figure 2.6(d).

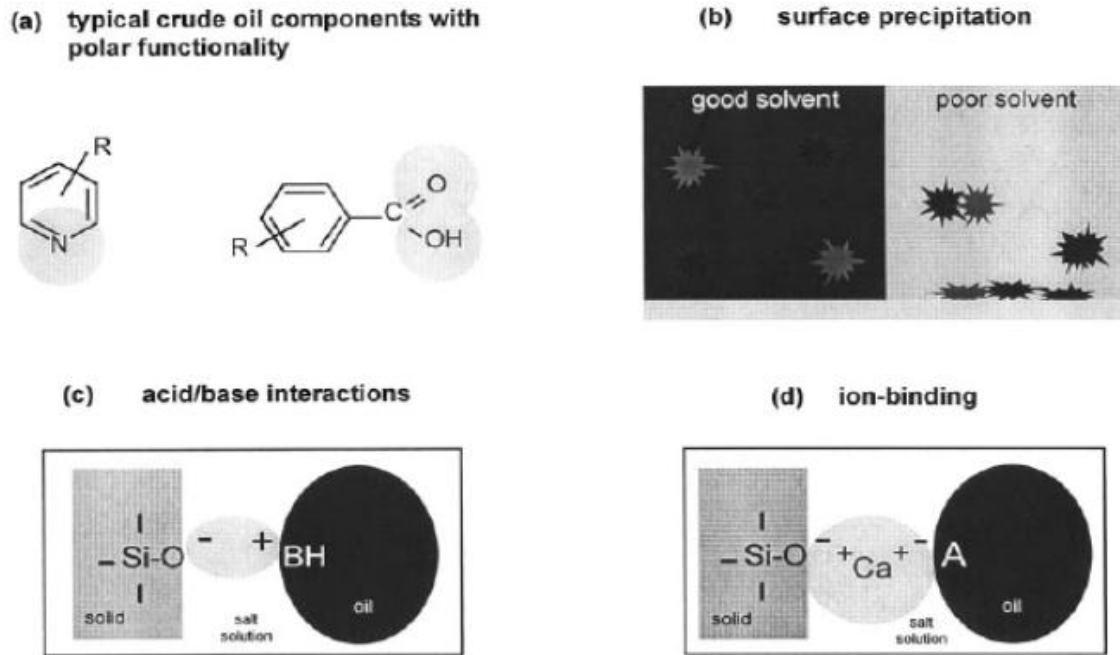


Figure 2.6 Mechanisms of interaction between crude oil components and solid surfaces [11].

2.3 Capillary Pressure

Capillary pressure, P_C , can be defined as the difference in molecular pressure across the interface between two immiscible fluids. In terms of the experimental work performed in this thesis, the immiscible fluids are respectively the wetting phase and non-wetting phase. This is expressed by the following equation [2]:

$$P_C = P_{non-wetting} - P_{wetting} \quad (2.3)$$

Capillary phenomenon is observed in a capillary tube when immersed in two immiscible fluids (oil and water), as illustrated in figure 2.7.

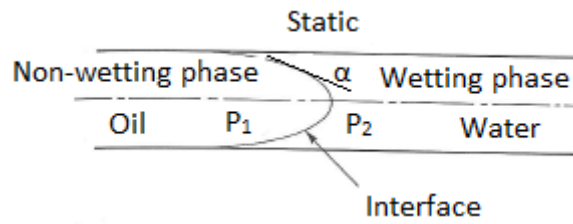


Figure 2.7 Configuration of an interface between a wetting phase (water) and a non-wetting phase (oil) in a capillary tube [13].

The pressure difference in this case results from the difference in both internal (cohesive) and external (adhesive) electrostatic forces acting upon the two fluids. Phase 1 (water) wets the tube surface because the contact angle θ , measured through this phase is less than 90° .

If the two phases and the interface are not moving, a higher pressure is required in the non-wetting phase than in the wetting phase to keep the interface stationary. The pressure difference from these two immiscible fluids is then expressed by the following equation:

$$P_c = \frac{2\sigma \cdot \cos \theta}{R} \quad (2.4)$$

This is a simple form of Laplace's equation, where R , is the curvature of the interface R , σ is the IFT between the two phases in contact, and θ is the wetting angle between solid surface and the tangent to the interface between the two phases in contact. The contact angle can take all values between 0° and 180° , and if it becomes greater than 90° , the wetting pattern of the two fluids will be reversed, and the capillary pressure becomes negative [13].

3 Electrokinetic Interactions

Introduction

Electrokinetic phenomena are a term which describes the electrokinetic interactions between heterogeneous fluids and surface active solids.

This chapter will describe the different properties and composition of crude oil, brine and solid which affects the interactions between them. The theory presented is emphasized on the experimental work in this thesis to provide a fundamental understanding of the interaction between COBR.

3.1 Fundamentals of Electrokinetic

3.1.1 Van der Waals Interactions

Van der Waals forces are universal forces which exist between all atoms and molecules. These forces are not dependent on the electrolyte concentration or pH, but as a function of the distance between the interacting particles [1].

Van der Waals forces can be divided in three categories;

- 1) Dipole-dipole interactions.
- 2) Dipole-induced dipole interactions.
- 3) Induced dipole-induced dipole interaction (London forces).

The net interactions between macroscopic objects (*i.e.* a pair of molecules, or oil/solid) are calculated from the summation of pair of interaction between all molecules in one object with all molecules in the other object.

The attractive forces are a function of the Hamaker constant (material constant), Φ_A , which provides the means of van der Waals interactions between macroscopic bodies. This constant is an experimental measurable parameter [1].

3.1.2 Electrostatic Interactions between Electrical Double Layers

One of the most important aspects of interfaces is the electrical charge separation that exists between them. Regardless of how the charge separation is generated, a structure will be developed such that the surface charge is neutralized by an adjacent layer in the solution containing an excess of electrolytes of opposite charge to the surface, *i.e.* counterions [1]. At equilibrium, a diffuse layer of counterions neutralizing the surface charge is formed with high concentration next to the surface, and it diminishes moving away from the surface. This, together with the surface charge, would produce a variation of potential in the solution, from its surface charge to zero far from the surface, which is represented in figure 3.1.

The electrical double layer is formed by two layers, an inner layer (stern layer) which is the monolayer of stationary counterions (not equal to the amount required for neutralization), and a diffuse layer (Gouy-Chapman layer) consisting of free ions that moves in the fluid under the influence of electric attraction. The slip plane is located between these two layers and thus is the plane between the stationary and mobile ions.

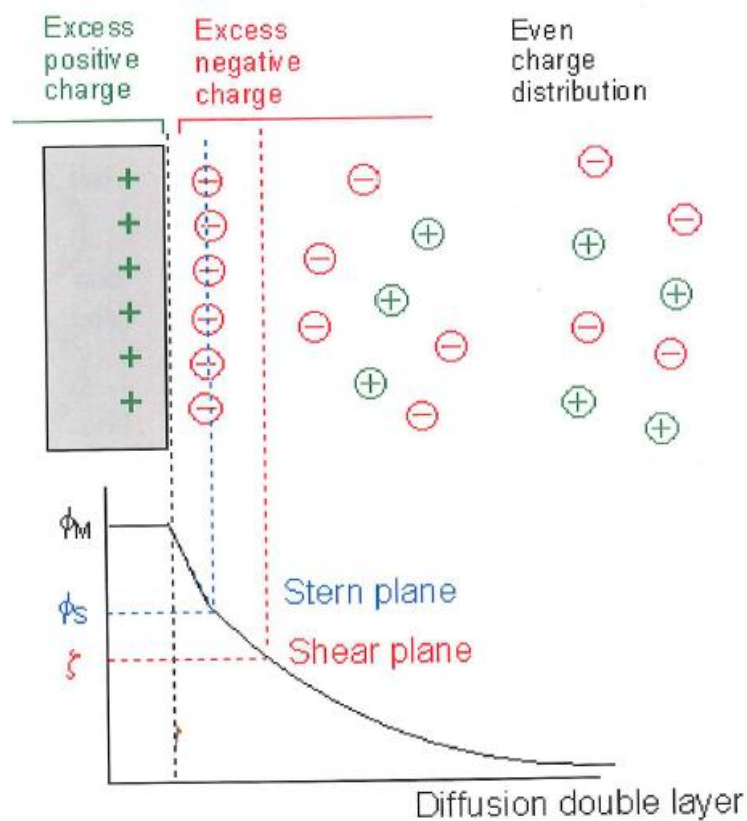


Figure 3.1 Schematic illustration of the electrical double layer for a positive charged solid surface, and the corresponding electrostatic potential curve [14]

As two charged surfaces approaches each other, electrostatic interaction between the electrostatic double layer will occur. These interactions can be either attractive, repulsive, or a combination of them both. The forces will vary, and is dependent of the pH and salinity in the aqueous phase.

A measure of the “thickness of the double layer” is called Debye length, κ^{-1} [nm], and is also appropriately termed as the electrostatic screening length. When the concentration and/or valence of counterions increases, the double layer thickness decreases as a consequence of improved screening. This makes the Debye length simply a property of the electrolyte concentration and is illustrated in figure 3.2. In a solution with mixed electrolytes, the Debye parameter is dependent on the ionic strength of the solution [1].

Ionic strength, I , is a measure of the total electrolyte concentration in a solution and is defined as:

$$I = \frac{1}{2} \sum_{i=1}^n (c_i \cdot z_i^2) \quad (3.1)$$

In this expression z_i is the charge number of the i 'th species (positive for cations and negative for anions) and c_i is the concentration of the ion i . The sum extends over all the ions present in the solution [15].

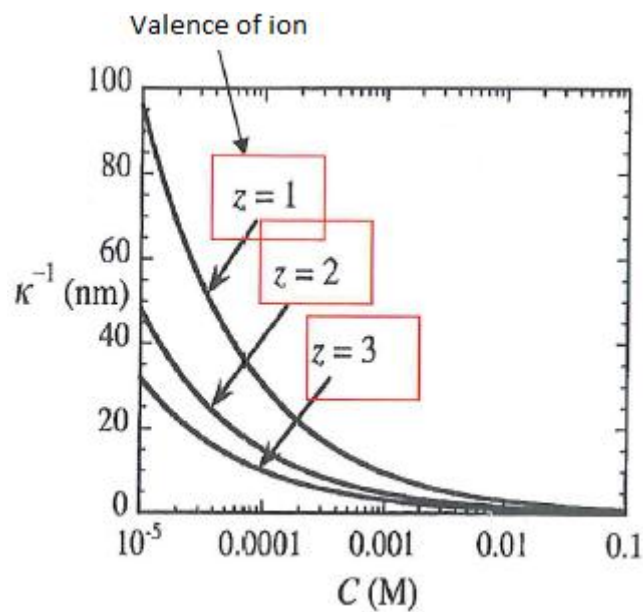


Figure 3.2 Schematic illustration of Debye length, κ^{-1} , in presence of salt with varying concentration, as well as different valence of the ions [1].

The dependency on the aqueous saline is illustrated in figure 3.3. When high salinity is present, the diffuse layer decreases, and vice versa for low salinity brine.

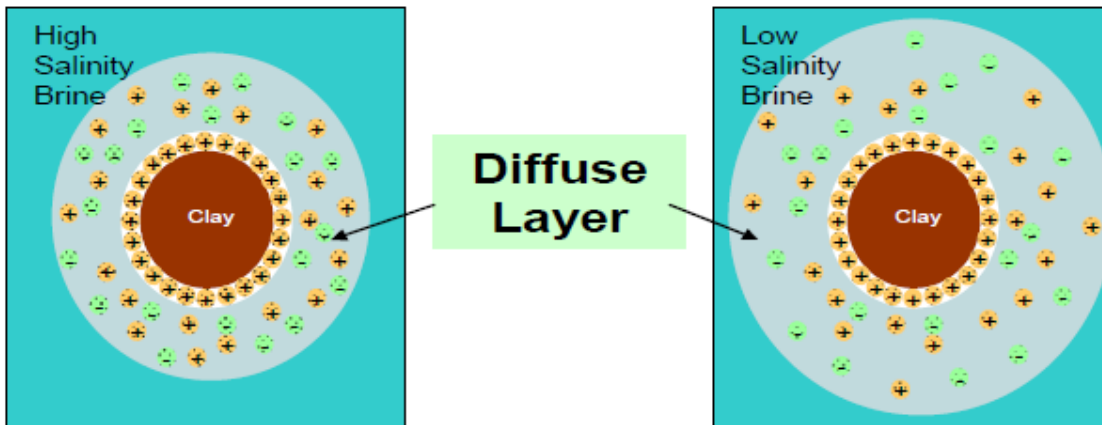


Figure 3.3 Impact of salinity on negative charged clay. When the salinity is reduced, the diffuse layer expands [16].

3.1.3 Zeta-Potential

The zeta-potential is taken to be the electrostatic potential at the interfacial layer located at the slipping plane, as displayed in figure 3.4.

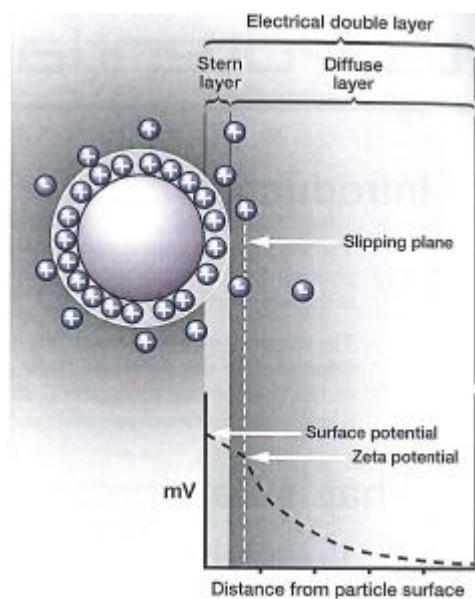


Figure 3.4 Schematic illustration of the zeta-potential located between a charged surface and counterions [17].

The magnitude of the zeta-potential gives an indication of the potential stability of a colloidal system, *i.e.* crude oil/brine or crude oil/solid system. If the zeta-potential is either large positive or negative, the particles will tend to repel each other and there is no tendency to flocculate. However, if the particles generate a low zeta-potential then there is no force to prevent the particles coming together and flocculate. The dividing line between a stable or unstable emulsion or suspension is generally taken to be either higher than +30 mV or less than -30 mV [17].

The zeta-potential of oil droplets dispersed in water is dependent on the pH in the aqueous phase. The potential decreases as the pH increases, and the point where the zeta-potential is equal to zero is called the isoelectric point (IEP). At this point, the dissociated acid and base groups on the surface between the oil and water contribute equally to the total charge on the surface, *i.e.* the colloidal system is least stable [17, 18].

3.1.4 Structural Forces

When the distance between brine/solid, oil/brine or oil/solid surfaces approaches within a few tenths of a nanometer (close to overlap), then short range interactions will appear in the system and the surfaces will be repelled.

These repulsive forces are called solvation, structural, or hydration forces (one type of solvation forces) when the medium is water, and is a result of the intermolecular structure of water [1].

3.1.5 Summary – Electrostatic Interactions

The interactions of aqueous colloidal dispersions is a result of van der Waals forces, electrostatic forces and structural forces [18].

The sum of these three forces as a function of distance to the interfering particles is commonly referred to as DLVO (Derjaguin and Landau, Verwey and Overbeek) theory and is illustrated in figure 3.5.

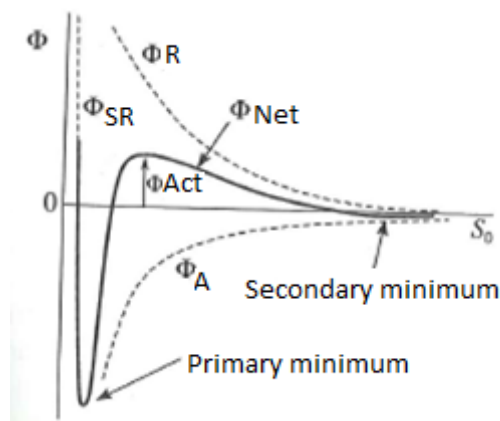


Figure 3.5 Illustration of interaction potential for a pair of spheres as a function of their distance of closest approach, S_0 [1]. Φ_{SR} is the structural, Φ_A is the attractive, and Φ_R is the repulsive forces. Φ_{Net} is the sum of the three forces.

The DLVO curve illustrates that when two particles are separated by long distance, the net force acting on them goes to zero. As the particles approach each other, a secondary minimum is reached where the particles flocculate. An intermediate potential barrier is reached by further reducing the distance. This barrier represents the energy needed to aggregate. When the energy barrier has been overcome, a primary minimum is reached where the particles aggregate. If the distance between them is further decreased, structural forces will repel them [1].

3.2 The Oil, Brine and Solid Phase

This sub-chapter will describe generally the different properties of crude oil, brine and solid phase which contribute to the CORB interactions.

3.2.1 The Oil Phase

The composition of the crude oil has an important influence on the COBR interactions.

Crude oils are not a uniform material but complex mixtures of hundreds of components ranging in size from one carbon atom to one hundred and more. The composition of the reservoir oils may vary considerable with geological locations and geological age of the field [19].

Crude oil cannot be readily separated and identified by standard techniques, but instead characterized by dividing the components into a few groups based on physical and chemical separation [20].

One such separation technique used is SARA-fractionation (Saturates, Aromatics, Resins and Asphaltenes) [21] shown in figure 3.6. The asphaltene fraction of the oil is identified by precipitation in a 40:1 volume mix with n-pentane. The remainder of the oil can be separated chromatographically based on polarity, with saturates as the least polar fraction, followed by the aromatic hydrocarbons. The resins consist of hydrocarbons with small percentages of polar heteroatoms [20].

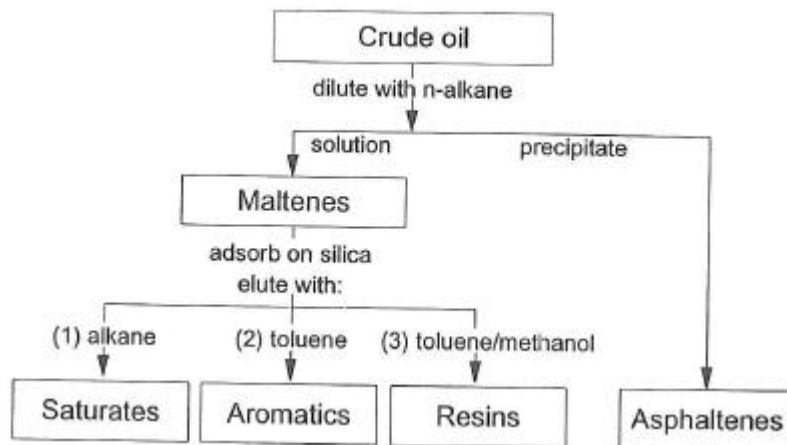


Figure 3.6 SARA separation scheme divides crude oil into Saturates, Aromatics, Resins and Asphaltenes [20].

Crude oils contain appreciable amounts of organic non-hydrocarbons constituents, which is mainly sulfur-, oxygen-, and nitrogen-containing compounds (NSO) [21]. Figure 3.7 presents typical structures of NSO present in crude oil.

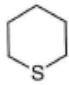
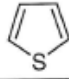
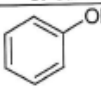
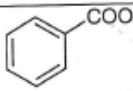
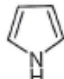
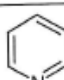
Name of Compound		Molecular structure
Sulphur Compounds	Sulphides	R-S-R'
	Cyclic sulphides	
	Thiophenes	
Oxygen Compounds	Alcohols	R-OH
	Phenols	
	Carboxylic acids	
Nitrogen Compounds	Pyrroles (non-basic)	
	Pyridines (basic)	

Figure 3.7 Typical structures of NSO (Nitrogen, Sulfur and oxygen) compounds present in crude oil [19].

Sulfur compounds are heteroatomic constituents of crude oil. There are many varieties of sulfur compounds in petroleum and in general, the higher the density of the crude oil, the higher the sulfur content is [21].

Oxygen can occur in a variety of forms in organic compounds, and it is estimated that the oxygen content in petroleum is usually less than 2%. Large amounts have also been reported, but when the oxygen content is phenomenally high, the crude oil may have been exposed to atmosphere over a prolonged time [21].

These oxygen compounds can have an acidic character in the petroleum, and is then termed as naphthenic acids. This is substances containing carboxyl groups (-COOH). In addition to the carboxylic acids, crude oil can also contain phenol which is mildly acidic [21].

Nitrogen compounds in crude oil may be classified arbitrarily as basic or non-basic. The basic nitrogen compounds are composed mainly of pyridine, whereas the non-basic compounds are usually pyrrole, indole, and carbazole types [21].

In general, the nitrogen content of petroleum is low and generally falls within the range of 0.1-0.9%.

3.2.2 The Aqueous Phase

The aqueous phase composition represents one of the main variables in this thesis and has been varied with regards to pH, salinity and ionic strength.

Both the oil/brine and solid/brine interfaces have ionizable sites.

Thus the aqueous phase impacts the oil/brine and brine/solid interface through acid/base reactions since the electrical surface charge and the electrical charge at oil/brine interface is a function of the brine`s pH [22].

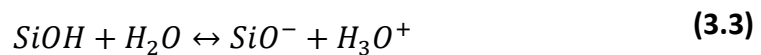
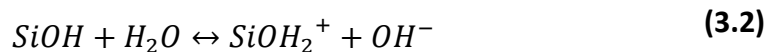
3.2.3 The Solid Phase

The most common mineral type in sandstone reservoirs is mineral quartz (SiO_2), in addition to feldspar and clay minerals. Compared to the bulk mineralogy, a variety of minerals may be present at the pore surfaces. As a consequence of the mineral heterogeneity and surface roughness of reservoir rock, large hysteresis is observed which can impact wettability measurements [19]. Thus, as a representative reservoir rock, smooth surface quartz crystalline slides were used for measuring wettability in CORB system.

When quartz is contacted with aqueous solutions, hydrolysis of the surface species takes place generating silanol groups (SiOH) [23].

Depending on the pH of the aqueous phase, acid/base reactions can take place by ionizing the hydroxide functional groups, resulting in a change of the interface properties between brine/solid [24].

This is shown by equation 3.2 and 3.3, where the first represents an acidic and the second a basic surface after the silanol group has been ionized [24].



3.3 Crude Oil/Brine Interactions

As mentioned earlier, the crude oil/brine interface is affected by acid/base reactions. Charged species at the oil/brine interface give rise to a net charge at the interface. The pH, salinity, and ionic strength will impact the accumulation of surface-active species at the crude oil/brine interface and the electrostatic forces between them [19].

It has been proven by for instance Buckley [20] that the interface of emulsified crude oil droplets in brine of varying composition have a net positive charge at low pH and net negative charge at high pH.

Buckley [20] explained that organic acids and bases dissociate at the oil/brine interface which impacts the zeta-potential. The oil/brine interface will then be dominated by positively charged bases at low pH, and negatively charged acids at high pH.

This is presented in figure 3.8 which illustrates the measured zeta potential for crude oil A-93 (figure 3.8 a), and Mountrary crude oil (figure 3.8 b) emulsified in NaCl brines.

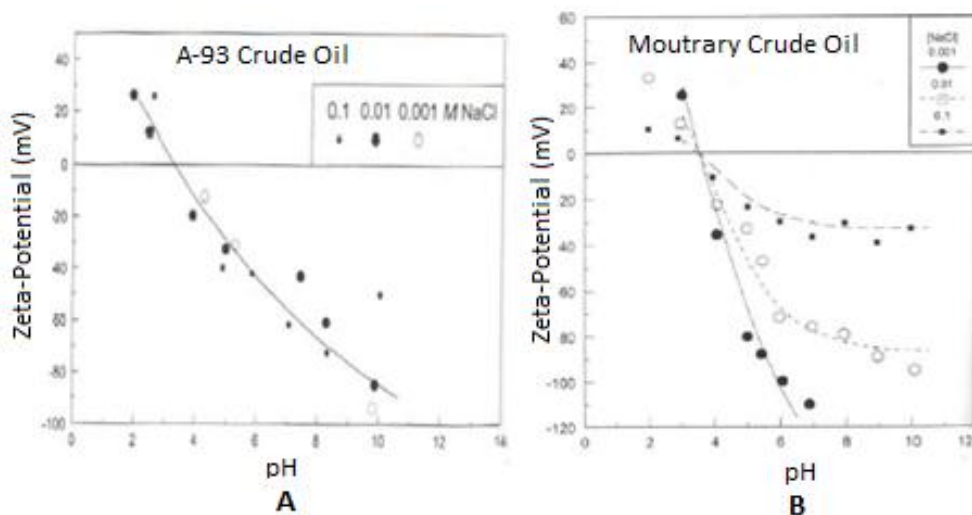


Figure 3.8 Zeta potential data for a) A-93 crude oil and b) Mountrary crude oil as a function of pH in 0.001, 0.01 and 0.1 M NaCl, measured by Buckley [20].

Nasralla *et al.* [22] studied the impact of pH on the zeta-potential and reported that the negative charge at the oil/brine interface reduces as the pH is decreased, as seen in figure 3.9.

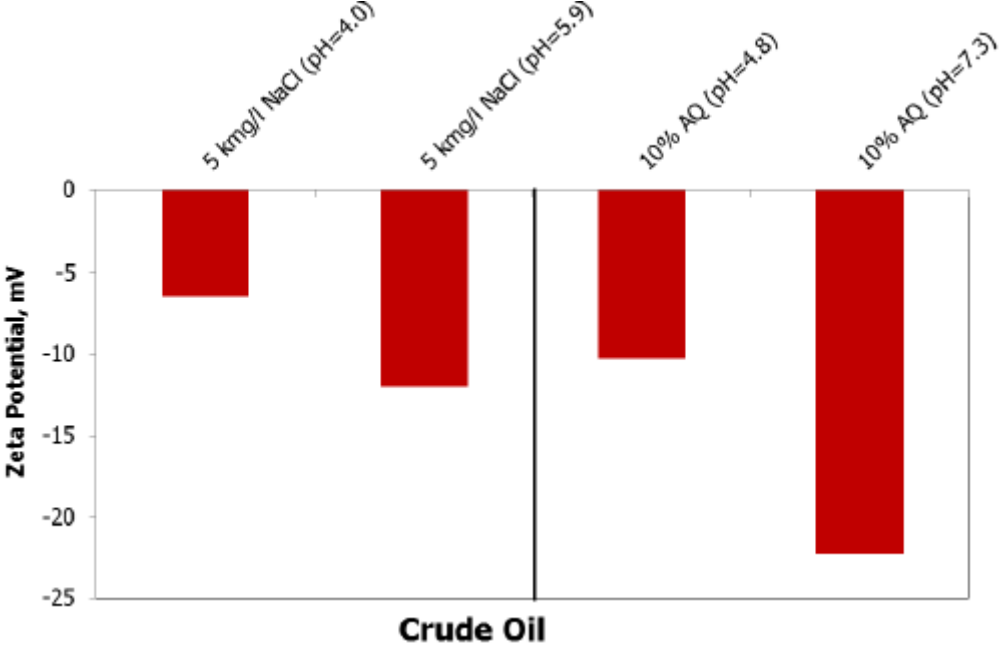


Figure 3.9 Impact of pH change on zeta-potential at crude oil/brine interfaces [22].

The acid and base reactions between the crude oil/brine interfaces also change the interfacial tension which makes the IFT a function of pH. The IFT is found to be highest near the neutral pH range, and decreases as pH is either increased or decreased [25].

This is shown in figure 3.10 between Ventura crude oil and water as a function of pH.

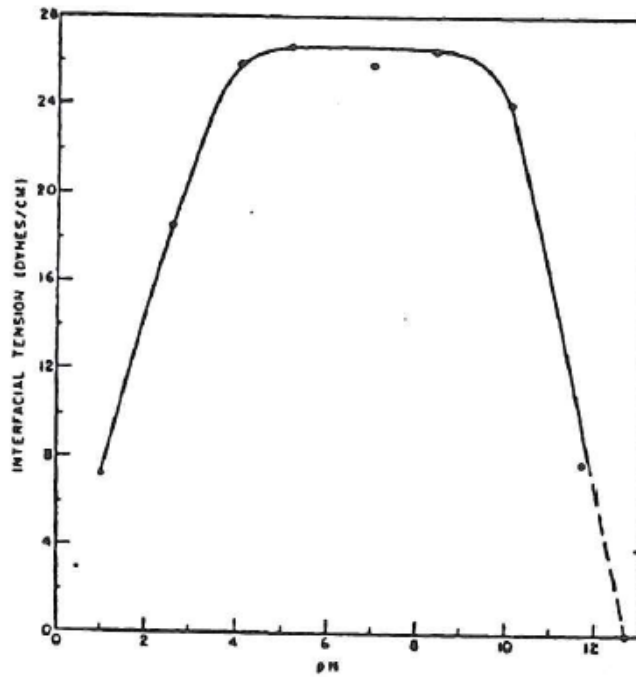


Figure 3.10 Interfacial tension between Ventura crude oil and water as a function of pH [19].

The effect of increasing salinity of the aqueous phase generally lowers the interfacial tension between oil and water [20]. The solubility of surface-active compounds will tend to be reduced by the salting out effect (precipitation) in the aqueous phase, and thereby increase the amount of surface-active species at the interface. In addition, salt may act as counterions at the interface causing a reduction in the electrostatic repulsion between equally charged molecules. Hence, the interfacial tension will decrease as the concentration of surface-active compounds at the interface increase [19].

4 Enhanced Oil Recovery (EOR)

Introduction

There exist many methods to reduce the residual oil saturation, and thus increasing the production of the reserves. These methods include for instance low salinity flooding to enhance the sweep by wettability alteration, surfactant flooding to reduce the interfacial tension between crude oil and water, polymer flooding to increase the viscosity of the injected water for an improved sweep etc.

Common for most EOR methods is that the improved effect can be explained through the capillary desaturation curve (CDC) [2]. This curve is illustrated in figure 4.1.

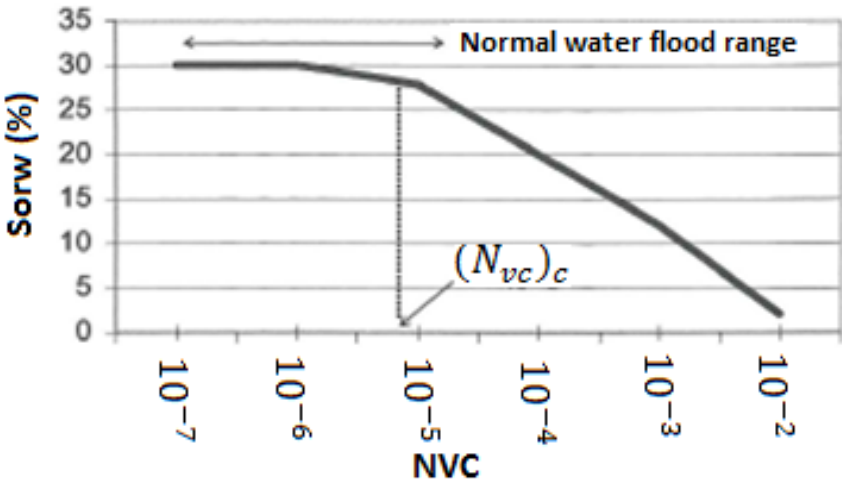


Figure 4.1 Schematic illustration of the Capillary Desaturation Curve (CDC). Residual oil saturation is reduced when the capillary number is increased [9].

The capillary number is a dimensionless ratio of viscous forces to local capillary forces and is expressed by equation 4.1 [9].

$$N_{vc} = \frac{\text{Viscous force}}{\text{Capillary force}} = \frac{u_w \cdot \mu_w}{\sigma_{o,w}} \quad (4.1)$$

Where, u_w is the Darcy velocity of water (displacing fluid), μ_w is the viscosity of water and $\sigma_{o,w}$ is the IFT between crude oil and water.

The CDC curve shows that at low capillary number, N_{vc} , the residual oil saturation is roughly constant at a plateau value. At a critical value, $(N_{vc})_c$, a drop in the curve occurs and the S_{orw} begins to decrease. The capillary number follows a logarithmic scale so in order to significantly reduce the oil saturation, N_{vc} needs to be increased by at least 2-3 orders of magnitude [9].

4.1 Low Salinity Waterflooding

For many decades, secondary recovery by water injection has been successfully used to increase the production of hydrocarbons. The purpose of the waterflood is i) to displace the oil towards a producer and ii) to give pressure support to the reservoir.

In 1971 Ekofisk (oil field in the North Sea) started production and the anticipated recovery factor was calculated to 17% by primary drive mechanism.

In 1987 through 1994 a full field waterflood was implemented, and the success was outstanding. The recovery factor was expected to exceed 50% which is illustrated in figure 4.2. This leaves Ekofisk as an example of the importance of water injection [9, 26].

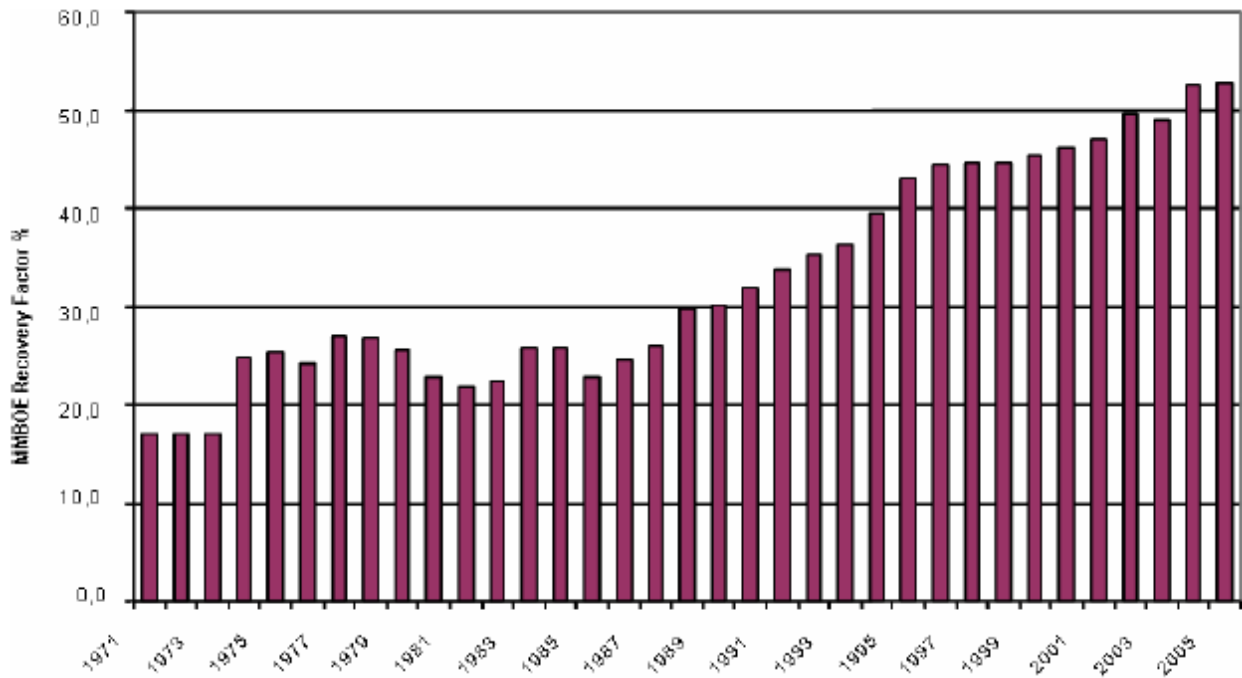


Figure 4.2 Expected ultimate recovery at Ekofisk from 1971-2005 [26].

In recent years, there has been more attention drawn towards the chemistry of the injected water. There is evidence from both laboratory and field tests that reduction of salinity in the injected water has an impact on the oil recovery [27-45].

The primary reported observation of low salinity brine affecting the oil recovery was made by Martin (1959) [32]. He suggested that the observed increase in the oil recovery factor in sandstone reservoir when salinity of injected brine was reduced was related to swelling of clays and emulsification.

The first observation of improved oil recovery with fresh water injection was made by Bernard (1967) [33]. He reported that injection of fresh water can increase oil recovery from sandstone cores containing clay. This was ascribed to sweep efficiency improvement caused by clay swelling and pore throat plugging from fines migration, which resulted from hydration of clays by fresh water. Unfortunately, this work did not capture the attention of the petroleum industry at that time.

More extensive research started in the 1990's to confirm the capability of low salinity water to improve oil recovery in sandstone reservoirs.

In 1995 Jadhunandan and Morrow [35] studied the effect of wettability on oil recovery in Berea sandstone based on results from more than 50 slow-rate laboratory waterfloods. They concluded for crude oil/brine/rock systems that oil recovery by waterflooding increases with change in wettability from strongly water-wet to a maximum close-to-neutral wet. Skauge and Ottesen [46] discovered the same type of relationship based on a large set of waterflood data from 30 different reservoirs and found a trend of lower remaining oil saturation when the cores were intermediate wet.

In 1996 Yildiz and Morrow [36] investigated how brine composition influenced the oil recovery in aged Berea sandstone cores with Moutray crude oil and two different brines, i) 4.0% NaCl + 0.5% CaCl₂ (brine 1) and ii) 2.0% CaCl₂ (brine 2). The cores were saturated with the brines thus representing the connate water. When connate and injected brine were the same, brine 2 gave highest recovery but imbibition test shows that brine 2 gave less water-wet conditions. The highest recovery was achieved by initial saturation of the cores with brine 2 and using brine 1 as the primary injection brine and brine 2 as the secondary injection brine.

Extensive research on the low salinity effect (LSE) was performed by Tang and Morrow [37]. In 1997, Tang and Morrow [37] published their study based on displacement tests in Berea sandstone with three crude oils and three reservoir brines (RB's). Salinity of the synthetic brine was varied by changing the concentration of total dissolved solids (TDS's). They reported an increase in oil recovery (~5% incremental oil recovery) by decreasing the concentration of injected brine by a factor of 10 and 100, as displayed in figure 4.3.

Other important results were also obtained;

When the connate and invading brine was identical, the final oil recovery (~30% incremental oil recovery) increased with decreasing salinity concentration. However, the most diluted brine gave slowest initial recovery but the highest final recovery.

When connate brine salinity was varied and concentration of invading brine held constant, decreasing connate brine salinity dramatically increased recovery (~35% incremental oil recovery).

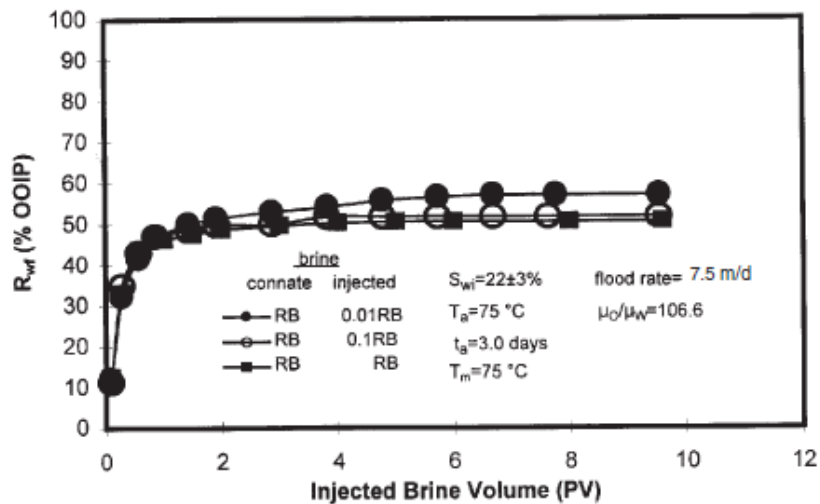


Figure 4.3 Effect of altering injected brine concentration on recovery with Dagang crude oil. Connate water was Dagang RB [37].

Morrow et al. [38] published one year later their work showing that wettability and laboratory recoveries of COBR ensembles can be strongly dependent on brine composition and on related COBR (using aged Berea sandstone) interactions. Four ions were considered at ambient temperature, sodium, potassium, calcium and aluminum(III), all at 0.09 M. For the monovalent-cations, the imbibition was relatively fast were potassium gave the highest recovery. Initial imbibition by multivalent-cations was slow and recovery curves fell closely to each other. But the final recoveries exceeded those for brines with monovalent-cations which gave a correlation for very strongly water-wet conditions.

Experiments by altering the sodium chloride concentration to observe the influence on oil recovery were also conducted. They observed an extent and rate of spontaneous imbibition, and an increase in breakthrough and final waterflood recoveries with decreasing sodium chloride concentration.

Throughout the years there has been more focus on understanding low salinity effects.

In 1999, Tang and Morrow [39] observed an increase in oil recovery by low salinity waterflooding (LSW) in two different cores. Core 1 was Berea sandstone and core 2 was Bentheim which is clean sandstone with much less clay content than Berea sandstone. The increase in oil recovery with a decrease in brine concentration was less for core 2. This led to a

discussion about potentially mobile fines by COBR interactions and the effect mobile fines had on oil recovery.

However, in 2000 Sharma and Filoco [40] did not observe any beneficial LSW effect. They flooded Berea sandstone while varying the injected brine from 0.3-20.0% NaCl and kept the connate water fixed at 3.0% salinity. They suggested the oil recovery is not sensitive to the salinity of the injected brine, but rather dependent on the salinity of connate water. In addition, based on the results they also suggested that residual oil saturation decreases as the wetting properties of the rock surface changes from water-wet to mixed-wet by low salinity connate brine.

Enhanced oil recovery in both secondary and tertiary mode has been reported by Zang and Morrow [41] in 2006 and by Zang et al. [42] in 2007.

Zang and Morrow [41] performed numerous core flood experiments on Berea sandstone with permeability of 60, 400, 500 and 1100 mD. Synthetic brines were prepared from deionized water and reagent grade chemicals. The oils were CS crude, Minnelusa crude from the Gibbs field in Wyoming and crude oil A. For all experiments with low salinity flooding, the synthetic reservoir brine was diluted with a factor of 0.01.

Based on their observation they concluded that sandstone properties are the most significant factor improving the oil recovery by injection of low salinity brine. Results also showed no low salinity effect on the core with 60 mD. They suggested that Berea sandstone with permeability in range of 40 to 140 does not usually respond to injection of low salinity brine.

When improved recovery due to LSW was observed, it was usually witnessed in both secondary and tertiary mode.

Zang et al. [42] in 2007 performed their experiment by using two consolidated reservoir sandstone cores which was rich in chert and kaolinite. Cores established mixed-wet wettability after absorption of two crude oils (named WP and LC) in presence of connate water by 10 days aging. The synthetic connate water was reservoir brine (RIB) and the injected low salinity brine was diluted to 0.05 RB (factor of 20) named LSB.

They accomplished to prove an increase in oil recovery by injection of low salinity water in both secondary and tertiary mode, displayed in figure 4.4. The core was first flooded with HS RIB which gave a secondary recovery of 55% original oil in place (OOIP). When the core was flooded with 8000 ppm NaCl to observe the effect of removing divalent ions by the previous injected RIB, only a slight increase in oil recovery was observed above the projected trend for RIB injection. This showed no increased oil recovery in tertiary mode but when switching to 1500 ppm NaCl an increase of 12.7% OOIP in tertiary recovery was observed. Finally the core was flooded with LSB which resulted in 4% OOIP additional recovery. Effluent pH and pressure drop was also monitored. For all cases, with WP crude oil as the oil phase, the effluent pH decreased by low salinity brine injection whereas when LC crude oil was used as the oil phase, the effluent pH increased.

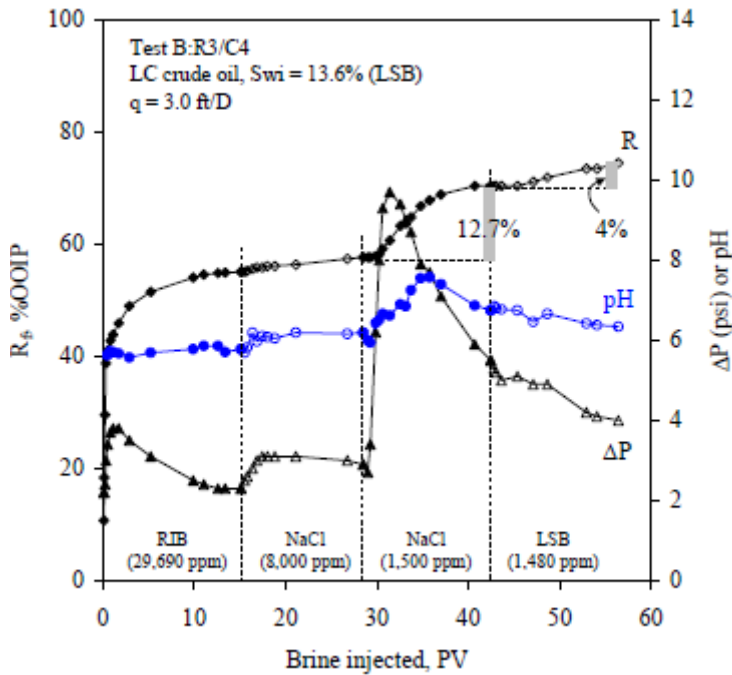


Figure 4.4 Oil recovery by injecting four sequences of different brine compositions. Incremental oil recovery is observed at every stage [42].

Nasralla *et al.* (2011) [31] investigated how type and ion concentration in the injected water influenced oil recovery. Coreflood experiments were conducted on Berea sandstone cores by injecting NaCl, CaCl₂ and MgCl₂ at concentrations of 0.2, 1.0 and 5.0 wt%.

The cores were saturated with formation brine at connate water saturation and crude oil (A) and (B).

Zeta potential was measured between crude oil/brine and rock/brine to examine electrical surface charges. For this, Berea sandstone and four different types of clays (illite, kaolinite, montmorillonite and chlorite) were crushed to very fine particles and added in the solution. In addition, cation exchange tests were run to investigate the interactions between rock and brine.

Results from coreflood experiments demonstrated that injection of the lowest concentration of sodium chloride gave the highest oil recovery (0.2 wt% recovered 85% OOIP) compared to calcium chloride (0.2 wt% recovered 77% OOIP) and magnesium chloride (0.2 wt% recovered 80% OOIP). They concluded that the type of cation had a significant impact on oil recovery, and was more dominant than the cation concentration in the injected brine.

By injecting a constant concentration of sodium in dry cores and measure the ion type and concentration in the effluent water, they were able to observe cation exchange. After some pore volumes (PV) injected, the concentration of sodium in the effluent water stabilized equal to the amount injected. The magnesium and calcium concentration declined in the effluent water until it stabilized at a constant concentration resulting from cation exchange.

Investigating the surface charge by measuring the zeta potential, they observed that sodium chloride changed the charges at rock/brine and oil/brine interfaces to highly negative compared to magnesium and calcium, see figure 4.5. As a conclusion, Nasralla *et al.* pointed out that oil recovery can be improved due to the expansion of electrical double layer, which causes the wettability towards a more water-wet system.

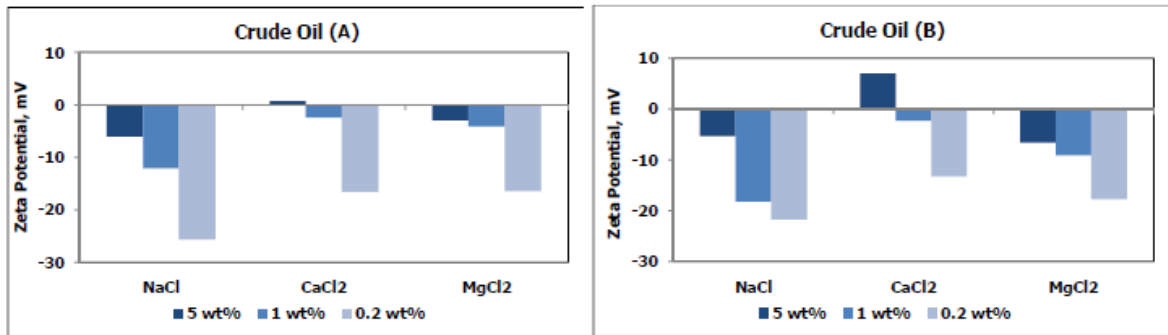


Figure 4.5 Impact of cation type and concentration on zeta potential at oil/brine interface with crude oil (A) and (B). For both oils, the zeta potential is highly negative with 0.2 wt% NaCl [31].

In 2011 Robin Gupta *et al.* [44] published their research on carbonate coreflood experiments by selectively adding and/or removing ions from the injected water. They called it AIMSM, Advanced Ion Management.

All brines were synthetic and the crude oil used was from a Middle Eastern reservoir and had a total acid number of 0.11 mg KOH/g. The cores, named D1, D2 and L1 to L6 were saturated with formation brine, flowed with dead crude oil and aged at reservoir temperature for six weeks to restore wettability towards reservoir conditions.

In their approach they flooded the cores with formation water (FW), followed by different sequences of adding/removing ions from the injected sea water (SW)/FW.

Figure 4.6 shows that they obtained incremental oil recovery by flooding core L5 with FW (recovered 63.2% OOIP), followed by synthetic sea water (SSW) without sulfate (recovered additional 7-9% OOIP), and then three sequences with SSW w/o SO_4^{2-} but with added 1/100, 1/10 and 1/1 times base phosphate ion concentration. Brines containing 1/100 and 1/10 times base phosphate ion concentration in SW w/o sulfate produced minimal oil, but an increase in oil recovery was observed with the highest concentration. In total, 15.7% OOIP was recovered by the combined floods of modified brines.

In another coreflood experiment they examined the influence of adding/removing calcium and magnesium from the injected brine to capture hardness vs. total salinity, as seen in figure 4.7. They measured incremental oil recovery in every step by first flooding core L6 with FW (recovered 57.7% OOIP) containing 15992 ppm calcium and 1282 ppm magnesium and then

continued flowing the core with the following sequence: FW w/o magnesium and calcium, FW w/o calcium (1282 ppm Mg^{2+}) and then SW w/o sulfate (521 ppm Ca^{2+} and 1094 ppm Mg^{2+}). The resulting recovery was 11.4% OOIP, compared to sea water w/o sulfate (see figure 4.6) which is relatively lower in salinity but harder.

An interestingly observation they also made was that after flooding core L2 with FW that recovered 57.7% OOIP before oil production ceased, additional incremental oil recovery of astonishing 15.6% OOIP was measured with SW w/o sulfate but containing borate salt.

Robin Gupta *et al.* concluded from this study that improved oil recovery results from reducing hardness, not from lowering total dissolved solids, and additional oil can be recovered with softened water alone.

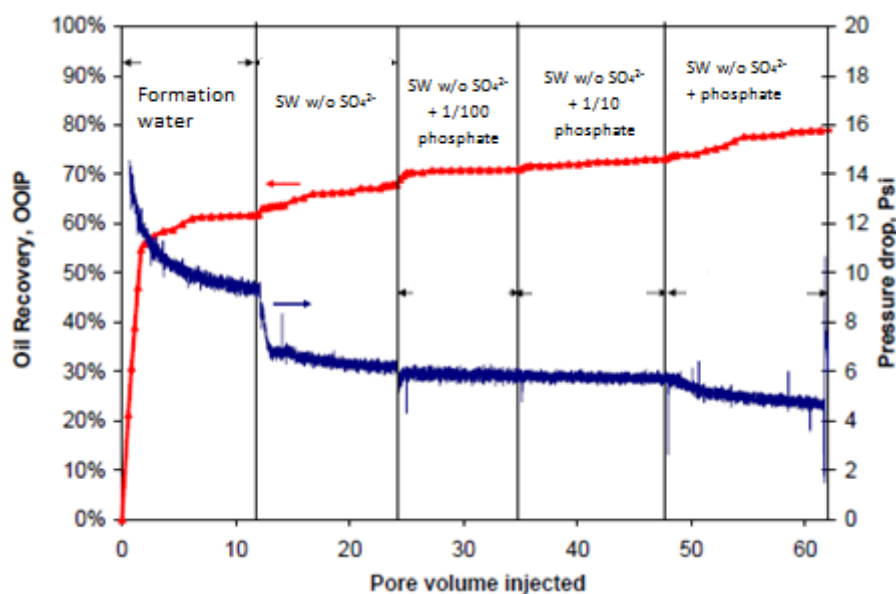


Figure 4.6 Coreflood experiment by injecting the core in the following order: FW, SW w/o sulfate and SW w/o sulfate but added 1/100, 1/10 and 1/1 times base phosphate ion concentration [44]. Incremental oil recovery is observed only for FW, SW w/o sulfate and 1/1 base phosphate added to SW w/o sulfate.

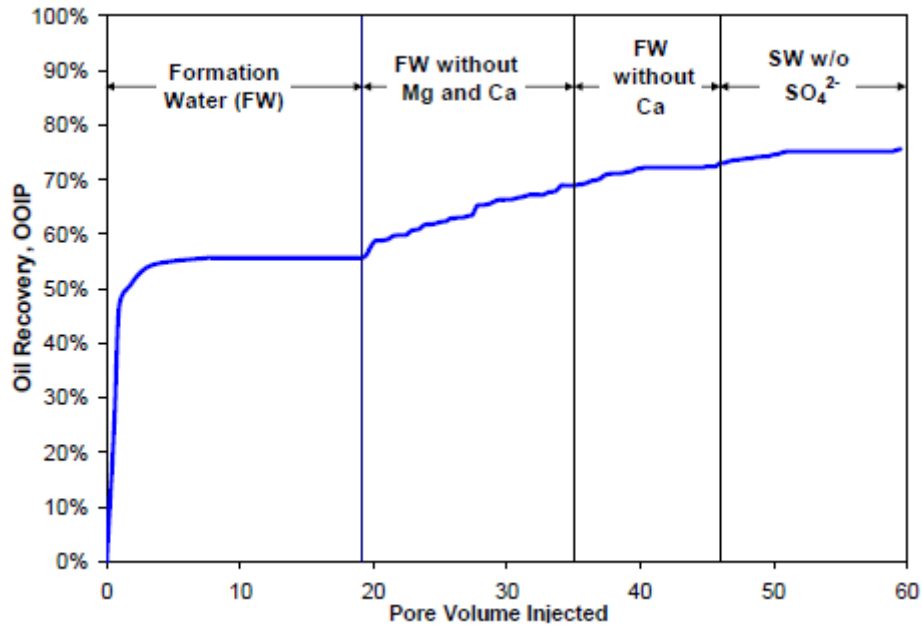


Figure 4.7 Coreflood experiment by selectively removing magnesium and/or calcium in the injected FW [44]. Incremental oil recovery was observed in every step.

From all the research done throughout the years it is evident that by manipulating the type of ions and concentration in the injected water it is possible to increase the oil recovery.

No one yet can thoroughly explain the reason behind the observed effect of LSW but many mechanisms have been suggested, and are explained in chapter 4.3.

One explanation which is supported by many scientists is the alteration of rocks wettability from water-wet to mixed-wet by LSW, which is more beneficial for oil production.

4.2 Field Scale LSW

Webb et al. (2004) [43] performed a field test study on LSE by measuring residual oil saturation (S_{orw}) with log inject log method. It was necessary to inject a minimum of three different brines based on the sodium chloride content to measure S_{orw} after high and low salinity waterflood. The quality of sodium chloride was checked with mass spectroscopy to ensure no contamination in the injection water. First an injection of high salinity (220000 ppm, approximately the same as the reservoir connate brine) brine was performed. The inject sequence followed by an intermediate (170000 ppm) brine, low salinity (3000 ppm) brine and then re-inject high salinity brine. The low salinity waterflood produced significant incremental oil compared to high salinity waterflood. Data from the field experiment showed that the oil saturation ranged from 30.0-50.0%.

In 2010 a group of scientists including Jim Seccombe, Kevin Webb, and Ester Fueg published a paper describing the first comprehensive inter-well field trial of low salinity EOR at the Endicott field, North Slope Alaska [45]. This was selected as the first BP (British Petroleum) initiated tertiary LS EOR pilot. Previously a comprehensive study had been made to evaluate Endicott field. This was presented by Seccombe *et al.* in 2008 [47] and included core measurements, numerous Endicott field single well chemical tracer tests (SWCTT) and simulation studies. Results from SWCTT demonstrated that a reduction in the remaining oil saturation ranged from 6.0%-12.0% OOIP, resulting in an increase in waterflood recovery of 8%-19% [48].

An increase in oil recovery by LSW at an Alaskan reservoir was also reported by Lager et al. (2008) [27]. In May 2005, it was decided to inject low salinity water and produce from a well that had been previously subjected to natural depletion, injected seawater and a slug of miscible injectant (MI). The LSW was successful with the oil production increasing to a peak of 320 bbls/day from 150 bbls/day, followed by a decrease to 200 bbls/day, shown in figure 4.8.

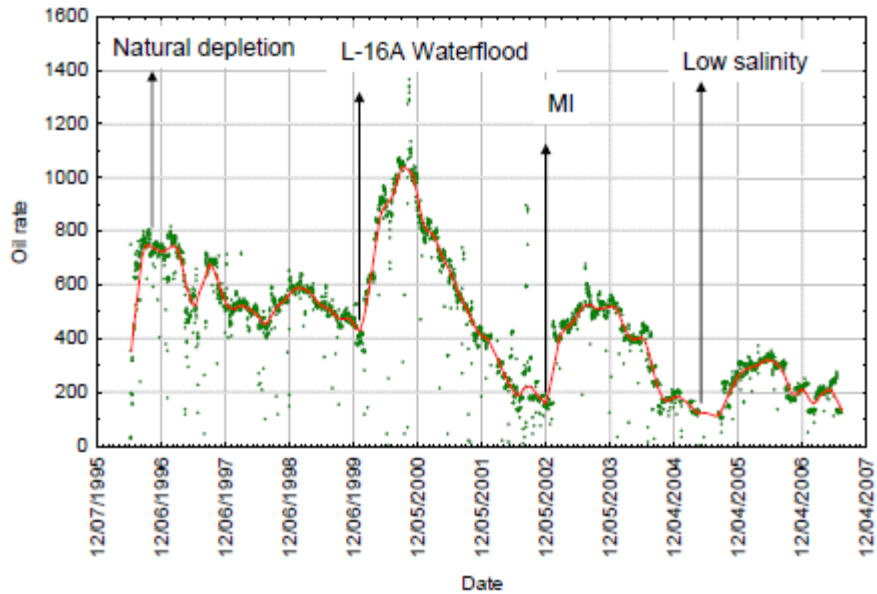


Figure 4.8 Production from a well after different enhanced oil recovery processes had been implemented at an Alaskan reservoir. Incremental oil recovery was observed after low salinity waterflooding [27].

The potential for low salinity waterflooding is not always optimal. Snorre field, located in the North Sea area, has also been evaluated through both laboratory measurements and a field test. Results from both investigations indicated that the potential is low. The anticipated reason for this is believed to be the wetting conditions at Snorre field is naturally close to optimal (neutral-wet to weakly water-wet) such that seawater injection already is efficient [49].

The success of any EOR technique is the ability to recover significant volumes of oil rapidly and at low cost. But there are also concerns with low salinity waterflooding despite the success from previously field trials. One of the concerns regarding LSW is the detrimental rock/fluid interactions, causing reduction in permeability and therefore reducing injectivity capacity into the reservoir [50]. Another concern is the economic issue rising from injection of LS water when there is no presence of fresh water.

4.3 Suggested Mechanisms for Low Salinity Effects

Improved oil recovery by LSW has been successful in both laboratory and field trials. But the mechanism behind the effect is not fully understood yet. Many mechanisms have been suggested in the literature, but because of the complex COBR interaction involved in the LSW process, none has to current date been accepted as the prevailing mechanism.

The crude oil/brine/rock interactions that have been proposed [12, 22, 51] as the main mechanism behind LSE is:

- Wettability alteration
- Fine migration
- pH variation
- Double layer expansion
- Multicomponent ionic exchange (MIE)

4.3.1 Wettability Alteration

Wettability alteration has been the most frequently suggested cause of increased oil recovery [52]. Historically it was believed that reservoirs were either water-wet or oil-wet [53], but it's not a defined property. Reservoirs can cover a broad spectrum of wetting conditions that range from strongly water-wet to strongly oil-wet and between these two conditions exist mixed-wet [54]. It is more favorable to produce oil from a weak water-wet to neutral-wet reservoir [9].

Wettability is dependent on the adhesive and cohesive interactions between crude oil/brine/rock. When the three interfaces come together at a contact line, the interfaces interact with each other and the forces that tend to disjoin or separate them is called disjoining pressure. This pressure results from intermolecular or interionic forces and is identified as Van der Waals, electrostatic and hydration forces. Electrostatic forces can be repulsive, attractive or

a combination. Thus the stability of the water film is dependent on a negative disjoining pressure that will promote water-wet conditions. But the disjoining pressure is strongly affected by brine pH and salinity, as well as crude oil composition and mineral composition [55].

Tang and Morrow (1997) [37] studied how low salinity waterflooding impacted the oil recovery. They reported an increase in oil recovery by diluting the ionic strength of invading brine. Tang and Morrow also reported wettability alteration towards more water-wet conditions as the salinity of injected brine decreased. Contrary, Sandengen *et al.* (2011) [56] observed that the wettability changed from water-wet to more oil-wet during LSW.

Ashraf *et al.* (2010) [57] performed core flood experiments on Berea sandstone with the objective to investigate the relationship between rock wettability and oil recovery with low salinity water injection as secondary recovery process. Brines used were synthetic (SB, 10.0% SB and 1.0% SB) and made out of different salts in deionized water. Four types of oils were made out of refined n-decane as base oil and additives. The experiment was conducted with four different wetting conditions, respectively water-wet, oil-wet, neutral-wet and neutral-wet TOW (towards oil-wet). In general, they observed that oil recovery increased as the invading brine salinity decreased. Maximum beneficial recovery was observed for water-wet cores (70.0% OOIP), contrary to lowest recovery, which was measured for oil-wet conditions (up to 7.0% OOIP). Figure 4.9 shows the effect of LSW on residual oil saturations under the four different wettability conditions. The general trend indicates that when the wettability changes from water-wet to neutral-wet, the final recovery increased to a maximum and then the oil recovery decreased with an increase in oil wetness.

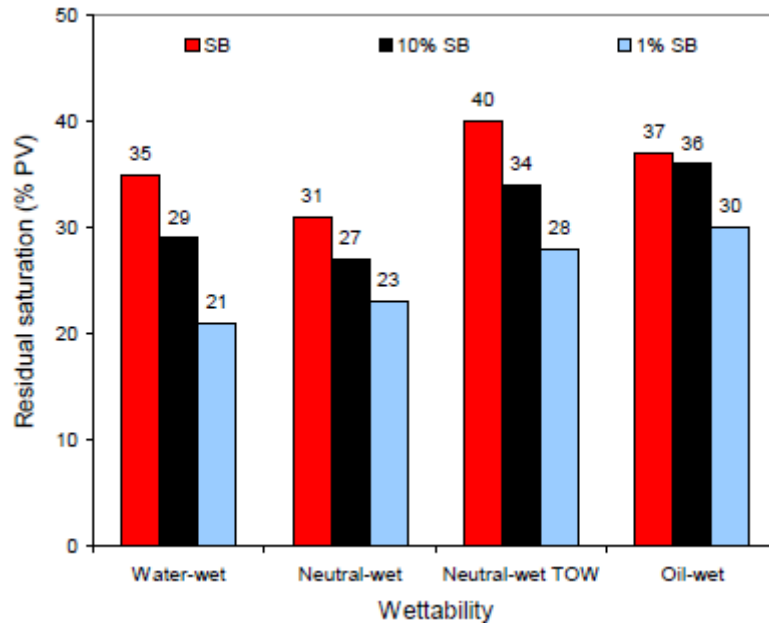


Figure 4.9 Relationship between wettability and residual oil saturation after injecting three different concentrations of synthetic brine [57].

Lee *et al.* (2010) [16] published a study on the water film thickness by examination of the interactions between brine (LiCl, NaCl, KCl, MgCl₂, CaCl₂, Na₂SO₄, MgSO₄) and LUDOX AM (both clay or sand like particle). For these measurements they used Small Angle Scattering (SAS). For the sand like particle, the water film thickness did not differ much but did indicate some increase in thickness by decreasing the ionic strength of the brine. The same was observed for clay like particles, except that the increase in size of the water film was greater for divalent ions, compared to monovalent ions.

It is evident that wettability alteration is an important mechanism affecting the oil recovery and the support is increasing. Wetting alteration involves complex interactions between many parameters which makes it difficult to draw conclusions regarding the responsible mechanism.

4.3.2 Fine Migration

A proposed mechanism that potentially plays an important role in enhancing the oil recovery by LSW is the mobilization of mobile fines.

Tang and Morrow (1999) [39] studied the effect brine chemistry had on oil recovery and pointed out particularly that fine migration played an important role in their observations. They conducted cyclic waterflooding on different cores by incrementally reducing the salinity of the injected brine. By examining the effluent water after flooding a Berea sandstone core with x-ray, they discovered an amount of fines produced (mainly kaolinite). They also used Berea sandstone after fines had been stabilized by firing and acidizing. Recovery of crude oil was essentially independent of salinity in this core. In addition, Tang and Morrow flooded Bentheim and Clashach stones which contain much lower clay content than Berea sandstone. The increase in oil recovery as a function of decrease in salinity was less than for Berea sandstone and there was only observed a slight production of fines after flooding the Bentheim sandstone. In addition, LSW had no effect when refined oil was used rather than crude while all other conditions were held constant.

Tang and Morrow explained these observations through DLVO theory of colloids. When the salinity is reduced, the electrical double layer in the aqueous phase between particles is expanded and the tendency for stripping of fines is increased. Further, the release of fine particles may contribute to an increase in oil recovery due to (A) wettability alteration and (B) flow path, shown in figure 4.10.

In the first case (a), presence of high salinity brine causes clay to be undistributed and will retain their oil-wet nature which leads to an inferior displacement efficiency. The fine particles (mixed-wet) will then detach from the pore surface when contacted with low salinity water. When these clay particles are mobilized, the wettability will be altered towards more weakly water-wet conditions which is more optimal for the oil production [37, 57] (figure 4.10 b).

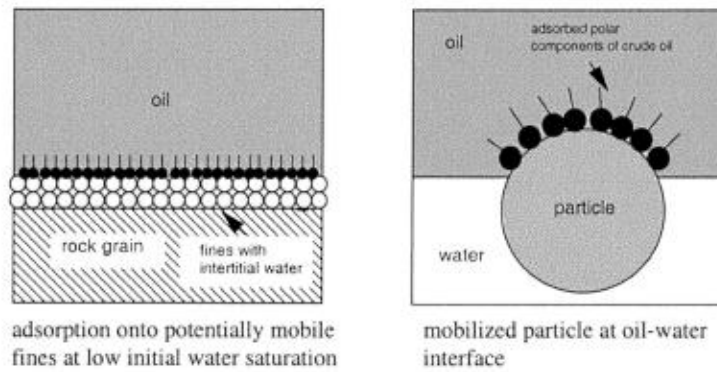
In addition, detachment of crude oil droplets that are attached to fines at pore walls with dilute brine injection will contribute to a further incremental in oil recovery (figure 4.10 c).

The second case (b) is related to reduction of permeability in pore channels. Tang and Morrow [39] observed a decrease in permeability when the injected low salinity (<1550 ppm) brine replaced the initially high salinity brine. It was suggested that particles follow the flow path and

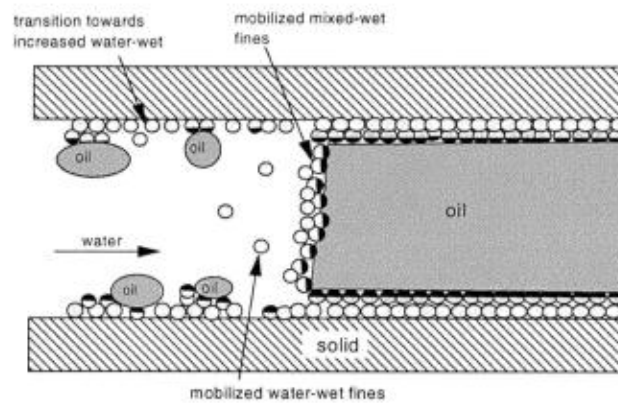
eventually block the pores, which leads to a diverted flow path to unswept zones. The result is an increase in oil recovery by the sweep of new zones.

Fine migration is seen as a contribution to enhance the production of oil, but not as the main mechanism. Contradictory results where additional oil recovery has been reported but no fines were observed has also been published [41, 42, 51].

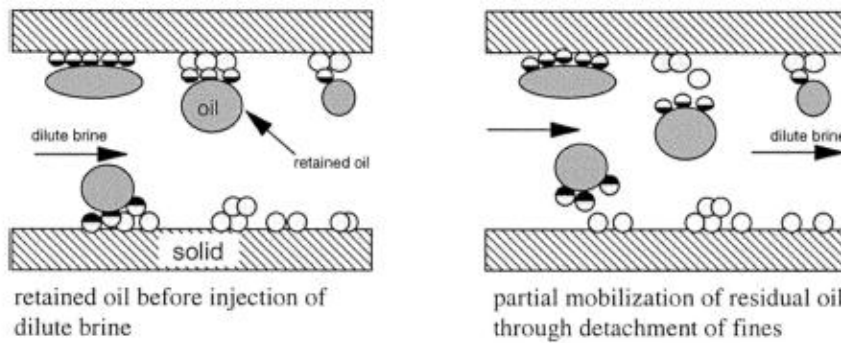
To observe the effect of fine migration with LSW it is evident that clay needs to be present and the amount and type of clay plays an important role.



a) Adsorption of polar components from crude oil to form mixed-wet fine.



b) Partial stripping of mixed-wet fines from pore walls during waterflooding.



c) Mobilization of trapped oil.

Figure 4.10

Role of potentially mobile fines by crude oil/brine/rock interactions as a function of reducing the brine salinity [39].

4.3.3 pH Variation

In numerous laboratory experiments, there has been observed a rise in pH in the effluent water during low salinity production [39, 48, 51].

This rise in pH is due to two concomitant reactions: carbonate dissolution and cation exchange.

Carbonate dissolution is represented by the chemical equilibrium;



The dissolution of carbonate (i.e. calcite and/or dolomite) results in an excess of hydroxide which induces an increase in pH, as illustrated by equation 4.2 and 4.3.

This reaction is relatively slow and depends on the carbonate content present in the rock.

Cation exchange has a much faster reaction time compared to carbonate dissolution and is an interaction between the clay surface and the liquid present. In this reaction, the mineral surface will substitute H^+ ions present in the liquid phase with cations previously adsorbed which will result in an increase in pH.

Tang and Morrow (1999) [39] observed an increase in pH of the effluent water by flooding Berea sandstone with low salinity brine. The same observation was reported by McGuire *et al.* (2005) [48] on North Slope field samples.

Austad *et al.* (2010) [58] investigated the chemical mechanism responsible for LSE in sandstone cores. At reservoir conditions, the pH of formation water was approximately 5 due to dissolved acidic gases like CO_2 and H_2S . At these pH conditions, Austad *et al.* suggested that clay minerals are adsorbed by acidic and protonated basic components from the crude oil, and cations

(favoring divalent ions, especially Ca^{2+}) from FW. Invading low salinity brine will create a local increase in pH were Ca^{2+} has been substituted by H^+ from the water. A fast reaction between OH^- and the adsorbed acidic and protonated basic material will cause desorption of organic material from the clay. The result is a more water-wet state of the rock surface which favors the production of oil. These reactions are illustrated in figure 4.11.

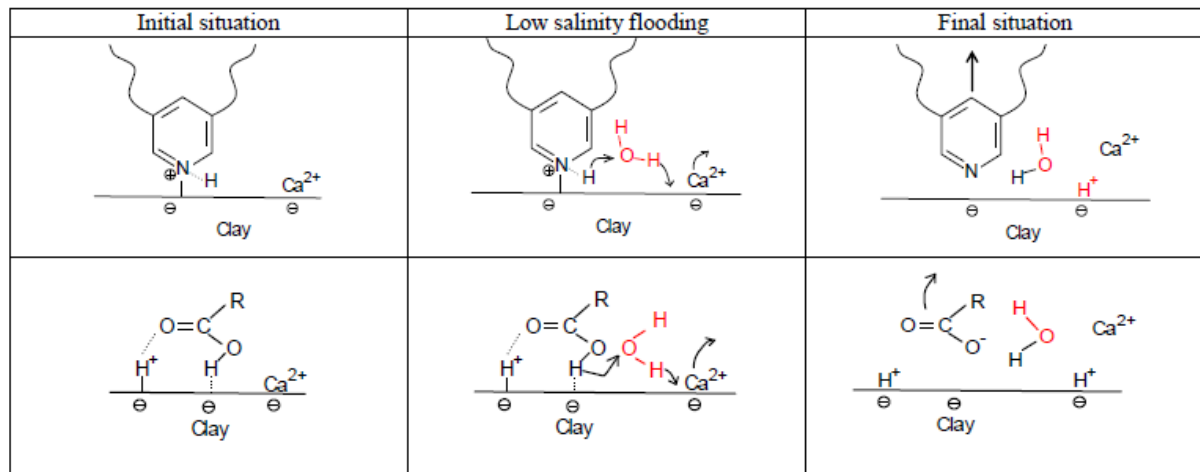


Figure 4.11 Proposed mechanism for low salinity EOR effect [58].
Upper: Desorption of basic material.
Lower: Desorption of acidic material.

McGuire *et al.* (2005) [48] suggested that low salinity flooding altered the pH to a more alkaline which generated in situ surfactants. When oil is in contact with an aqueous phase at high pH, the acidic and polar components in the oil is saponified which will reduce the interfacial tension between the oil and the brine, and in addition alter the wettability to more water-wet conditions.

However, conflicting evidence to McGuire *et al.* [48] suggestion of saponification has been published. In their suggestion, the type and amount of organic acid in the oil is essential for the saponification to occur. Ehrlich and Wygal (1997) [59] stated that an acid number (AN) of > 0.2 mg KOH/g is needed to generate enough in situ surfactant to alter the wettability and/or emulsion formation. One of the best LSW result obtained came from a North Sea reservoir (ca.

40.0% increase in oil recovery), which had crude oil with AN <0.05 [51]. In other cases, it has been observed that particularly when the initial pH is low, there is little change in pH and it does not reach the levels associated with either wettability-change or low IFT based on caustic flooding [60].

4.3.4 Multicomponent Ionic Exchange (MIE)

Multicomponent ionic exchange is based on the affinity each individual ion/molecule has to the mineral matrix. If the charged particles in the invading water has a higher affinity to the mineral surface it will exchange sites until equilibrium is reached. MIE is actually the basis for geochromatography.

Studies on MIE goes back to 1981 were Valocchi *et al.* [61] noticed that the concentration of magnesium and calcium in different control wells were lower than the invading water and connate brine.

Later, Lager *et al.* [51] analyzed the effluent water from a North Slope core by LSW. The injected brine had a lower salinity than the connate water. Results showed that the concentration of magnesium and calcium dropped lower than the concentration in the invading brine which indicated that the ions had been adsorbed by the rock matrix.

Supporting evidence of this mechanism having a significant impact on the oil recovery is supported by Nasralla *et al.* (2011) [28, 29, 31]. This group did an extended research on MIE and concluded that this mechanism was responsible for the improved oil recovery. After flooding Berea sandstone cores with low salinity brine, they observed a stabilized concentration of calcium (between connate and injected water) from the effluent water. This indicated that the mineral surface exchanged calcium with the invading sodium.

Multicomponent ion exchange has eight different possible mechanisms of organic matter adsorption onto clay matrix according to the extended DLVO theory by Amarson and Keil [62], and Sposito [63]. Lager *et al.* (2006) [51] concluded that out of these eight mechanisms, only four are strongly affected by cation exchange during a low salinity brine injection. Table 4.1 summarizes the eight mechanisms, but only cation exchange, ligand bonding and cation and water bridging is essential.

Table 4.1 Mechanisms of association between organic functional groups and mineral surface [63]. A Green line indicates the mechanism which is involved by low salinity flooding.

Mechanism	Organic functional group involved
<u>Cation exchange</u>	Amino, ring NH, heterocyclic N (aromatic ring)
Protonation	Amino, heterocyclic N, carbonyl, carboxylate
Anion exchange	Carboxylate
<u>Water bridging</u>	Amino, Carboxylate, carbonyl, alcoholic OH
<u>Cation bridging</u>	Carboxylate, amines, carbonyl, alcoholic OH
<u>Ligand exchange</u>	Carboxylate
Hydrogen bonding	Amino, carbonyl, carboxyl, phenolic OH
Van der Waals interaction	Uncharged organic units

These four possible mechanisms are represented in figure 4.12, and are defined:

-*Cation exchange* occurs when molecules containing quaternized nitrogen or heterocyclic ring replace exchangeable metal cations initially bound to clay surface [51].

-*Ligand bonding* is the direct bond formation between a multivalent cation and a carboxylate group. These bonds are stronger than cation bridging and cation exchange bonds and lead to detachment of organo-metallic complexes from clay surface [51].

-*Cation bridging* is a weak adsorption interaction between polar functional groups and exchangeable cations on the mineral surface [51].

-*Water bridging* will occur if exchangeable cation is strongly solvated (i.e magnesium). It involves water molecules solvating the exchangeable cation and the polar functional group of the organic molecule [51].

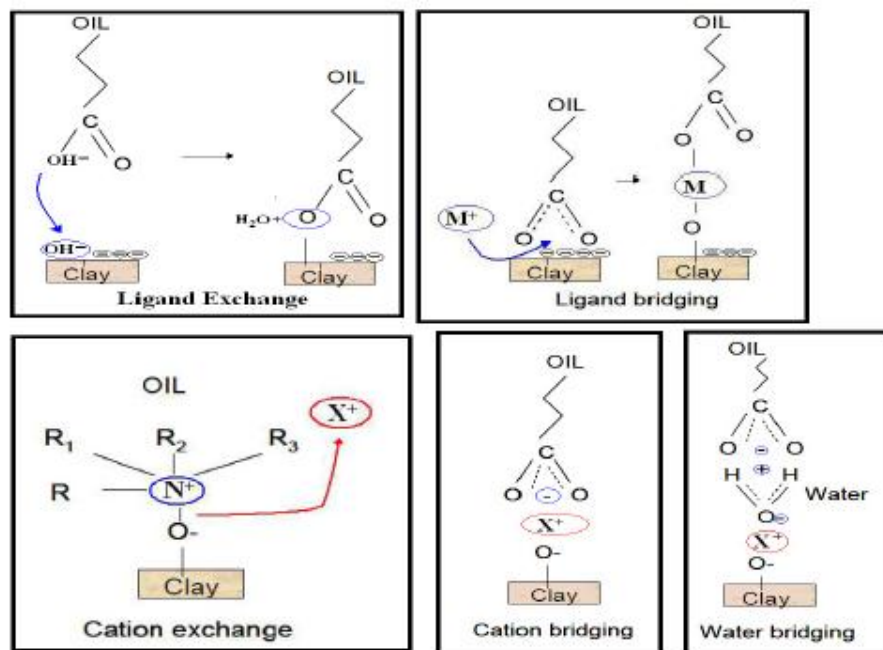


Figure 4.12 Representation of the diverse adhesion mechanisms occurring between clay surface and crude oil. Illustration taken from [64].

It is clear that the mechanisms underlying MIE has an impact on oil recovery by LSW. Lager *et al.* (2006) [51] suggested that when MIE takes place, organic polar compounds and organo-metallic complexes from the mineral surface are removed by replacing them with cations. Desorption of these polar compounds from the clay surface should lead to a more water-wet surface, which enhances the oil recovery.

4.3.5 Double Layer Expansion

It is believed that expansion of the double layer between the oil and clay surface has an important influence on reservoir wettability and hence microscopic sweep efficiency by LSW [22, 31, 65]. Clay minerals are negatively charged on surface due to imperfections in the crystal lattice and the pH range encountered in reservoirs [66].

Multivalent cations like magnesium and calcium act as bridging agents between the negatively charged oil and clay surface [51]. In presence of a sufficiently high salinity level, sufficient cations are available to screen-off their negative electrical charges with a decrease in the electrostatic repulsion as a result [65]. In addition, if the double layer becomes significantly small enough, then the crude oil can react with the clay surface and form an organo-metallic complex [67]. As a result, the clay becomes hydrophobic and a local oil-wet surface is created [68].

Ligthelm *et al.* (2009) [65] explained that when the invading salinity level is reduced significantly (especially multivalent cations), the screening potential will drop which yields an expansion of the electrical diffuse double layer that surrounds the clay and oil particle. This causes an increase in zeta potential and in turn yields an increase in the electrostatic repulsion between the clay and crude oil. It is believed that once the repulsive forces exceed the binding forces via the multivalent cation bridge, the oil particles may be desorbed from the clay surface which alters the wetting conditions to more water-wet.

They also pointed out from their coreflood results that it's not just the reduction of divalent cations which contribute to an expansion of the double layer and wettability modification, but also a substantial decrease in total ionic strength of the brine is essential.

This theory is illustrated in figure 4.13.

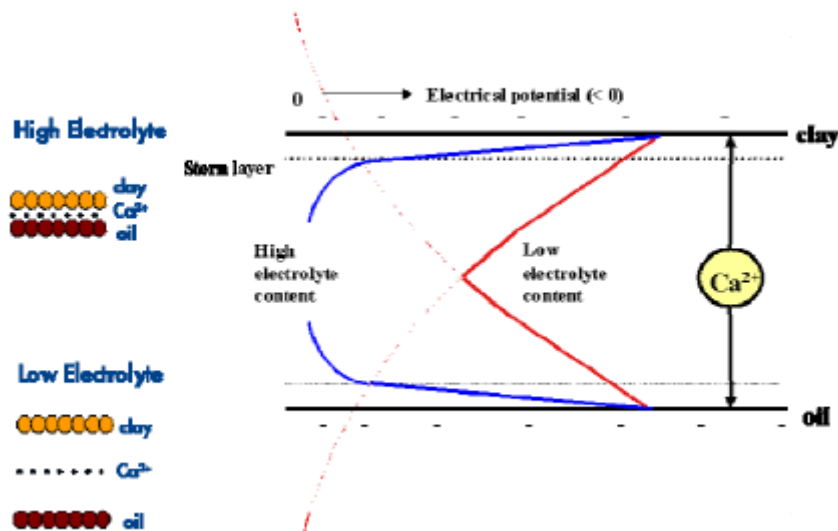


Figure 4.13 Representation of bonding between clay surface and oil in high- and low saline brine environment. The calcium ion represents the multivalent cation which acts as a bridge between clay and oil particles. Redrawn from [65].

Nasralla *et al.* (2012) [22] investigated the dominance of the electrical double layer expansion as a mechanism of improved oil recovery by LSW.

Important observations were highlighted in their publication, in summary:

- Zeta potential at the oil/brine and rock/brine interfaces was highly negative with low salinity water, and close to zero with seawater.

- Zeta potential between oil/brine and rock/brine became more negative as pH increased.

- A bigger fraction of mica surface became water-wet by low salinity water compared to high salinity water.

- Mica surface became less water-wet as pH of the low salinity water decreased.

These observations made by Nasralla *et al.* imply that pH and the salinity level has a strong influence on the double layer expansion which affects the wettability conditions.

4.4 Perception of LSW as an EOR Method

It's evident that low salinity waterflood can in some way or another enhance the production of oil. Only a part of the diverse literature on this subject has been presented in this chapter with empathize on the positive effects and the suggested mechanisms influencing the oil recovery. The COBR interactions encountered in the reservoirs are very complex and it's clear that it is not one prevailing mechanism responsible, but rather an interplay between all of them. The literature demonstrated in this thesis draws the attention to the wettability alteration being dominant. Many scientists support this theory with confidence and explains that the other mechanisms work to enhance the wettability shift, but other studies have proven an increase in oil recovery without witnessing any wettability alteration.

It is important to keep investigating the LSE since LSW can cause a significant increase in the production of oil. Although the dominant mechanism is still uncertain, one conclusion can be made which is not stressed enough in the literature, a negative effect with LSW by inhibiting the oil recovery has not been observed.

It is not efficient to perform a large scale waterflood by reducing the brine salinity of economic reasons if no incremental oil recovery is present. But the LSW has a high potential and the attention to this EOR method is increasing in the scientific community.

5 Experimental Equipment and Procedures

The experimental research performed in this master thesis was emphasized on the interfacial tension, zeta-potential and electrophoretic mobility generated through the surface interactions between the crude oils and brines. In addition, adhesion tests were conducted to observe wettability trends between crude oil/brine/quartz.

Three general categories of experimental equipment were used:

1. *Equipment to prepare the samples for further analysis.*

This equipment includes an ultrasonic bath to homogenize the emulsion generated between crude oil and brine, and a centrifuge to separate suspension by precipitation.

2. *Equipment to analyze fluid properties.*

A densitometer was used to measure the fluid density, a pH-meter to record the pH, bond elute to separate saturated, aromatics and resins in the crude oils and automatic titrator to measure the total acid number in the crude oils.

3. *Equipment to perform the experimental work.*

This includes a micrometer syringe to measure IFT, nanosizer for electrophoretic mobility and zeta potential measurements and goniometer to measure contact angles.

5.1 Chemicals and Fluids

In this subchapter the fluid properties are listed for all the brines and crude oils.

5.1.1 Brines

SSW, HS water and LS water were used in interfacial tension, electrophoresis and adhesion measurements.

In addition, brines containing single electrolytes dissolved in low salinity water were prepared to compare the impact of each individual ion on these measurements.

Synthetic seawater was prepared based on a recipe generalized by the amount of salts in seawater. These salts were sodium, potassium, magnesium and calcium as chloride salts and sulfate and bicarbonate as sodium salts. Distilled water was mixed with the salts and set on a magnetic stirrer for two hours. SSW had an ionic concentration of 42665 ppm.

High salinity water was prepared in the same manner as SSW. The main difference between these two brines is the concentration of magnesium and calcium as well as the HS water did not contain carbonate or bicarbonate. HS water had an ionic concentration of 35267 ppm.

Low salinity water contains <4000 ppm TDS [43]. The LS water was made by dissolving sodium chloride in distilled water to a concentration of 3000 ppm and set on magnetic stirrer for two hours.

Brines containing 10, 50 or 100 ppm Ca^{2+} , CO_3^{2-} , Mg^{2+} , SO_4^{2-} , PO_4^{3-} or $\text{B}_4\text{O}_7^{2-}$ were made by mixing the corresponding salts and distilled water, and set on a magnetic stirrer for two hours.

The ionic strength of the solutions with a single electrolyte was in the interval;

$$[(\text{Solvent}(\text{ppm})), (\text{Solvent}(\text{ppm}) + 100 \text{ ppm } \text{Mg}^{2+})]$$

The max range in the interval was due to 100 ppm magnesium was the solution with the highest concentration.

0.1 M hydrochloric acid and 0.1 M sodium hydroxide was used to adjust the pH of the brines in all cases it was altered.

For a more detailed list of the brines recipe and concentrations, see appendix A.1

5.1.2 Crude Oils

Two crude oils named A-12 and Exp-12 were supplied by Arne Skauge at Centre of Integrated Petroleum Research (CIPR). Both A-12 and Exp-12 came from Heidrun, a field in the North Sea operated by Statoil, but were produced from two different wells. Exp-12 was diluted with 20% xylene and 20% iododecane to reduce the viscosity. Physical and chemical properties of the oils are listed in chapter 6.1.

In the following, the mixture of 60% Exp-12, 20% iododecane and 20% xylene is termed as Exp-12_{x&i}.

5.2 Equipment for Sample Preparation

5.2.1 Ultrasonic Bath

Introduction

To measure the electrophoretic mobility of oil droplets dispersed in brine (or distilled water), an ultrasonic bath was used to generate the micro emulsion.

When ultrasonic waves are sent through the solution, large oil droplets originally formed from the instability between oil/water interface are disintegrated into smaller ones by cavitation until stable droplet size is reached, a critical size characteristic of the particular oil/water system [69].



Figure 5.1 Ultrasonic bath, Sonorex Super RK 102 H from Bandelin.

Materials

All samples which were needed to emulsify in order to experimental determine the zeta-potential and electrophoretic mobility.

Experimental method

The ultrasonic bath was filled with distilled water and set to 25.0°C.

After the temperature was reached, the sample was transferred to a glass container and submerged in the water for 5 minutes.

Errors

The zeta-potential and thus electrophoretic mobility measured from the micro emulsions generated by the ultrasonic bath will not be consistent if the emulsion is not homogenous.

After many trials it was proven that the most homogenous emulsion were created by shaking the sample well in advance.

Washing procedure

Normal cleaning detergents were used to wash the glass tubes, then flushed with distilled water and finally dried in an oven at approximately 80.0°C.

5.2.2 Centrifuge

A universal 320R centrifuge from Hettich Zentrifugen was used to separate suspension samples between –pentane and asphaltenes for further analysis.



Figure 5.2 A universal 320R centrifuge from Hettich Zentrifugen .

5.3 Equipment for Fluid Analysis

5.3.1 pH-Meter

Introduction

The pH was measured with a Hach-Lange pH-meter with a glass electrode from Nerliens Mezansky AS. The electrode is an ion-sensitive field-effect transistor (ISFET) probe.

The pH is determined by the ion concentration in the solution (such as H_3O^+ or OH^- ions). When the ion concentration is changed, the current through the transistor will change accordingly [70].



Figure 5.3 Hach-Lange pH-meter with a glass electrode.

Materials

The pH was measured for different brines and emulsions.

Experimental method

The electrode was submerged in the sample and held steady until a constant pH value was recorded.

Errors

There are two important errors which limit the accuracy of pH measurements by using glass electrode [70].

1. A pH measurement cannot be more accurate than the standards used, which are typically ± 0.01 pH unit.
2. There exists a junction potential at the porous plug near the bottom of the electrode. If the ionic composition of the analyte solution is different from the standard buffer, the junction potential will change and the effect gives an uncertainty of at least ~ 0.01 pH unit.

Washing procedure

The probe was washed immediately with distilled water after each measurement.

When measuring pH of crude oil/brine emulsions, the probe was washed with ethanol and then distilled water.

5.3.2 Densitometer

Introduction

For an accurate measurement of fluid densities an Anton Paar DMA60 densitometer with a 602 cell was used. This instrument can measure at temperatures ranging from -200.0°C to +150.0°C, where the temperature is controlled by an external water bath connected to the densitometer.

The DMA60 densitometer measures density based on the law of oscillation. The fluid is injected into a vibrating U-shaped tube (1 mL) where an electromagnet unit forces harmonic waves through the fluid which makes the wave period dependent of the density.

The density, ρ , is defined as the mass, m , of a substance divided by its volume, V :

$$\rho = \frac{m}{V} \quad (5.1)$$

The density of a fluid increases as the temperature decreases and the pressure increases [71]

The density of a fluid, ρ_{fluid} , can be expressed as a function of its period, T_{fluid} , as expressed by equation 5.2.

$$\rho_{fluid} = \frac{1}{A} \cdot (T_{fluid}^2 - T_{water}^2) - \rho_{water} \quad (5.2)$$

Where T_{water} and ρ_{water} are the reference points of deionized water and, A , is the apparatus constant.



Figure 5.4

Anton Paar DMA60 densitometer.

Materials

The density was measured for crude oil A-12 and Exp-12_{x&i} and all brines used through the experimental work in this master thesis.

Experimental method

The densitometer has to be calibrated at the same temperature as the fluids shall be measured at. All fluid densities were measured at 22.5°C.

It is important that the densitometer holds a firmly stabilized temperature before it is calibrated. The instrument was calibrated by measuring the periods (T_{water} and T_{air}) of two known fluids (deionized water and air at 25.0°C). By the use of equation 5.3, the instrument constant, A , was calculated.

$$A = \frac{(T_{\text{air}}^2 - T_{\text{water}}^2)}{(\rho_{\text{air}} - \rho_{\text{water}})} \quad (5.3)$$

After calibration, the fluid was injected into the densitometer with a syringe in the bottom opening. To fill the test tube properly, it is important to keep pushing the syringe stamp slowly until fluid comes in return from the top opening. The syringe was left in the bottom opening while the densitometer constantly measured the fluids period. The measurements continued until the period stabilized (altered less than $\pm 10^{-5}$).

Errors

The largest deviation from the true density is in range of $\pm 10^{-4}$ g/cm³.

It is also important to prevent air bubbles from settling in between the test tube and fluid. This is easily detected by non-stabilizing periods.

Washing procedure

Two washing procedures were used, depending on the fluid.

Aqueous sample: The test tube was cleaned with ethanol, distilled water and finally air dried.

Oil sample: The test tube was washed in the sequence: toluene, acetone, distilled water and then air dried.

5.4 Experimental Apparatus and Equipment

5.4.1 Drop Volume Method

Introduction

To investigate the effect of altering pH and the type and concentration of different brines on the interface between oil and brine, the interfacial tension was measured by the drop volume method. The IFT was measured either at first contact between crude oil and brine or after an amount of time in contact. Since the pH can alter with time, the measurements were conducted immediately after the pH in the brine phase was determined.

There are many ways to measure the interfacial tension between oil and brine, but only the drop volume method was used in this study.

The IFT is determined by squeezing out crude oil from the syringe and record the volume which eventually detaches from the needle tip (oil droplets).

This is a direct consequence of the interfacial tension which is dependent on the gravitational force, buoyancy force, and the radius of the needle tip, and is the basic principle behind the drop volume method, expressed by equation 5.4.

$$\sigma = \frac{\Delta V \cdot \Delta \rho \cdot g}{2\pi \cdot r \cdot F_c} \quad (5.4)$$

Where:

- σ is the interfacial tension, mN/m.

- g is the gravitational force, 9.80665 m/s².

- ΔV is the average volume oil squeezed out from the needle tip, m³.

- $\Delta \rho$ is the buoyancy force, $\Delta \rho_{\text{brine}} - \Delta \rho_{\text{oil}}$, kg/m³.

- r is the radius of the needle tip, m.

F_c is a dimensionless correlation factor that accounts primarily for liquid retained on the needle tip after detachment [1] and is a function of (V/r^3) . F_c is expressed by equation 5.5.

$$F_c = 0.14782 + 0.27896 \left(\frac{r}{V^{1/3}} \right) - 0.1662 \left(\frac{r}{V^{1/3}} \right)^2 \quad (5.5)$$

Harkins and Browns [72] showed that the correlation factor is most accurate when

$$0.6 < \left(\frac{r}{V^{1/3}} \right) < 1.0.$$

The method is very simple due to accurate measurement of only length and mass is required [73].

The probable error of the mean value is in range of ~ 0.01 mN/m [73, 74].



Figure 5.5 Micrometer syringe from Burkard (to the right) used to measure the interfacial tension. The inverted needle is also shown.

Materials

The interfacial tension was measured for different systems. Two crude oils were used, A-12 and Exp-12_{x&i}. The brines were SSW, HS water and LS water, and brines containing 10, 50 and 100 ppm Ca^{2+} , CO_3^{2-} , Mg^{2+} , SO_4^{2-} , PO_4^{3-} or $\text{B}_4\text{O}_7^{2-}$. The IFT was also measured after Exp-12_{x&i} had been in contact with the brine phase for fixed time to compare the IFT generated between a more equilibrated than non-equilibrated system. Exp-12_{x&i} had been in contact with the magnesium solutions for 11 days, and borate and LS water for 14 days.

For comprehensive information of the brines and the measurements see appendix A.5 .

Experimental method

A micrometer syringe with an inverted needle was used to determine the drop volumes. All measurements were conducted at ambient temperature.

To calculate the IFT between crude oil and brine, two calibrations were first needed.

Calibration with distilled water:

Distilled water was used to determine the slope between mass fluid released from the needle per millimeter squeezed from the syringe stamp. The slope was calculated by pushing out ten drops distilled water and measuring the total weight. Three parallels were performed.

Calibration with decane and water:

A fluid with a known IFT with distilled water can be used to calculate the radius of the syringe needle and thus F_c . Decane was used in all calibrations.

The calculation was done by:

1. Determined rF_c from equation 5.4 (assume $F_c=1$). The IFT between decane and deionized water used was 51.00 mN/m. IFT values of ± 51.00 mN/m has also been

reported at 25.0°C, for instance 50.50 mN/m from Harley Y. Jennings, Jr. [75] and 51.98 mN/m by Z. Susana, R. Jhosgre, and A.L. López de Ramos [76].

2. Inserted r value obtained from equation 5.4, into equation 5.5, and solved for F_c .
 3. Inserted the F_c value obtained from equation 5.5, into equation 5.4, and solved for r .
- The rest of the parameters were known.

To measure the oil drop volume, the following procedure was followed:

80% of the oil drop volume was squeezed out at a moderate speed from the capillary needle tube. The oil drop was held in the brine phase for 30 seconds for equilibration, before the rest of the drop was pushed out. It is important to slowly squeeze the rest out, otherwise the volume will not be reliable. The Volume of the oil droplets is read from the micrometer syringe once the oil has detached from the capillary needle tip.

Errors

The relative uncertainty of the IFT measurements was calculated to 5% based on equation A.1.4.

Errors will occur if some objectives are not satisfied [18];

When squeezing out oil, the needle tip needs to be horizontal in the water phase, if not the oil drop will be misshaped and thus not maintain its oval figure which is essential.

When alkalinity of the brine phase is significantly too high, oil droplets will be misshaped and detach from the needle tip before equilibration is reached. This is a consequence of dramatic reduction in the IFT. To compensate for this error, the inverted needle can be replaced with another needle which has a smaller radius to increase the drop volume.

It is very important that the inverted needle tip has been cleaned in a reliable manner (which is described below) so it maintains its hydrophilic character.

If the needle tip is tainted with some organic impurities, it will adapt to a more hydrophobic character which will make the measurements unreliable, as illustrated in shown figure 5.6.

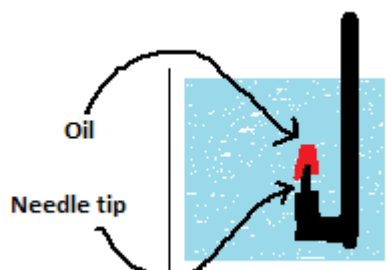


Figure 5.6 Schematic illustration of a needle tip contaminated with organic impurities.
The red drop represents the oil which is wetting the needle tip. This contributes to an increased volume of oil measured.

Washing procedure

The syringe was washed inside first with toluene, followed by methanol and finally distilled water. To protect the needle tip from organic impurities, it was submerged in ~3.0 wt% sodasil and thereafter in hot water (~90.0°C) for 5 minutes. The equipment was then blown dry. This cycle was repeated for every new measurement.

5.4.2 Nanosizer

Introduction

Zetasizer nano ZS from Malvern was used to measure the zeta-potential and thus the electrophoretic mobility of crude oil dispersed in brine or water.

When an electric field is applied across charged particles, the particles suspended in the solvent are attracted towards the electrode of opposite charge. Viscous forces will act opposite to this movement of the particle, but when equilibrium is reached between these two opposite forces, the particle will move with constant velocity. The velocity that the particle reaches is defined as the electrophoretic mobility.

The zetasizer nano instrument calculates the electrophoretic mobility by applying the Henry equation, equation 5.6, to determine the zeta-potential.

$$U_E = \frac{2\varepsilon Z f(\kappa a)}{3\eta} \quad (5.6)$$

Where:

- U_E is the electrophoretic mobility, $\mu\text{mcm/Vs}$.

- ε is the dielectric constant.

- Z is the zeta-potential, mV.

- $f(\kappa a)$ is Henry's function.

- η is the viscosity, cP.

The electrophoretic mobility is measured by filling electrolyte and dispersant in a cell with electrodes at both ends to which a potential is applied. Particles move towards the electrode of

opposite charge and the technique used to measure this velocity is called Laser Doppler Velocimetry (LDV). LDV is based on light scattering combined with a reference beam. When the light is sent through the cell with the sample, the light is scattered, which produces a fluctuating intensity signal where the rate of fluctuation is proportional to the speed of the particle. A digital signal processor is used to extract the characteristic frequencies in the scattered light.

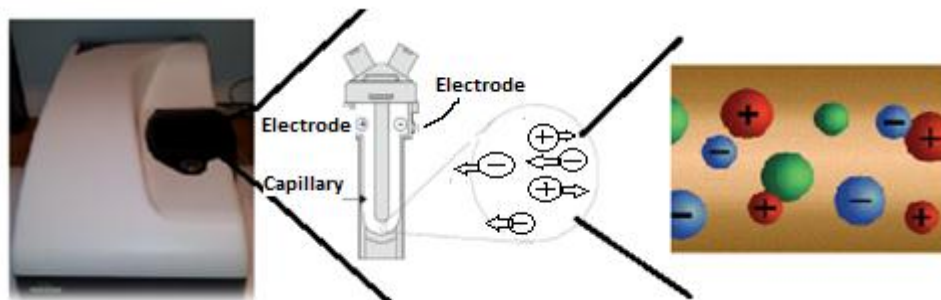


Figure 5.7 Picture of Zetasizer nano ZS from Malvern displayed to the left. Illustration of the movement of charged particles in an electrolyte solution under an applied electric field in the measuring cell is shown to the right. The charged particles will move to the opposite charged side [17].

Materials

The zeta potential and electrophoretic mobility was measured for crude oil A-12 and Exp-12_{x&i}. The brines used was SSW, HS water, LS water, and brines containing 10,50 or 100 ppm Ca^{2+} , CO_3^{2-} , Mg^{2+} , SO_4^{2-} , PO_4^{3-} , $\text{B}_4\text{O}_7^{2-}$. Solutions of $6.61 \cdot 10^{-8}$ mole/kg of Ca^{2+} , CO_3^{2-} , Mg^{2+} , SO_4^{2-} , PO_4^{3-} and $\text{B}_4\text{O}_7^{2-}$ were made to compare the electrophoretic mobility and zeta potential generated between the different ions.

For comprehensive information of the brines and the measurements see appendix A.4.

Experimental method

The procedure used had been written by Anders Ekberg Nymark [77]. Some changes were made on his approach to optimize the results.

To a small glass container, 10.0 mL brine or distilled water and 5.0 μL crude oil was mixed and submerged in an ultrasonic bath for 5 minutes to generate a micro emulsion.

The sample was then immediately injected slowly into the polystyrene cell with a syringe to prevent trapping air bubbles, and thereafter inserted in the nanosizer. The software was programed to continuously take a measurement every 3 minutes for 20-30 minutes, depending on the emulsion stability.

The nanosizer software was configured manually instead of using standard operational procedure (SOP) to optimize the performance with these configurations:

- *Sample*: Polystyrene latex cell.
- *Dispersant*: Temperature on 25.0°C. Viscosity on 0.8872 CP. RI – 1.330.
- *Temperature*: 25.0°C and equilibrium time: 120 sec.
- *Model*: Henry's function ($f(\kappa a)$) in equation 5.6 can either follow a Smoluchowski or Huckel approximation. In all measurements performed, the Smoluchowski approximation was used since the electrophoretic determination of zeta-potential was from an aqueous media with moderate electrolyte concentration.
- *Cell*: Clear disposable zeta cell.
- *Measurements*: minimum 10, maximum 100.

The zetasizer nano instrument was programmed such that so each obtained result consisted of an average of 10-100 continuous measurements, depending on the standard deviation. Each result presented in chapter 6.2 is an average of two or three parallels which means that the reported results consist of a large underlying database of measurements.

After measuring the electrophoretic mobility of crude oil A-12 in 1/22 HS water and 1/22 SSW, it was concluded that these results were not consistent since they proved no trend, just

fluctuations as seen in figure 5.8 and 5.9. It was found that the reason for these unreliable measurements came from the emulsions generated by the ultrasonic bath which were not homogeneous enough.

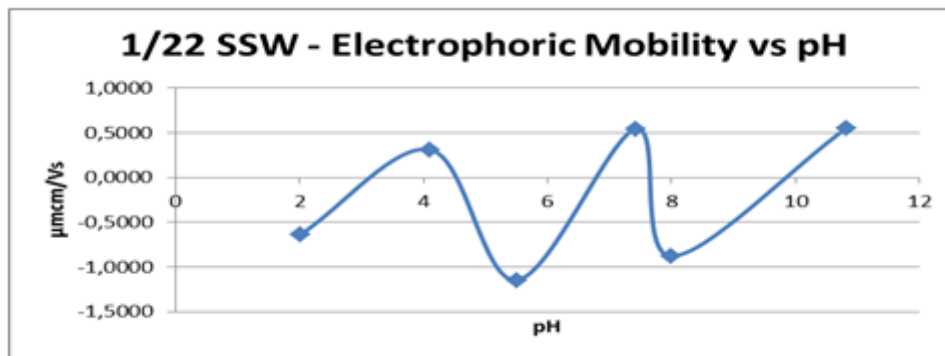


Figure 5.8 Electrophoretic mobility of 5.0 μL crude oil A-12 in 10.0 mL 1/22 SSW. pH ranging from 2-11.

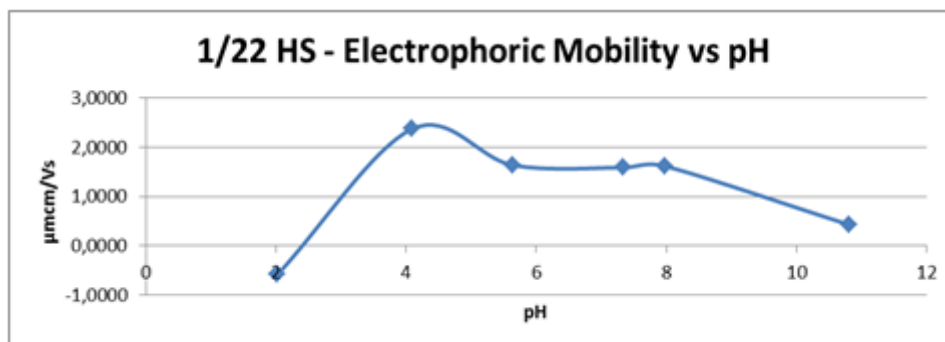


Figure 5.9 Electrophoretic mobility of 5.0 μL crude oil A-12 in 10.0 mL 1/22 HS water. pH ranging from 2-11.

The problem was solved by shaking the sample in the glass container before generating the emulsion. This is presented in figure A.4.2, A.4.3 and A.4.4 which shows a consistent trend.

Errors

The reproducibility of the measurements was dependent on different factors.

The direction of the crude oil particles and the size of the dispersed oil droplets are uncertain, but the parameter which significantly affected the reproducibility was the time. As a micro emulsion is generated, the system will be unstable and tend to separate. Thus, it was very important to create a consistent procedure and follow it on every measurement.

Since these factors may have affected the measurements to some degree, it was of interest to examine trends by internal variation instead of each single result.

It is important to make sure that no air bubbles are trapped in the measuring cell after injecting the sample. To prevent this, the cell has to be turned upside down and sample injected upwards (against gravity) until the sample reaches halfway, then the cell must be turned over again and slowly filled until it overflows.

Washing procedure

The polystyrene cell was cleaned first with ethanol, followed by distilled water and finally air dried.

5.4.3 Adhesion Map

Introduction

In this study, adhesion map was used to build a systematic map to observe whether crude oil would adhere to brine-covered glass (smooth quartz) when pH and brine concentration were altered.

Different qualitative and quantitative methods are used to determine the wettability of a system. These methods include contact angles, imbibition and forced displacement (Amott), USBM wettability etc. [78]. In this experiment, only contact angles were measured.

A contact angle goniometer with a telescope was used to measure the contact angles between the crude oil and brines.

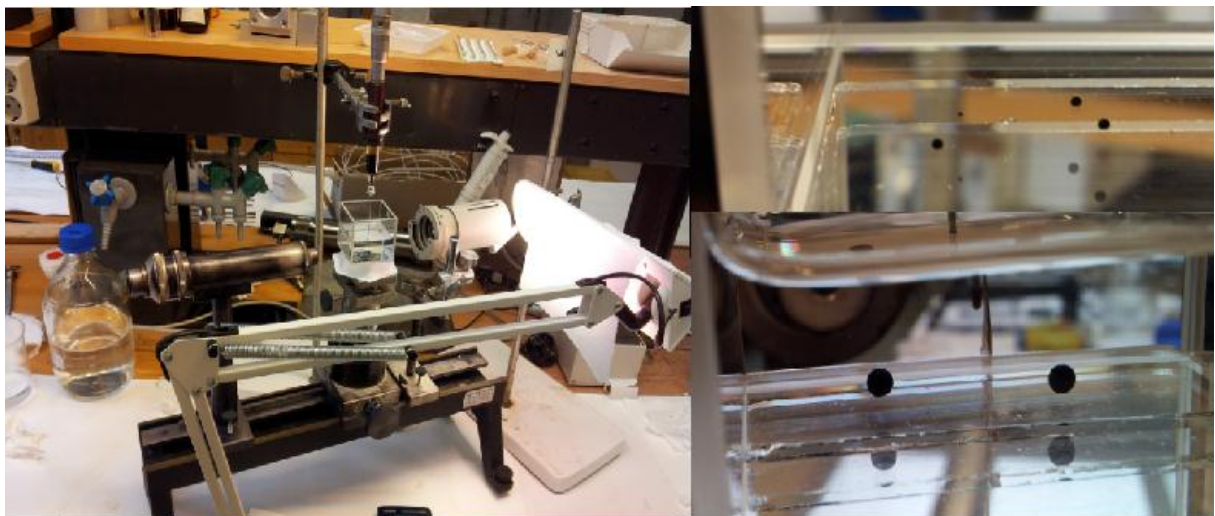


Figure 5.10 From left (a): Goniometer to measure the contact angles.
From upper right (b): Temporary adhesion.
From lower right (c): adhesion of crude oil onto glass surface.

Materials

The substances used for measuring the contact angles were between crude Oil A-12 and SSW, HS water and LS water.

Experimental method

The adhesion of crude oil was measured on glass surface in the presence of a brine phase at pH 2/4/6/8.5/10/12 and concentration of 100.00%/50.00%/10.00%/6,67%/4,55%/0.00% (distilled water).

All measurements were conducted at room temperature (22.5-25.0°C).

The glass and brine had been left in a cuvette with the measuring pH for three hours to equalize the hydroxide functional groups (see section 3.2.3) before the adhesion test.

A micrometer syringe was used to squeeze out one drop of crude oil onto the glass surface where it was left for 5 minutes before the needle was gently removed out to see whether it would adhere.

Distinguished between three possible outcomes:

- Adhesion: The oil drop releases from the needle tip and adheres to the glass surface, see figure 5.10 (b).
- Temporary adhesion: The oil drop is partly attached to the needle tip and to the glass surface. Once the needle is slowly pulled out, the oil drop detaches from the glass surface. This system differs from non-adhesion by a small drop remaining adhered to the glass surface after the majority has been released, see figure 5.10 (c).
- Non-adhesion: The oil drop does not adhere to the glass surface and remains attached to the needle tip.

Minimum three oil droplets were tested at different spots at each glass surface.

The contact angle was measured through a telescope in which the maximum error was set to $\pm 10.0^\circ$.

Errors

When the brine phase reaches a certain alkalinity, it will ionize possible polar groups (carboxylic groups) in the oil which makes it more hydrophilic. This results in an IFT so low that the oil will flow out from the needle tip as a thin film when it is in contact with the brine. This was observed from crude oil A-12 at pH 12.

Magnesium hydroxide will precipitate, depending on the alkalinity and magnesium concentration.

Washing procedure

The glass surface was washed with zalo (washing detergent), followed by distilled water and finally left to be air dried.

5.4.4 SARA-Analysis and Determination of TAN

Introduction

The total acid number (TAN) is a measure of how much KOH (potassium hydroxide) is required to neutralize one gram of oil [79]. The total acid number is given in mg KOH/g oil and is determined by acid/base titration. Once the equivalence point is found, equation 5.7 is used to calculate TAN.

$$TAN = \frac{(C_{KOH} \cdot EQP - B) \cdot Mm_{KOH}}{m_{oil}} \quad (5.7)$$

Where:

- C_{KOH} is the concentration of the titrant, mol/L.
- EQP is the equivalence point, mL KOH.
- B is the blank value of the solvent, mmol.
- Mm_{KOH} is the molar mass of KOH, g/mol.
- m_{oil} is the mass of the oil, g.

SARA-fractionation is a method which separates crude oil into Saturated, Aromatic, Resins (polar) and Asphaltene compounds. Saturated, aromatics and resins is chromatographically separated as different solvents flow through the column, each component is adsorbed to a greater or lesser extent depending on their chemical nature which is the fundamentals behind the separation. Asphaltene content is determined by precipitation [21].

Materials

Crude oil A-12, Exp-12 and Exp-12_{x&i} was analyzed through SARA-fractionation and TAN method.

Experimental method

All measurements were conducted at room temperature (22.5-25.0°C).

Determination of TAN

For the TAN analysis, some of the guidelines developed by Yu Bian, a student at Rice University in Houston were used [80].

A blank value was determined for the solvent system.

The electrode (DGI113-SC) on the automatic titrator (Mettler Toledo TSO) was calibrated using buffers of pH 4.00±0.02, 7.00±0.02 and 11.00±0.05. The titrant used was 0.05 M KOH in iso-propanol and was standardized by using potassium hydrogen phthalate.

1-2 g of the crude oil A-12, Exp-12 and Exp-12_{x&i} were first dissolved in 40 mL of 50.0/49.5/0.5 (v/v) mixture of toluene/2-propanol/deionized-water. The samples were transferred to the automatic titrator and stirred for 2 minutes. The titration curves used to identify the TAN of the crude oils were found as mL titrant against signal from electrode in mV.

Each oil sample was tested with parallels of two.

SARA-Fractionation

The SARA-analysis was divided into two parts, asphaltene precipitation and quantitative chromatographic determination of saturated, aromatic, resins content.

The NIGOGA guide [81] was used for asphaltene precipitation.

0.5 g of crude oil A-12, Exp-12 and Exp-12_{x&i} was dissolved in 3 μL of 93/7 (v/v) dichloromethane/methanol and added 15.2 g pentane. The solutions were set in ultrasonic bath for 10 minutes to release the asphaltenes from the tube walls. The samples were stored for 24 hours in a dark room at ambient temperature. The samples were further centrifuged for 10 minutes at 3000 rpm. The excess solvent was extracted out, and then the precipitated asphaltenes were washed with 5 mL pentane and centrifuged again. This washing cycle was

repeated until the excess pentane was colorless. The amount of asphaltene was determined when the weight recorded was constant on a microbalance in pre-weighted vials.

The experimental procedure used to chromatographic determine the amount of saturated, aromatic and resins content in the crude oils had previously been performed by Linda Kristine Moen [82]. The chromatographic column used was bond elute with silica as the bonded phase. The silica-column was cleaned with total of 3 mL hexane, added in 1 mL portions.

100 mg of the crude oils were solved in 1 mL hexane and added to the column.

The aliphatic fraction was eluted with 2 x 1 mL hexane, aromatic fraction with 2 x 1 mL DCM (Dichloromethane)/hexane (10/90) and the polar fraction with 2 x 1 mL DCM/MeOH (50/50).

Each fraction was collected in a separated glass container which had previously been weighted.

To determine the amount of each compound, 5 μ L of each fraction was injected onto a micro-weight by a Hamilton syringe. The amount of residual fraction was recorded when the solvent had evaporated, which was observed when the weight was constant (after 15-20 minutes).

Each fraction in each crude oil sample was weighted with parallels of two.

Errors

The uncertainty of measuring the amount of saturated, aromatic and resins in the crude oils was set to 2% [82].

Washing procedure

The electrode on the automatic titrator was washed with toluene and then rinsed with distilled water.

6 Main Results and Discussion

In this chapter, all the results obtained and observations from the experimental work will be presented and discussed. The objective in this study was to investigate which effect individual ions, ion concentration and pH, in relationship, had on IFT and zeta-potential with crude oil. Adhesion tests of crude oil A-12 onto smooth quartz surface in brine solution were also investigated. A comparison to previous studies in the literature will be a part of the discussion.

This chapter is structured by first presenting the SARA-analyses results without any further discussion because these results are included in the electrophoresis and interfacial tension discussion.

The second and third part consists of the electrophoresis and IFT results which will be presented and discussed.

In the end, the adhesion results of crude oil A-12 in brines will be listed.

6.1 SARA-Analyses

Total acid number was determined by acid/base titration, asphaltene content by precipitation and saturated, aromatic and resin content by chromatography. The crude oils were A-12, Exp-12 and Exp-12_{x&i}.

All relevant data to calculate the results is shown in appendix A.4.

Table 6.1 lists the total acid number obtained from the different oils. It is observed that both crude oil A-12 and Exp-12 has a high acidic content. Exp-12_{x&i} has 60% of the total acid amount as Exp-12, which was expected since adding 20% xylene and 20% iododecane will dilute the oil.

Table 6.1 Total acid number in crude oil A-12, Exp-12 and Exp-12_{x&i}.

Oil	TAN [mg KOH/g]
A-12	3.84±0.01
Exp-12 _{x&i}	1.68±0.01
Exp-12	2.83±0.01

Table 6.2 shows the asphaltene content obtained in the oils. Crude oil A-12 contains half of the amount as Exp-12. The asphaltene content in Exp-12_{x&i} was not 60% of Exp-12 (55.6%) which may have been caused by a small solvating effect of xylene and iododecane.

Table 6.2 Asphaltene content in the oils.

Oil	[mg/g]
A-12	33.2±1.7
Exp-12 _{x&i}	38.5±1.9
Exp-12	67.5±2

The amount of saturated, aromatic and resins obtained from chromatography separation is presented in table 6.3.

Table 6.3 Saturated, aromatic and resins content in the oils.

Component	A-12 [mg/g]	Exp-12 _{x&i} [mg/g]	Exp-12 [mg/g]
Aliphatic	704±14	598±12	692.6±14
Aromatic	110.6±2.2	80.5±1.6	115.8±2.3
Polar	134.8±3	73.4±1.5	67.6±1.4

Theoretically, the sum of asphaltene, saturated, aromatic and resin content in the oils will add up to 1 gram since in total 1 gram is used. In practice, when weighing the constituents, some of the oil will evaporate with the solvent and thus reduce the total content.

6.2 Electrophoresis

The effect of pH, electrolyte concentration and ion-valence on the crude oil/brine interface was investigated through electrophoresis measurements at 25°C. The net charge of the crude oil/brine interface is a function of the aqueous pH through ionization of acidic and basic species in the oil phase, and electrolytes by screening the charged constituents. This was explained in chapter 3.

As mentioned in section 5.4.2, all result listed in this chapter consist of a large database of measurements. Three parallels were taken for each measurement, but only two replications are presented when the third was an outlier.

Results

Electrophoretic mobility is linearly dependent on the zeta-potential as shown in equation 5.6. Thus, only the zeta-potential is presented in this chapter and the electrophoretic mobility is listed in appendix A.4 with all tables showing the results with standard deviation and pH measurements of the crude oil/brine systems.

Section 6.2.1 presents the zeta-potential results for crude oil A-12 in diluted SSW, HS water and LS water. Further, in section 6.2.2 the generated potential between dispersed crude oil Exp-12_{x&i} in LS water containing electrolytes of 10, 50 or 100 ppm Ca^{2+} , Mg^{2+} , CO_3^{2-} , SO_4^{2-} , $\text{B}_4\text{O}_7^{2-}$ or PO_4^{3-} is shown. Finally, section 6.2.3 covers the results obtained for emulsified droplets of crude oil Exp-12_{x&i} in LS water containing a constant electrolyte concentration of $6.61 \cdot 10^{-8}$ mole/kg Ca^{2+} , Mg^{2+} , CO_3^{2-} , SO_4^{2-} , $\text{B}_4\text{O}_7^{2-}$ or PO_4^{3-} at pH 4.0 and 9.0.

6.2.1 Dispersed Crude Oil A-12 in Diluted SSW, HS Water and LS Water

Figure 6.1 presents the zeta-potential generated between emulsified droplets of crude oil A-12 in 2.3% SSW and 2.3% HS water, and 50% LS water as a function of the brines pH. The pH was varied from 2.00-11.00, but as the micro emulsion was generated, the pH changed through acid/base reactions, as shown in table A.4.3. The zeta-potential was recorded as a function of the stabilized pH.

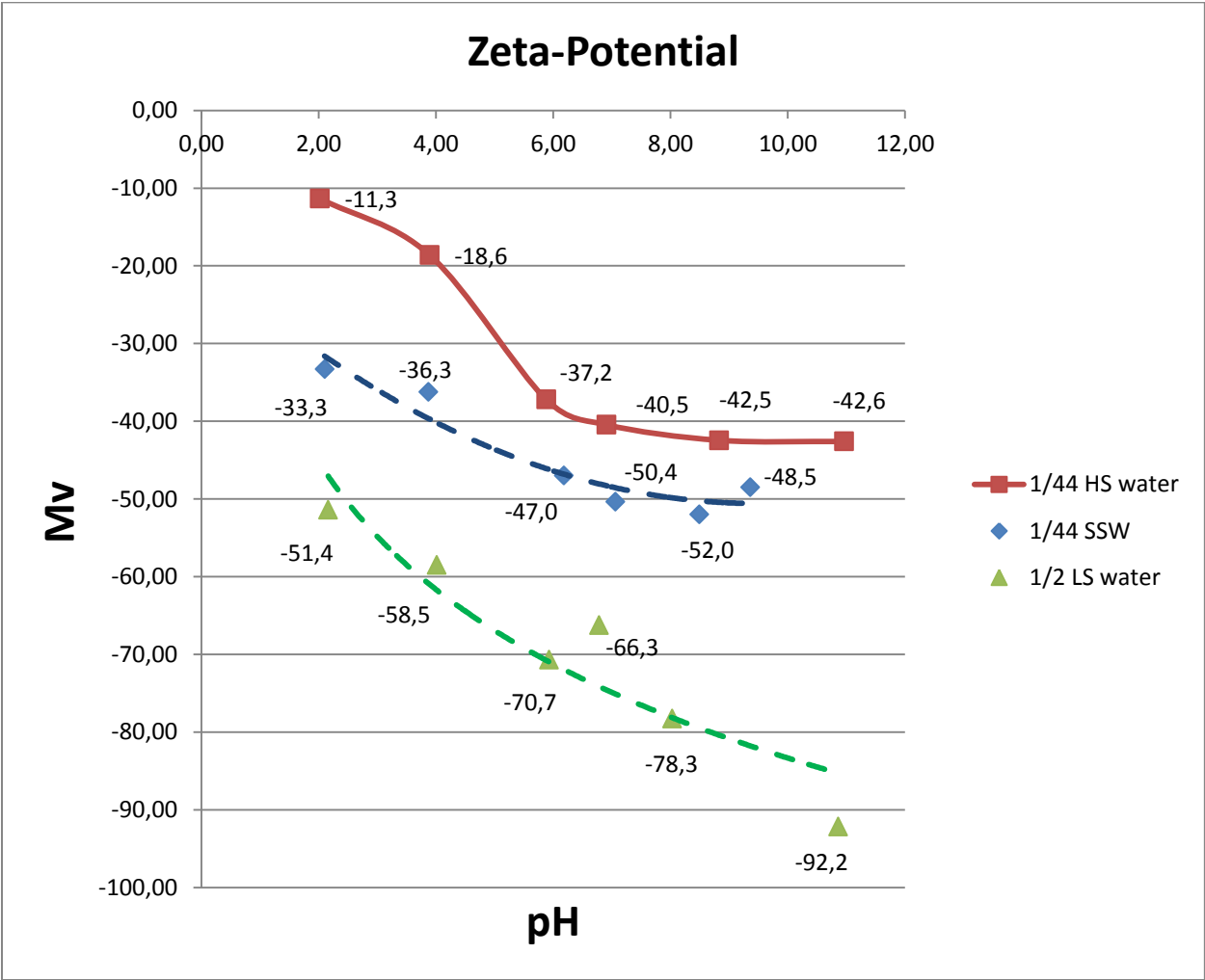


Figure 6.1 Zeta-potential of crude oil A-12 dispersed in 2.3% diluted SSW and 2.3% HS water, and 50% LS water. The pH was varied from 2.00-11.00.

Discussion

The results presented in figure 6.1 strongly indicate a dependent relationship between zeta-potential and pH. All three micro emulsions showed a decreasing zeta-potential as the pH increased.

This is explained by the magnitude of net negative charge between the crude oil/brine interfaces increases as the acidic species in the crude oil ionizes. As a consequence, the electrical double layer expands which causes increased emulsion stability.

The stabilization is caused by the oil phase gaining a higher hydrophilic character at the surface when organic acids dissociates as the pH increases, which favors its solubility in the aqueous phase.

Theoretically, the zeta-potential between the crude oil/brine will become constant when all acidic functional groups in the oil phase are ionized as the pH increases. This was observed for emulsified droplets of crude oil A-12 in 2.3% HS water at pH ~9 as the curve flats out. A trend line was drawn for the emulsions with 2.3% SSW and 50% LS water. The trend line clearly indicates the same relationship as for 2.3% HS water which was expected. The curve for 2.3% SSW seems to flat out at pH 9.4, but the zeta-potential generated with 50% LS water did not stabilize in the pH range.

Buckley [20] presented same type of relationship for Mountrary crude oil as a function of pH, as shown in figure 3.8 (b).

Kaliyugarasan [83] observed the same zeta trend when pH was altered. She investigated the zeta-potential of emulsified droplets of crude oil Exp-12 in 50%-, 10%,- and 1%,- SSW in a pH range of 3-10. Her study revealed that as the pH of the aqueous phase increased and the salinity was held constant, the zeta-potential decreased until the curve flatted out. In addition, the pH region where she observed no change in the zeta-potential by further increment the pH, increased as the salinity of the aqueous phase decreased.

At the same pH values, the results in figure 6.1 show that the 2.3% HS water emulsion obtained the highest zeta-potential followed by 2.3% SSW and finally 50% LS water with the lowest potential. It is evident from these results that the zeta-potential is also dependent on the salinity and ion-valence.

50% LS water contained 1500 ppm sodium chloride which is mono-valence ions. These electrolytes reduce the screening potential of the net negative charge at the interface, compared to HS water and SSW.

Both the HS water and SSW contains divalent ions which contributes to an improved screening of the net surfaces charge, and thus reduces the diffuse layer as shown in figure 3.2. The 2.3% SSW had an ionic strength of 16.5 mmol/L compared to 2.3% HS water with 15.3 mmole/L, but figure 6.1 shows that the micro emulsions generated by 2.3% HS water resulted in a less net negative charge than for 2.3% SSW at the same pH. A possible explanation is the charge on the divalent ions present in the aqueous phase. The 2.3% HS water contained 0.48% positively charged divalent ions (magnesium and calcium), but the 2.3% SSW contained only 0.30% positively divalent ions (magnesium and calcium) in addition to 0.21% negatively charged divalent ions (carbonate and sulfate). The divalent ions will impact the zeta-potential by either increasing or decreasing the Debye length. Crude oil A-12 is highly acidic which leads to a greater negative surface charge when the pH of the aqueous phase increases as explained above. Divalent cations will be attracted to the interface and thus screen the potential. Divalent anions will experience a repulsive force to the negatively interfacial charge and thereby increase the double layer.

Nasralla *et al.* [31] compared the impact on zeta-potential by different cation types and presented the same results as figure 6.1 shows.

They observed the zeta-potential to be significantly affected by the cation type, as sodium chloride changed the charges at crude oil/brine interface to highly negative compared to the emulsions containing same wt% calcium chloride or magnesium chloride, as seen in figure 4.5.

Crude oil A-12 has a total acid number of 3.84 ± 0.01 mg KOH/g compared to Moutrary crude oil with a TAN of 0.55 ± 0.10 mg KOH/g. Thus, one can expect crude oil A-12 to generate a higher electronegative zeta-potential as the pH increases due to ionization of more acidic species. By comparing the zeta plots of these two oils presented in figure 3.8 (b) and figure 6.1 it is observed that Moutrary crude oil in all salinity regions has a higher net negative charge, even compared to 50% LS water.

The isoelectric point (see section 3.1.3) was not observed for the micro emulsions.

Kaliyugarasan [83] found that the IEP for emulsified droplets of crude oil Exp-12 with a TAN of 2.96 ± 0.05 in 50% SSW was at pH 3 and in 10% SSW at pH 4. It is evident that the salinity and concentration of divalent ions impacts the IEP, but the total acid number of crude oil A-12 had almost 1 mg KOH/g more compared to crude Exp-12 which can imply that the TAN of the crude oil is more dominant than the salinity, even at low pH.

6.2.2 Dispersed Crude Oil Exp-12_{x&i} in LS Water Containing Different Ions

Figure 6.2 presents the zeta-potential obtained for emulsified droplets of crude oil Exp-12_{x&i} in different brines. Respectively, these brines were LS water containing 10, 50 and 100 ppm Ca^{2+} , CO_3^{2-} , Mg^{2+} , SO_4^{2-} , PO_4^{3-} or $\text{B}_4\text{O}_7^{2-}$. pH of the aqueous phase were not modified to a fixed value, but kept at the solutions natural pH, as shown in table A.4.6. The measurement of LS water was used as a reference point.

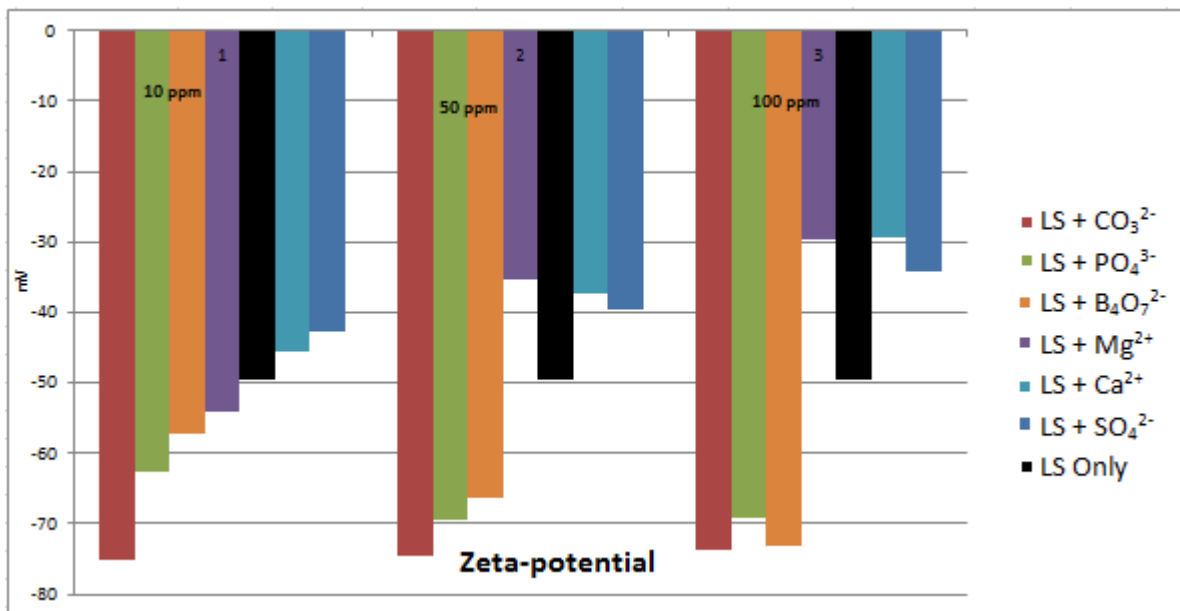


Figure 6.2 Zeta-potential for 5 μL crude oil Exp-12_{x&i} in 10 mL LS water containing 10, 50 or 100 ppm Ca^{2+} , Mg^{2+} , CO_3^{2-} , SO_4^{2-} , $\text{B}_4\text{O}_7^{2-}$ or PO_4^{3-} . pH was not held constant, see table A.4.6 for pH measurements.

Discussion

By examining the results listed in figure 6.2 it becomes evident that each aqueous phase generated different zeta-potential values at their respective pH regions. A very interesting observation was the impact on the emulsion stability by positive and negative charged divalent ions present in the aqueous phase. How the different ion charges affects the zeta-potential is explained in the discussion in section 6.2.1. Table A.4.6 provides information of the measured pH after generation the emulsions of crude oil Exp-12_{x&i} in the different brines.

Magnesium and calcium provided positively divalent charged ions in the aqueous phase. It is observed from table A.4.6 that when the ion concentration increased in the emulsions, the pH decreased from 6.58 to 5.99 by addition of magnesium, but only a partial increase was observed by adding calcium.

Both emulsions resulted in a greater zeta-potential by the increase of concentration from 10 to 100 ppm which was expected since divalent cations accumulate to the negative charged interface between crude oil/brine and screens the potential. The pH increased by incremental addition of calcium which should imply a decrease in zeta-potential, but the increase was within the uncertainty of the pH-meter and thus cannot be discussed.

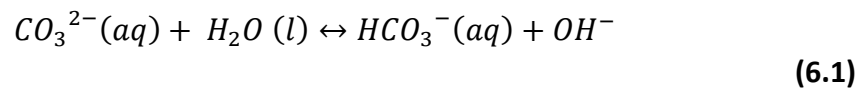
Nasralla *et al.* [31] experienced the same zeta behavior when the ionic concentration was altered. They investigated the impact of incrementally increasing the concentration of magnesium and calcium present in a crude oil/brine emulsion. Their results showed that the charge at the oil/brine interfaces was significantly affected by changing the concentration. When the concentration was lowered from 5 wt% to 0.2 wt%, the zeta-potential was dramatically reduced as shown in figure 4.5.

The emulsions containing borate and phosphate showed a trend where the net negative charge at the crude oil/brine interface increased with incremental electrolyte concentration. In addition, the pH increased in both cases which indicated that the acidic species in the oil phase dissociated.

The impact of sulfate in the emulsions caused the zeta-potential to increase slightly as the pH dropped. Theoretically, as explained in section 6.2.1, divalent anions should cause the zeta-

potential to decrease by expanding the diffuse layer when the net interface charge is negative due to repulsive forces. An explanation for these observations may be that the pH is more dominant than the concentration of sulfate.

The measured results for the emulsions containing carbonate were approximately -74.0 mV at all concentrations. The pH increased from 8.87 to 9.93 in the emulsions consisting of 10 ppm to 100 ppm carbonate. A possible reason which could cause the zeta-potential to not alter much is that the carbonate ions reacted with water molecules and initiated acid/base equilibrium reactions as shown in equation 6.1. A shift in equilibrium from left to right will cause an increase of hydroxide ions present in the emulsion and thereby contribute to a rise in pH. Through these acid/base reactions the carbonate concentration will be reduced by formation of bicarbonate, which has a lower repulsion potential contributing to an increased diffuse layer.



Zeta-potential generated by LS water was measured as a reference point.

It is observed by comparing the zeta results presented in figure 6.2 that the emulsions containing carbonate, phosphate, borate and magnesium generated a higher net negative charge at the interface than the LS water, contrary to calcium and sulfate, all at 10 ppm. When the electrolyte concentration was increased, magnesium, calcium and sulfate generated a higher zeta-potential compared to the solvent. One possible reason explaining why sulfate generated a higher zeta-potential compared to the LS water may be the dominance of pH. It is observed from table A.4.6 that sulfate generated a lower pH at all salinity levels compared to LS water. Correlation between the electrical charge and pH has been reported by Nasralla *et al.* [22] who demonstrated the impact of pH change on zeta-potential at oil/brine interfaces, where the electrical charge reduced as the pH was decreased, as shown in figure 3.9.

6.2.3 Dispersed Crude Oil Exp-12_{x&i} in LS Water with Constant Electrolyte Concentration

Figure 6.3 shows the zeta-potential results of crude oil Exp-12_{x&i} dispersed in LS water containing a constant electrolyte concentration of $6.61 \cdot 10^{-8}$ mole/kg Ca^{2+} , CO_3^{2-} , Mg^{2+} , SO_4^{2-} , PO_4^{3-} or $\text{B}_4\text{O}_7^{2-}$.

The measurements were conducted at an acidic and alkaline environment for comparison.

The measurement of LS water was used as a reference point.

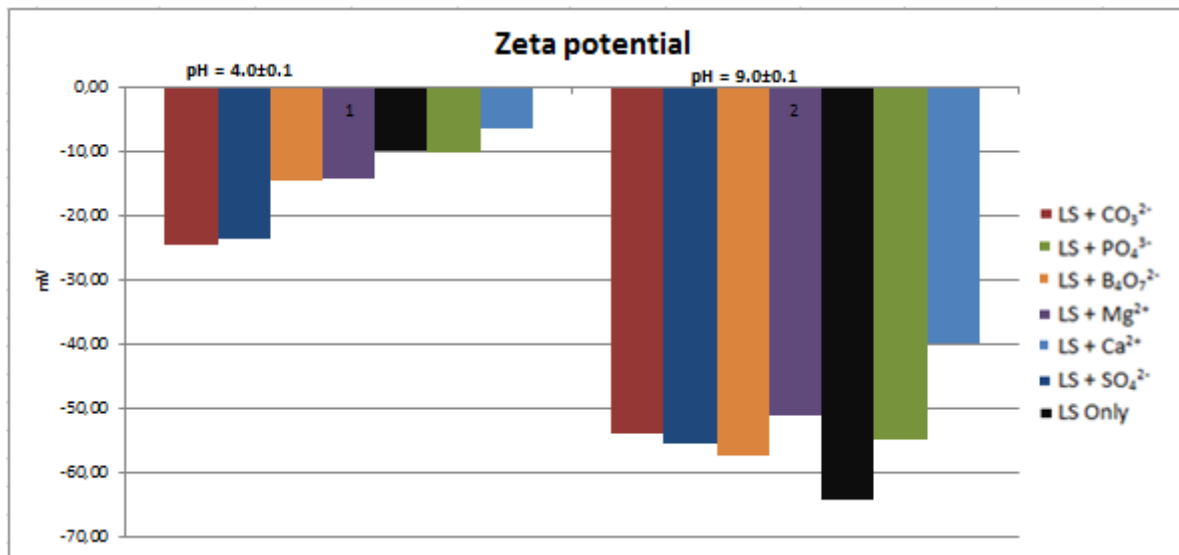


Figure 6.3 Zeta-potential for 5 μL crude oil Exp-12_{x&i} in 6 mL LS water containing constant ionic molality of Ca^{2+} , Mg^{2+} , CO_3^{2-} , SO_4^{2-} , $\text{B}_4\text{O}_7^{2-}$ or PO_4^{3-} . pH was maintained at 4.00 ± 0.1 and 9.00 ± 0.1 .

Discussion

As these measurements were taken, the pH-meter stopped functioning. The pH listed in table A.4.7 and A.4.8 is recorded as the pH of the aqueous phase. Thus, comparing the impact of different electrolytes on the zeta-potential by the emulsion pH is not possible. Instead, the discussion will be emphasized on the brines pH being 4.0 and 9.0 before the micro emulsion was generated.

The zeta-potential results presented in figure 6.3 clearly show a significant gap in magnitude of the net negative charge between crude oil/brine interfaces when the micro emulsion is encountered in an acidic and alkaline region. The zeta-potential increased dramatically from highly to weekly negative by reducing the pH of the brine phase from 9 to 4. The most significant change in zeta-potential was encountered for the low salinity water by a variation of 54.1 ± 1 mV. The brine containing phosphate affected the charge potential the most by 44.7 ± 2 mV compared to the other multivalent electrolytes. This shows the importance of brine pH.

As demonstrated in section 3.3, Buckley [20] explained that through ionization of organic acidic and basic species, the net charge of oil/brine interface will be positive at low pH, and negative at high pH.

At pH 4.0, none of the brines generated a positive net charge between the oil/brine interfaces. Brine emulsion with calcium caused a zeta-potential of -6.6 mV which was the value closest to the isoelectric point. At this point, the zeta-potential is zero and the colloidal system is least stable. A possible reason for not observing the IEP at pH 4 may be due to low content of basic species in crude oil Exp-12_{x&i}. Buckley [20] presented in her study (figure 3.8) the zeta-potential of two different oils, respectively A-93 and Moutrary crude, emulsified in 0.1 M NaCl. At pH 4, crude oil A-93 with an acid/base ratio of 0.06 resulted in a zeta-potential of ~ 28 mV, compared ~ 4 mV by Moutrary crude with an acid/base ratio of 0.7. It is evident that the magnitude of basic species increases the positive charge at oil/brine interface as the pH becomes more acidic. The total base number has not been measured for crude oil Exp-12_{x&i}, but it is reasonable to believe that the base number is higher than crude oil A-12, since at pH 4, the emulsion of LS water generated a zeta-potential of -9.9 mV (table A.4.8) with Exp-12_{x&i} and -58.5 mV (table A.4.2) for A-12 in 50% LS water and continued to increase to -51.4 at pH 2. Thus, it is possible that a positive value of zeta-potential would have been encountered if the pH had been reduced below 4.

The zeta results presented in figure 6.3 were generated by different brine solutions containing a constant electrolyte concentration. By examining the results at pH 4, it is observed that carbonate, -24.7 mV, and sulfate, -23.7 mV, resulted in the highest electronegative crude oil/brine interface. Borate, -14.7 mV, and magnesium, -14.3 mV, increased the zeta-potential by

~10 mV. Interestingly, phosphate, -10.9 mV, resulted in approximately the same potential as LS water, -9.9 mV, where both further increased the zeta-potential by ~4 mV. Finally, calcium, -6.6, raised the zeta-potential by ~6 mV.

By comparing the impact of constant concentration of electrolytes present in the crude oil/brine emulsion at the alkaline environment, it was observed that the LS water, -64.1 mV, gave the largest net electric charge. By examining the electrolytes, all except calcium resulted in a zeta-potential within the range of -57 mV to -51 mV, where borate, -57.2 mV, generated the most electronegative interface. The zeta-potential was incrementally increased by sulfate, -55.4, phosphate, -54.9 mV, carbonate, -53.8 mV and magnesium, -51.0 mV. The lowest zeta-potential was encountered by calcium, -39.9 mV.

These observations summarize that not only pH, salinity and ion-valence affects the zeta-potential, but also the type of electrolyte present.

6.3 Interfacial Tension (IFT)

Interfacial tension studies were conducted between two crude oils, respectively crude A-12 and Exp-12_{x&i}, and different brines to investigate the impact of aqueous phase on the surfactant character of the crude oils. The aqueous phase was manipulated in respect to varying the pH, salinity and ion-valence.

All IFT measurements were conducted by the drop volume method at ambient temperature. Three parallels were taken, whereas only two was presented if the third replication was an outlier.

Appendix A.5 lists all the IFT measurements with relative uncertainty, pH measurements and all data obtained to calculate the interfacial tension, except density measurements of the crude oils and brines which was presented in appendix A.2.

Results

Section 6.3.1 summarizes the interfacial tension results between crude oil A-12 and incremental dilution of SSW, HS water and LS water. Further, section 6.3.2 lists the IFT between crude oil Exp-12_{x&i} and LS water containing 10, 50 or 100 ppm Ca^{2+} , Mg^{2+} , CO_3^{2-} , SO_4^{2-} , $\text{B}_4\text{O}_7^{2-}$ or PO_4^{3-} at a pH region from 2 to 10. Finally, section 6.3.3 presents the IFT obtained between crude oil Exp-12_{x&i} and LS water that contained 10, 50 or 100 ppm magnesium or borate as a function of time in contact before IFT was measured.

6.3.1 IFT between Crude Oil A-12 and SSW, HS Water and LS Water

Figure 6.4 displays the interfacial tension obtained between crude oil A-12 and SSW and HS water as a function of the brines salinity. Distilled water was measured as a reference point. The pH was not measured.

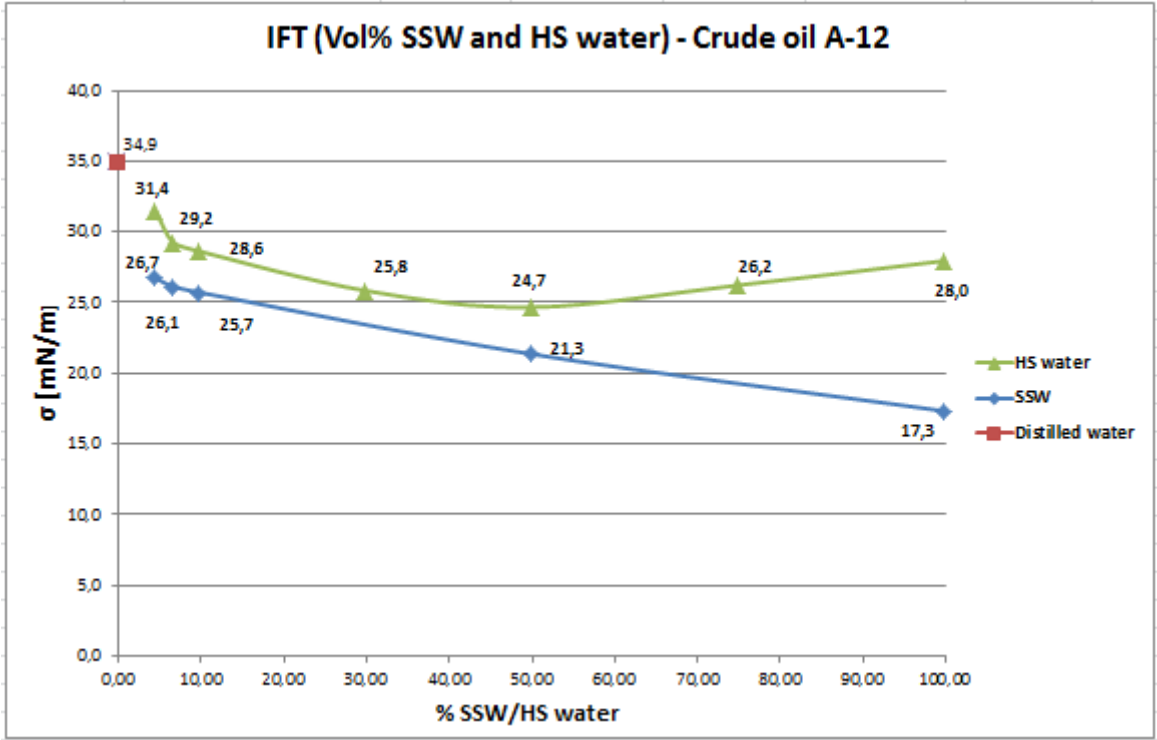


Figure 6.4 IFT between crude oil A-12 and SSW and HS water.

Discussion

By examining the IFT measurements presented in figure 6.4 it's observed two distinctive trends between crude oil A-12 and SSW/HS water.

The interfacial tension between crude oil A-12 and SSW increased as the salinity was reduced, and indicated a linear dependency on the salinity from 100% to 10%. In addition, the IFT measured at 100% SSW was 17.3 mN/m which is less than the average IFT observed for SSW that are normally encountered between 20-30 mN/m.

Contradictory, Tang and Morrow [84] showed that the measured IFT values between reservoir brine and CS crude oil decreased by reducing the brine concentration.

Kaliyugarasan [83] also investigated the IFT between crude oil A-12 and SSW without pre-equilibration prior to the measurements and showed same relationship as presented in figure 6.4. She observed that the IFT increased by diluting the brine concentration, but at 100% SSW, she obtained an IFT value of 12.3 mN/m and suggested that this low value may have been caused by the high acidic character of the crude oil (see table 6.1).

Standal *et al.* [85] showed that the lowest IFT measurements were accomplished by the oil with highest acid number in presence of all brine compositions.

Buckley and Fan [86] studied the IFT between crude oils and brine as a function of the oils acid and base number. They found a correlation where a higher base number contributed to an increased IFT, and increasing the acid number corresponded to a decrease in the IFT.

Synthetic seawater was one of the brines they tested and pointed out that SSW contains divalent cations such as magnesium and calcium which may have specific interactions with ionizable species at the oil/water interface.

The electrophoretic measurements presented in chapter 6.2 show that crude oil A-12 had a net negative charge at the crude oil/brine interface at neutral pH conditions. A possible explanation for the observed trend where the IFT increased by incrementally reducing the salinity may be that the attractive interactions impaired between the two phases. The surface of the dispersed crude oil droplets in SSW will remain negative through dilution from 100% to 2.3%, but the magnitude of the divalent cations (magnesium and calcium) diminishes and thus may cause a reduction of the solubility character between crude oil/brine.

The IFT between crude oil A-12 and HS water was reduced by diluting the brine concentration, until approximately 50%, where further dilution caused the IFT to increase. These IFT results are distinctly different from SSW by not continuously increasing or decreasing through the salinity region.

Vijapurapu *et al.* [87] showed the same trend as for HS water in figure 6.4, where the IFT initially decreased from a mixture of 100% deionized water to 50/50 mixture with Yates synthetic brine and then increased on further increasing the volume percent brine up to 100%. A possible cause for this observed trend may have been the magnitude of divalent ions present in the brine phase. As the surface of the oil particles are negative charged (surface active

components), increasing the content of divalent cations (magnesium and calcium) from zero will cause a migration of the ions to the oil/brine interface and increase the attraction forces between the two phases and thus reduce the diffuse layer. Nasralla *et al.* [31] showed that the zeta-potential increased by increasing the concentration of magnesium and calcium, but the increase in zeta-potential was significantly higher by adding calcium (figure 4.5). In correlation to the SSW and HS water used in the IFT measurements, the SSW contained a calcium/magnesium ratio of 0.36 (table A.1.1) and HS water had a ratio of 8.39 (table A.1.2). Thus, as the concentration of calcium is increased, the zeta-potential may become positively charged. When the zeta-potential changes from negative to positive, then at the IEP the IFT may have reached a minimum which was observed. A result of an excess of calcium ions in the brine and a positively charged interface between oil/brine causes the two phases to repel each other and thus increase the IFT.

Distilled water which does not contain any electrolytes generated the highest IFT with 34.9 mN/m. Together with the electrophoretic studies in section 6.2.1, where LS water gave the most electronegative interface between oil and brine compared to SSW and HS water, indicates that there is a relationship between the IFT and Debye length.

A comparison of the IFT results between crude oil A-12 and SSW, HS water and distilled water, makes it evident that surface active components in the oil phase along with ion type and concentration in the aqueous phase have an impact on the interfacial activity.

6.3.2 IFT between Crude Oil Exp-12_{x&i} and LS Water Containing Different Ions

Figure 6.5, 6.6 and 6.7 presents the results obtained for the IFT between crude oil Exp-12_{x&i} and LS water containing 10, 50 or 100 ppm Ca^{2+} , Mg^{2+} , CO_3^{2-} , SO_4^{2-} , $\text{B}_4\text{O}_7^{2-}$ or PO_4^{3-} as a function of pH. The pH was varied from 2.00 to 10.00. LS water was measured as a reference point.

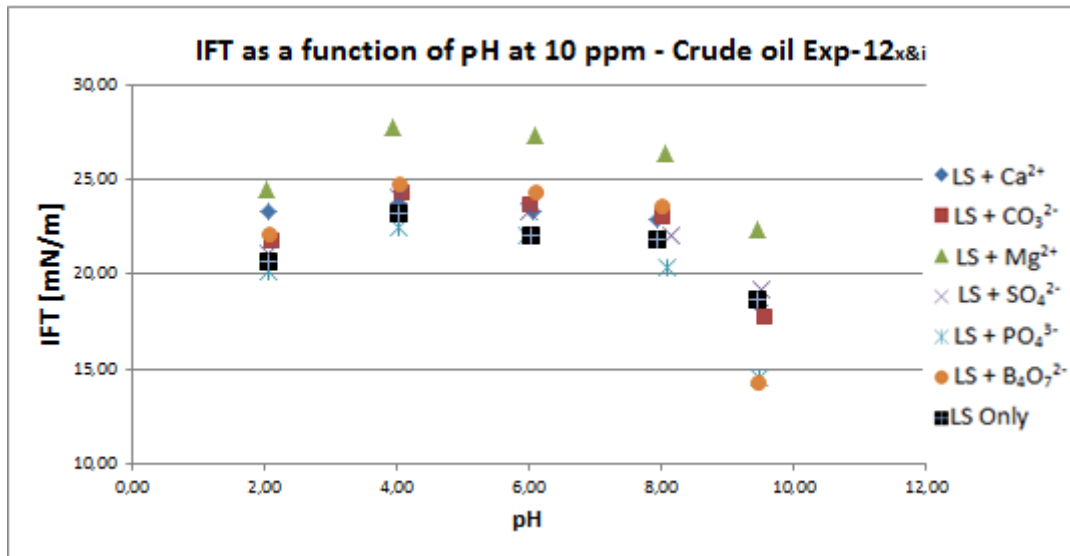


Figure 6.5 IFT between crude Exp-12_{x&i} and LS water containing 10 ppm Ca²⁺, Mg²⁺, CO₃²⁻, SO₄²⁻, B₄O₇²⁻ or PO₄³⁻. pH of the aqueous phase was varied between 2.00-10.00.

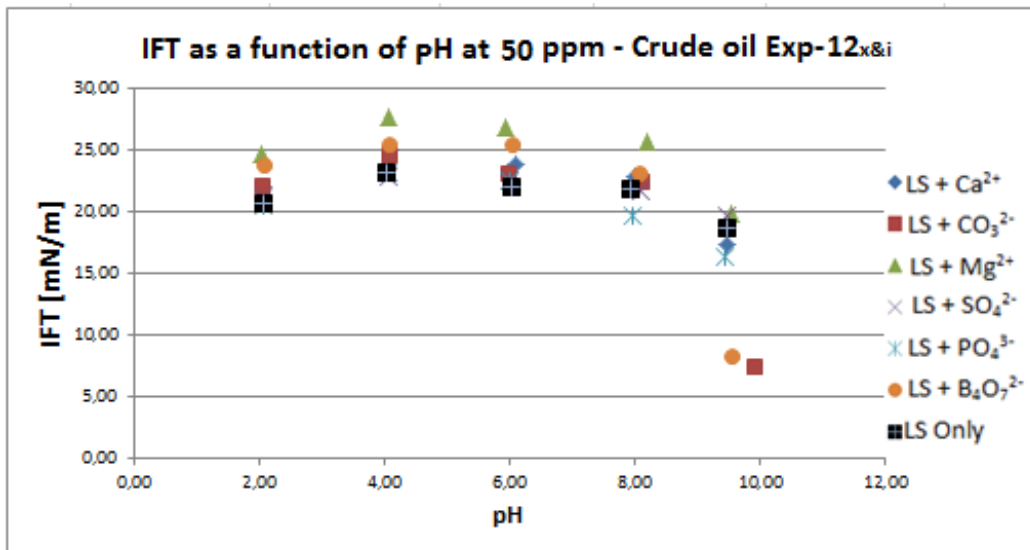


Figure 6.6 IFT between crude Exp-12_{x&i} and LS water containing 50 ppm Ca²⁺, Mg²⁺, CO₃²⁻, SO₄²⁻, B₄O₇²⁻ or PO₄³⁻. pH of the aqueous phase was varied between 2.00-10.00.

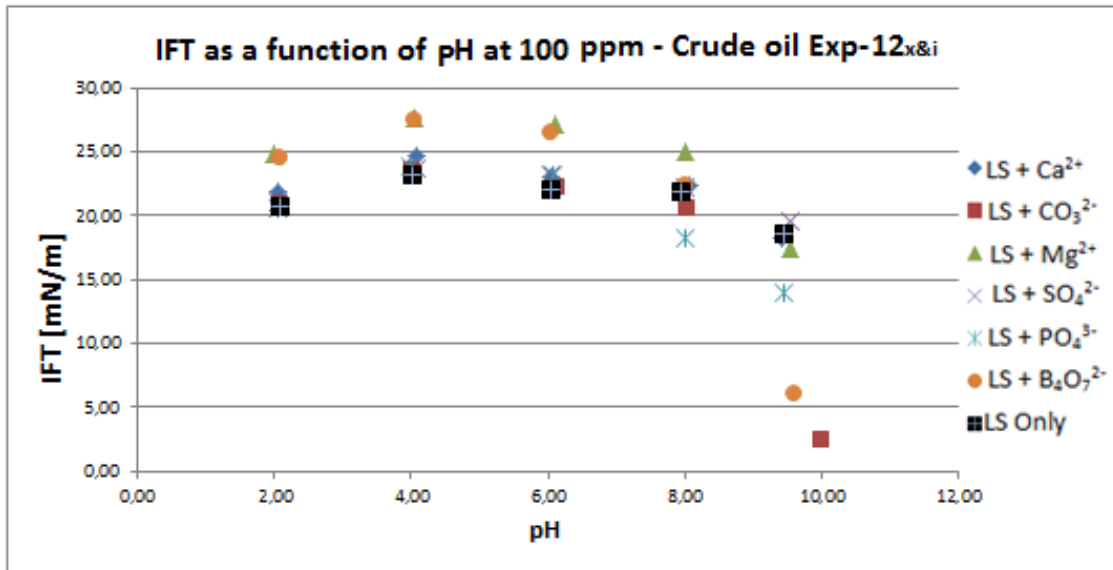


Figure 6.7 IFT between crude Exp-12_{x&i} and LS water containing 100 ppm Ca²⁺, Mg²⁺, CO₃²⁻, SO₄²⁻, B₄O₇²⁻ or PO₄³⁻. pH of the aqueous phase was varied between 2.00-10.00.

Discussion

All three figures presented above shares the same IFT trend by varying the pH from 2 to 10.

In general, the IFT increased at a pH range from 2-4, and then decreased by further increasing the pH from 4 to 10. An interesting observation is that all brines, in all salinity concentrations, reached a maximum in the interfacial tension at pH 4. This IFT curve was expected due to the high content of acidic constituents in crude oil Exp-12_{x&i}. When the pH was increased from extreme acidic environment, the ionized bases protonated and thus the IFT increased. When pH was further increased, the acidic species ionized and the IFT decreased.

Buckley and Fan [86] investigated the IFT relationship between high and low acid number oils and reported that two of the low-acid-number samples gave IFTs that decreased continuously with increasing pH. On the other hand, all the high-acidic-numbered oils exhibited a plateau or a maximum IFT value from low to intermediate pH, which was also observed for crude Exp-12_{x&i}. TAN of crude oil Exp-12_{x&i} was measured to be 1.68±0.01 mg KOH/g after being diluted by 20% xylene and 20% iododecane in volume, which classifies it to be an highly acidic oil.

Kaliyugarasan [83] used crude oil Exp-12_{x&i} (named Exp-12-D) in her IFT studies and investigated if xylene and iododecane impacted the IFT between original and diluted oil with SSW. Her results showed that only an increase of ~ 1 mN/m was measured.

There was no distinct change in the IFT between the crude oil and the individual brines by altering the electrolyte concentration at constant pH. The variation was within the relative uncertainty of $\pm 5\%$ which makes it impossible to discuss. In addition, the variation in the results fluctuated when the ionic concentration was increased from 10 to 100 ppm which made it impossible to prove a trend. The only exception was the brine solution containing borate. At pH 2-6, the increase of borate concentration in the emulsion caused the IFT to increase. By further increase of pH, the IFT seemed to stabilize except when pH approached 9 to 10 where the magnitude of ionized functional groups in the crude oils caused a solubilization effect in the aqueous phase due to the oil adapting a more hydrophilic character. This effect was common for all the oil/brine systems at a high alkaline environment. The result is a dramatic reduction in the IFT by a small increase in pH.

The IFT gap between the different concentrations could perhaps been higher if the difference in electrolyte concentration in the brines had been significantly increased.

The emulsion with absence of multivalent ions (LS water) caused the lowest IFT in all pH regions, except at pH 2 and 8 compared to the other brines. The extreme acidic environment caused the brine with phosphate to generate the lowest IFT, and again in the alkaline environment of pH 8. The impact of the brines at pH 9-10 will not be discussed due to the solubilization effect explained above.

These results justify that varying the ion-valence present in the emulsion will impact the IFT between the crude oil/brine.

An observation from the IFT measurements by the increase of electrolyte concentration is the impact of magnesium and calcium in relationship to the results obtained in section 6.3.1.

Figure 6.5, 6.6 and 6.7 showed that when brine concentration increased from 10 to 100 ppm, the emulsions with magnesium caused the highest IFT compared to calcium. SSW contained almost no calcium but a high content of magnesium and gave a lower IFT compared to the HS water which consisted of a high concentration of calcium and almost no magnesium.

These contradictory results are not easy to explain, but rather confirm that there exists a more complex interplay between the electrolytes present in the emulsion and the crude oil, making it difficult to draw a conclusion from examination of individual ions.

6.3.3 IFT as a Function of Time in Contact between Crude Oil Exp-12_{x&i} and Brines

Figures 6.8, 6.9 and 6.10 list the results obtained for the IFT between crude oil Exp-12_{x&i} and LS water containing 10, 50 or 100 ppm magnesium and borate as a function of pH. The pH was varied from 2.00 to 10.00. The IFT measurements were performed on two different systems, at first contact between the two phases and after an amount of time in equilibrium. Then the equilibrated crude oil was further extracted and used to measure the IFT with the identical synthetic brines which had not been in contact with the oil. The brines containing magnesium had been in contact with the crude oil for 11 days, and borate and LS water had been equilibrated for 14 days. LS water was measured as a reference point.

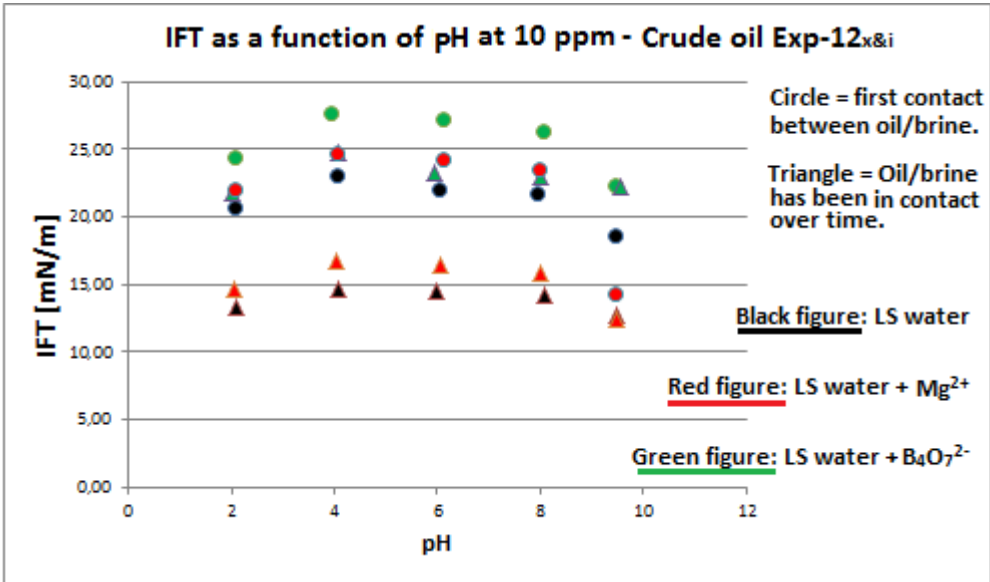


Figure 6.8 IFT between crude Exp-12_{x&i} and LS water containing 10 ppm magnesium or calcium. Measurements were taken at first contact and after a fixed time in equilibrium. pH of the aqueous phase was varied between 2.00-10.00.

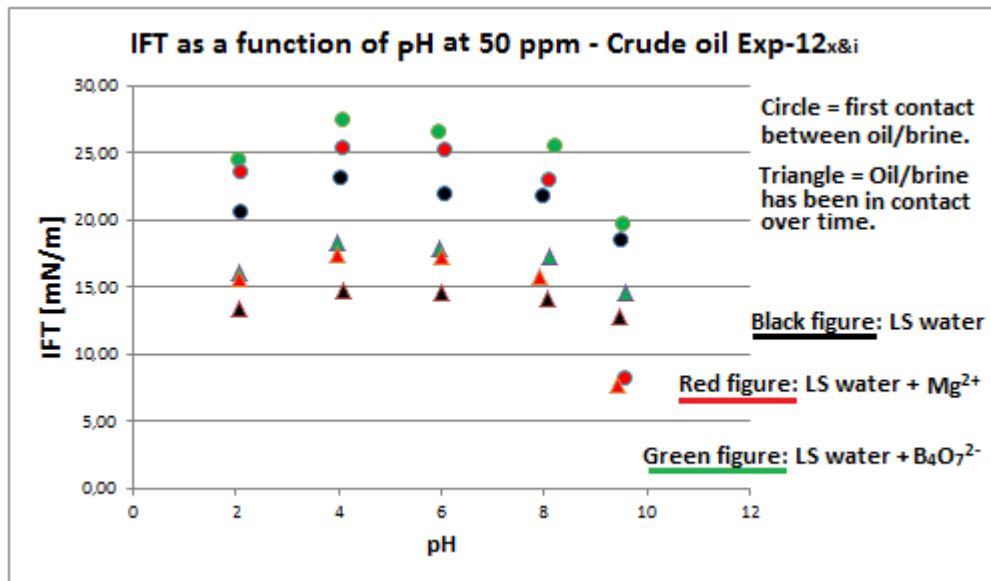


Figure 6.9 IFT between crude Exp-12_{x&i} and LS water containing 50 ppm magnesium or calcium. Measurements were taken at first contact and after a fixed time in equilibrium. pH of the aqueous phase was varied between 2.00-10.00.

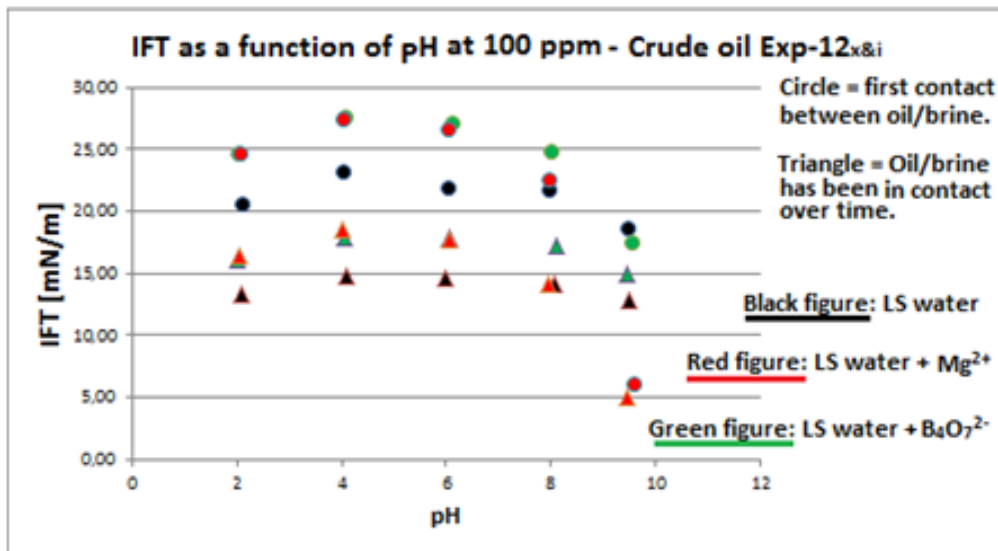


Figure 6.10 IFT between crude Exp-12_{x&i} and LS water containing 100 ppm magnesium or calcium. Measurements were taken at first contact and after a fixed time in equilibrium. pH of the aqueous phase was varied between 2.00-10.00.

Discussion

From the three different figures above it is evident that equilibration time between crude oil and brine has a positive impact on the IFT. In the entire pH span and all salinities the IFT measured by first contact between the two phases was higher than after 11-14 days in equilibrium. Still, after equilibration time, there was observed a maximum plateau for the IFT at pH 4, as discussed in section 6.3.2.

By excluding the measurements performed at pH 9-10 due to the surfactant character the crude oil adopts at these alkaline environments, the results showed that the average difference in the measured IFT between first contact and after time by a max variation in pH and salinity was more or less constant, as seen in table A.5.8. The only exception was 10 ppm magnesium which varied by 3.2 mN/m instead of ~ 7.8 - 8.8 mN/m which was observed for the rest of the measurements. A possible reason for this deviation may have been the sample preparation where all other measurements were equilibrated in advance in a of 50/50 oil/brine mix by volume, whereby the 10 ppm magnesium brine was a 25/75 oil/brine mix. By this observation one can speculate if the impact on IFT by volume present between the two phases affects the equilibrated system more than the salinity concentration of the brine present.

Buckley and Fan [86] presented the same IFT behavior between an equilibrated and non-equilibrated system. They investigated the IFT as a function of time between crude oil E-1XCO-01 and SSW by formation of new drops at an interval of 2000 s by pendant drop which is a static method. The average decrease in IFT from initial to equilibrated conditions was 4.7 ± 2.9 mN/m (about 23% initial IFT values) with larger changes occurring mainly in the higher pH measurements.

The IFT measurements performed in this thesis were implemented by the drop-volume method which is a dynamic method and does not show any variation with time. Despite it was only equilibrated crude oil that was measured instead of both phases, it was found the same trend as Buckley and Fan obtained.

The results obtained in this section clearly indicate that surface active compounds interact in the interface between crude oil and brine and alter the interfacial tension.

With respect to the results obtained, one can try to identify the mechanism providing the proven IFT behavior between an equilibrated and non-equilibrated system. The equilibrated

crude oil Exp-12_{x&i} was transferred by a micrometer syringe where the oil had been absorbed from the bulk and not from the interface. Since the IFT decreased after measuring the crude oil/brine system where the brine experienced first contact, but the crude oil had been equilibrated in advance with the identical same type of brine, it is most likely that the oil phase became more hydrophilic through activation of acidic and basic species which adsorbed into the bulk over time.

6.4 Adhesion Map (Wettability Alteration)

This section summarizes the wettability measurements of Crude oil A-12 on smooth quartz in presence of SSW, HS water and LS water, as shown in table 6.4, 6.5 and 6.6. An adhesion map was created with respect to pH and brine salinity. The pH was varies from 2 to 12 and the SSW and HS water was diluted from 100.0% to 50.0%, 10.0%, 6.8% and 4.6%, respectively.

Three parallels were taken for each measurement to confirm adhesion, non-adhesion or temporary adhesion. The contact angle was measured through a telescope where the relative uncertainty was set to $\pm 10^\circ$.

The adhesion map was emphasized on the wettability behavior as a function of pH and salinity, not by the contact angle.

Results

Table 6.4 Wettability of Crude oil A-12 onto smooth quartz surface in presence of SSW.
pH was varied from 2-12 and brine salinity from 100.0 to 0%.

		% - SSW					
		100.0	50.0	10.0	6.7	4.6	0.00
P H	12.0	No Adhesion	No Adhesion	No Adhesion	No Adhesion	No Adhesion	No Adhesion
	10.0	No Adhesion	No Adhesion	No Adhesion	No Adhesion	No Adhesion	No Adhesion
	8.5	No Adhesion	No Adhesion	No Adhesion	No Adhesion	No Adhesion	No Adhesion
	6.0	No Adhesion	No Adhesion	No Adhesion	No Adhesion	Adhesion $41.1^\circ \pm 10^\circ$	No Adhesion
	4.0	Adhesion $45.9 \pm 10^\circ$	Adhesion $49.4 \pm 10^\circ$	Adhesion $45.7 \pm 10^\circ$	Adhesion $41.6 \pm 10^\circ$	Adhesion $49.7 \pm 10^\circ$	Adhesion $38.3 \pm 10^\circ$
	2.0	No Adhesion	Temporarily	No Adhesion	Adhesion $46.7 \pm 10^\circ$	Temporarily	Adhesion $45.75 \pm 10^\circ$

Table 6.5 Wettability of Crude oil A-12 onto smooth quartz surface in presence of HS water.
pH was varied from 2-12 and brine salinity from 100.0 to 0%.

		%- HS water					
		100.0	50.0	10.0	6.7	4.6	0.00
P H	12.0	No Adhesion	No Adhesion	No Adhesion	No Adhesion	No Adhesion	No Adhesion
	10.0	No Adhesion	No Adhesion	No Adhesion	No Adhesion	No Adhesion	No Adhesion
	8.5	No Adhesion	No Adhesion	No Adhesion	No Adhesion	No Adhesion	No Adhesion
	6.0	No Adhesion	No Adhesion	No Adhesion	No Adhesion	No Adhesion	No Adhesion
	4.0	Adhesion 31.3±10°	No Adhesion	Adhesion 31.1±10°	Adhesion 48.2±10°	Adhesion 44.0±10°	Adhesion 38.3±10°
	2.0	Temporarily	Temporarily	Adhesion 53.9±10°	No Adhesion	Adhesion 51.8±10°	Adhesion 45.8±10°

Table 6.6 Wettability of Crude oil A-12 onto smooth quartz surface in presence of LS water.
pH was varied from 2-12 and brine salinity from 100.0 to 0%.

LS water		
P H	12.0	No Adhesion
	10.0	No Adhesion
	8.5	No Adhesion
	6.0	No Adhesion
	4.0	Temporarily
	2.0	No Adhesion

Discussion

The wettability alteration from water-wet to more oil-wet is a direct consequence of the interfacial tension between the oil and aqueous phase and its corresponding attraction to the solid surface.

It is observed from table 6.4 and 6.5 that adhesion of crude oil A-12 onto smooth quartz surface was recorded for all salinity levels at pH 4 for SSW and HS water, except at 50% HS water.

A key challenge was to identify if there was a correlation between the wettability alteration and the IFT measurements at pH 4 since the wettability is a function of the interfacial tension.

Equation 2.2 shows that when the IFT between oil and water increases, the contact angle also increases meaning the thin water film ruptures increasingly and thus an oil-wet surface can be formed. It was observed from section 6.3.2 and 6.3.3 that all IFT measurements between crude oil Exp-12_{x&i} and LS water containing different electrolytes showed a maximum IFT at pH 4 by varying the pH between 2 and 10. Section 6.3.1 shows that the IFT between crude oil A-12 and SSW increased when the salinity was reduced, which according to equation 2.2 gives a more favorable shift of the wettability towards a more oil-wet surface.

Interestingly, the one measurement at pH 4 for 50% HS water which showed non-adhesion was also the lowest IFT recorded through the salinity region, despite the pH was not measured, shown in figure 6.4. The contact angles seemed to fluctuate for both SSW and HS water in respect to the adhesion which makes it hard to discuss, although the variation can have been caused by the high relative uncertainty. Despite the fluctuations, it was observed that the lowest recorded contact angle after adhesion was measured to be $31.3 \pm 10^\circ$ for 100% HS water and $31.1 \pm 10^\circ$ for 10% HS water. This concludes a dependent relationship between wettability and IFT.

Table 6.6 summarizes the wettability results for LS water which did not generate any oil-wet surface with crude oil A-12. However, at pH 4 it was observed a temporarily adhesion. In relationship to the observed adhesion in presence of distilled water, which generated the highest IFT with crude oil A-12, and SSW and HS water at the same pH, it could indicate that not only is the pH dominant with respect to wettability alteration but also the salinity and ion-valence of the aqueous phase.

Above pH 4 there was only one adhesion recorded. Section 6.3.2 and 6.3.3 shows the IFT reduced after increasing the pH above 4. The domination of pH to reduce the IFT may have caused the surface to maintain its wettability preferences. In addition, section 3.2.3 shows that when pH is below 7, quartz surface will be negatively charged, and above 7 bear a positive charge. At alkaline environments the acidic functional groups of crude oil A-12 will be negative charged as well and thus as explained in section 4.3.5 magnesium or calcium can act as a cation bridge between the surface and oil. This was not observed for SSW or HS water as the salinity increased.

Standal *et al.* [85] measured the contact angles generated between different crude oils and silica surface and found a relationship where the water-wetness of the system increased with increasing acidic number.

The SSW and HS water generated an oil-wet surface, temporarily adhesion and non-adhesion at pH 2 by varying the salinity concentration. This wettability behavior is not easy to explain, but at these extreme acidic environments it could be due to domination of the surface charge by ionized basic species.

It was not easy to explain why 4.6% HS water caused an adhesion to the quartz surface at pH 6, but it could have been a result of bad washing routine where traces of organic solvent or impurities had been left on the quartz surface and caused an oil-wet region.

Buckley [20] reported contradictory results to those presented in this section. She investigated the wettability alteration of crude oil A-93 in presence of SSW and its corresponding dilutions. She reported non-adhesion of the oil in all salinity regions and pH ranges. In relationship to the adhesion results observed for crude oil A-12 and SSW one can confirm that crude oil composition has an important dominant impact on the wettability behavior.

7 Parameters Influence on the Results and Previous Work

The results obtained in the experimental work in this thesis were presented and discussed in chapter 6. This includes chemical analysis to examine the composition of the oils used, interfacial studies of crude oil/brine and adhesion behavior of crude oil/brine/rock systems.

All reservoirs with a potential of oil production is of high interests. They vary in oil composition, brine composition, pH, wettability preferences etc. Thus, the purpose of this thesis was to investigate the interactions between crude oil/brine with respect to varying the parameters that can be alternated to exploit the production opportunities. The attention has been on the promising results of low salinity waterflood at both laboratory and field trials by investigating the mechanisms responsible. The desirable situation is to fully understand the COBR interactions and thus know which parameters to alter to perform the most effective LSW.

In the following, a summary of the different parameters that were investigated (in this thesis) are described with emphasis on the impact on COBR interactions.

In addition, previous research with relationship to the experimental work in this thesis is presented.

Oil composition

The oil composition played an important role in the experimental work. To understand better the interactions between crude oil/brine, a lot of attention was drawn to the magnitude of acidic species in the oil phase.

Through the electrophoretic measurements it was observed that the magnitude of net negative charge at the oil/brine interfaces increased as more acidic constituents ionized.

Buckley [20] found a relationship where the magnitude of net negative charge between Moutrary crude and brine increased through incremental ionization of the acidic functional

groups in the oil. In addition, she proved that the acid/base content in the crude oils affected the zeta-potential where more acidic species caused a lower potential compared to a greater potential with higher total base number advantage.

Standal *et al.* [85] showed that the acid number impacted the interfacial tension between the crude oil/brine where the IFT reduced as a function of increased TAN.

Buckley and Fan [86] reported that when the pH of the aqueous phase increased, high acid-number oils reached a maximum IFT, whereby low acid-number oils caused the IFT to continuously decrease.

Standal *et al.* [85] showed that the wettability preferences of silica surface increased to more preferentially water-wet as the TAN of the crude oil increased.

pH

pH of the brine phase played a dominant role in the electrophoresis, IFT, and wettability measurements. Through results and discussion the attention was drawn towards the activation of acidic/basic species when altering the pH.

By varying the pH, it was observed that the interfacial properties between crude oil/brine changed where the zeta-potential decreased as the pH increased.

Kaliyugarasan [83] reported a decreasing trend in the zeta-potential between crude oil exp-12 and SSW interfaces as a function of increasing pH.

Nasralla *et al.* [22] showed that the electrical charge between oil/brine interfaces increased as a function of increasing pH, and reduced when the pH was decreased.

In the interfacial tension experiments it was observed that the IFT reached a maximum value as the pH increased from 2-10 in the brines consisting of individual ions. The plateau was witnessed at pH 4, and by further increase the alkalinity the IFT decreased continuously. At high alkaline environment the crude oil gained a surfactant character which caused the IFT to decrease dramatically.

With respect to the wettability studies, adhesion was mainly observed at pH 4.

Salinity, ion-valence and ion type

The brine composition had a prevailing effect on the experimental work.

By studying the electrophoresis measurements, it was observed that in general, cations caused a lower zeta-potential than anions through an improved screening of the negative charge at the crude oil/brine interfaces. The zeta-potential measurements of SSW, HS water and LS water revealed the impact of ion-valence, where multivalent cations increased the potential significantly compared to monovalent ions. By increasing the salinity it was observed that the zeta-potential either increased or decreased, depending on the ion charge.

Nasralla *et al.* [31] showed that the zeta-potential was significantly affected by the cation type, where sodium chloride caused the charge at crude oil/brine interfaces to become highly negative compared to emulsions with same wt% calcium chloride or magnesium chloride. In addition, the increase in magnesium and calcium concentration present in the emulsion caused the zeta-potential to increase dramatically.

The IFT experiments showed in general that the IFT between crude oil/brine increased when the salinity was reduced. An exception was the behavior of HS water where it was observed a minimum IFT value by reducing the salinity from 100 – 50%, by a further reduction the IFT increased.

It was not observed any significant advantages by examining the impact of individual ions on the IFT.

Vijapurapu *et al.* [87] reported the IFT to decrease when Yates synthetic brine was reduced from 100/0 to 50/50 brine/deionized water mix. After a minimum value had been reached, the IFT increased when the brine concentration was further reduced to 0/100 brine/deionized water mix.

The brines containing multivalent ions altered the wettability towards a more preferentially oil-wet surface compared to monovalent ions. This was only observed at acidic environment.

Buckley [20] observed non-adhesion between crude oil A-93 and SSW at all dilutions and pH ranges.

8 Summary and Conclusions

Main trends in measured data:

- Low salinity had a high impact on the net negative charge at the crude oil/brine interfaces. The interfacial tension was only partially affected by reduction in brine salinity. Adhesion map showed that low salinity did not shift the wettability preferences.
- The highly acidic oils used in this thesis caused a net negative charge between the crude oil/brine interfaces at all pH ranges and salinities measured.
- The net negative charge between crude oil/brine interfaces was highly dependent on the pH. High pH caused the zeta-potential to decrease.
- Zeta-potential for oil emulsified in brine at constant pH showed decreasing electronegative behavior with increase in salinity.
- The interfacial tension at constant pH was dependent on the brine composition. Reduction in salinity caused the IFT to increase.
- At low salinity, addition of specific ions (10-100 ppm) increased the IFT. The results showed that magnesium gave the largest effect on the IFT.
- A maximum IFT was observed at pH 4 between crude oil and brines containing different individually ions.
- Changes in IFT by varying the pH provided an indication that both acids and bases are active at crude oil/brine interfaces.
- Interfacial tension measurements showed that an equilibrated system generated a lower IFT between crude oil/brine compared to first contact.
- Crude oil adhered to quartz surface at low pH which is consistent with reduced surface charge from electrophoretic repulsion and less electronegativity between the crude oil and solid.

- Analysis of the impact of electrolytes on COBR interactions proved that magnesium and calcium dominated.
- The reduction in IFT in terms of general reservoir pH was insufficient to impact the capillary desaturation curve enough to reduce the oil saturation.
The capillary forces must be reduced by a factor of 10-100 to mobilize the capillary trapped oil.

General conclusion of LS mechanisms

Only minor changes in the interfacial tension between crude oil/brine, as effect of low salinity, was observed in this study. The results indicate that change in IFT is insufficient to play a major role in the LS effect on oil recovery.

Reduction in salinity causes a greater repulsion between the electronegative charged oil particles and the negative charged water-wet solid surface. As a consequence, the thickness of the water film increases and destabilizes the oil layers interacting with the rock surface. Thus, due to increased electronegative repulsion between oil and solid, the oil layers destabilized by water film become more mobile and the result can be a lowering of the oil saturation.

9 Further work

The prevailing mechanisms responsible for the positive effect of low salinity waterflooding are up to date still uncertain. Through continuous research and more data an extended knowledge of the low salinity effect may be achieved. The emphasis of this thesis was the physical chemistry of mechanisms for LSW. Dynamic coreflooding experiments must be performed to study the combined effect of these mechanisms. Some suggested further work is given in the following:

- Implement coreflood experiments by varying the same parameters under the same conditions as the experimental work performed in this thesis to observe the impact on oil recovery.
- Investigate the physiochemical interactions with high base-numbered oils to examine if other trends are observed. The oils used in this thesis had an unusual high acid number.
- Perform interfacial tension measurements between crude oils and brines with a wider salinity region than used in this thesis.
- Conduct more adhesion tests with brines composed of different salts to study the wettability behavior between NaCl brine and mixed brines.
- Investigate the wettability preferences at pH 4 with the same synthetic brines that generated a maximum IFT at pH 4 in this study.
- Implement electrophoresis measurements with crushed quartz in presence of brines of interest to study the COBR interaction in more detail.
- More interfacial tension measurements by altering the magnesium/calcium ratio in the aqueous phase to investigate the concave trend observed for HS water.
- Perform interfacial tension measurements between a high base-numbered oil and incremental dilution of SSW. Will an opposite trend form compared to high acid-numbered oils, in which case the dominance of magnitude of acidic/basic species in the oil phase may be concluded?
- Conduct interfacial tension experiments between crude oil/brine by incrementally varying the time in contact. Record the IFT as a function of time.

10 References

1. J. C. Berg, (2010). *"An Introduction to Interfaces & Colloids - The Bridge to Nanoscience"*. First ed.: World Scientific Publishing Co. Pte. Ltd.
2. A. B. Zolotuchin and J. R. Ursin, (2000). *"Introduction to Petroleum Reservoir Engineering."* Høyskoleforlaget AS - Norwegian Academic Press.
3. K. A. Dill and S. Bromberg, (2003). *"Molecular Driving Forces. Statistical Thermodynamics in Chemistry and Biology."* Garland Science, New York.
4. O. S. Hjelmeland and L. E. Larrondo, (1986). *"Experimental Investigation of the Effects of Temperature, Pressure, and Crude Oil Composition on Interfacial Properties."* Society of Petroleum Engineers.
5. W. Xu, (2005). *"Experimental Investigation of Dynamic Interfacial Interactions at Reservoir Conditions."* MSc Thesis, Louisiana, USA, May 2005.
6. Jr. Forrest and F. Craig, (1971). *"The reservoir Engineering Aspects of Waterflooding."* Society of Petroleum Engineers of AIME, Dallas.
7. J. R. Lien, (2010). *"PTEK212, Reservoir engineering I."* Compendium. University of Bergen.
8. K. S. Sorbie and M. I. J. van Dijke, (2005). *"Fundamentals of Three-Phase Flow in Porous Media of Heterogeneous Wettability."* Institute of Petroleum Engineering: Compendium.
9. A. Skauge and M. Skarestad, (2011). *"Reservoir engineering II, PTEK 213"*. Compendium. University of Bergen.
10. J. S. Buckley, et al., (1997). *"Asphaltenes and Crude Oil Wetting - The Effect of Oil Composition."* Presented at the SPE/DOE Improved Oil Recovery Symposium held in Tulsa, 21-24 April, 1996.
11. J. S. Buckley, et al., (1998). *"Mechanisms of Wetting Alteration by Crude Oils."* Presented at the 1997 SPE International Symposium on Oilfield Chemistry held in Houston, 18-21 February.
12. J. S. Buckley and Y. Liu, (1998). *"Some Mechanisms of Crude Oil/Brine/Solid Interactions."* Journal of Petroleum Science and Engineering 20 (1998) 155-160.
13. L. W. Lake, (1989). *"Enhanced Oil Recovery."* Prentice-Hall, Inc.
14. *"Double Layer Expansion"*.
http://web.nmsu.edu/~snsn/classes/chem435/Lab14/double_layer.html
[Downloaded 29.07.2013].
15. P. Atkins and J. D. Paula, (2006). *"Atkins Physical Chemistry."*, ed. E. Edition.: W.H. Freeman and Company.
16. S. Y. Lee, K. J. Webb, and I. Collins, (2010). *"Low-Salinity Oil Recovery: Increasing Understanding of the Underlying Mechanism."* Presented at the SPE Improved Oil Recovery Symposium, Tulsa, Oklahoma, USA. SPE 129722.
17. (2012). *"Zetasizer Nano User Manuel"*. Malvern Instruments Ltd, Instrumental Manual.
18. B. Fosse, (1995). *"Effect of Water Chemistry on Static and Dynamic Interfacial Tension at the Oil-Water and Oil-Water-Solids."* PhD Disseration. University of Bergen. .
19. S.H. Standal, (1999). *"Wettability of Solid Surfaces Induced by Adsorption of Polar Organic Components in Crude Oil."* Department of Chemistry, University of Bergen. Doctorial Thesis.

20. J. S. Buckley, (1996). *"Mechanism and Consequences of Wettability Alteration by Crude Oils."* Department of Petroleum Engineering. Heriot-Watt University. Doctorial Thesis.
21. J.G. Speight, (1991). *"The Chemistry and Technology of Petroleum." Second Edition, Revised and Expanded.*: Marcel Dekker, INC.
22. R. A. Nasralla and H. A. Nasr-El-Din, (2012). *"Double Layer Expansion: Is it a Primary Mechanism of Improved Oil Recovery by Low-Salinity Waterflooding?"*. Paper presented for presentation at the Eighteenth SPE Improved Oil Recovery Symposium held in Tulsa, Oklahoma, USA, 14-18 April 2012. SPE 154334.
23. R. D. Kulkarni and P. Somasundaran, (1976). *"Effects of Pretreatment on the Electrokinetic Properties of Quartz."* International Journal of Mineral Processing, 4 (1977) 89-09.
24. G. A. Parks, (1984). *"Surface and Interfacial Free Energies of Quartz."* Journal of Geophysical Research, June 10. **89**: p. 3997-4008.
25. J. Reisberg and T. M. Doscher, (1956). *"Interfacial Phenomena In Crude-Oil-Water Systems."* Producers Monthly. (Nov. 1956) 43-50.
26. H. Hermansen, (2008). *"The Ekofisk Field: Achieving Three Times the Original Value"*. 19th World Petroleum Congress, Spain 2008.
27. A. Lager, et al., (2008). *"LoSal™ Enhanced Oil Recovery: Evidence of Enhanced Oil Recovery at the Reservoir Scale"*. SPE/DOE Improved Oil Recovery Symposium held in Tulsa, Oklahoma, U.S.A 19-23 April 2008.
28. A. Ramez, et al., (2011). *"Efficiency of Oil Recovery by Low Salinity Water Flooding in Sandstone Reservoirs"*. SPE Western North America Regional Meeting held in Anchorage, Alaska, USA, 7-11 May 2011. SPE 144602.
29. A. Ramez, et al., (2011). *"Coreflood Study of Low Salinity Water Injection in Sandstone Reservoirs"*. SPE/DGS Saudi Arabia Section Technical Symposium and Exhibition held in Al-Khobar, Saudi Arabia, 15-18 May 2011. SPE 149077.
30. N. R. Morrow, M. Valat, and H. Yildiz, (1996). *"Effect of Brine Composition on Recovery of an Alaskan Crude Oil by Waterflooding"*. Western Research Institute/University of Wyoming . 47th Annual Technical Meeting of The Petroleum Society in Calgary, Alberta, Canada, June 10-12, 1996. Paper 96-94.
31. A. Ramez, et al., (2011). *"Impact of Electrical Surface Charges and Cation Exchange on Oil Recovery by Low Salinity Water."* Presented at Asia Pacific Oil and Gas Conference and Exhibition held in Jakarta, Indonesia, 20-22 September 2011. SPE 147937.
32. J. C. Martin, (1959). *"The Effect of Clay on the Displacement of Heavy Oil by Water"*. Society of Petroleum Engineering of A.I.M.E. Venezuelan 3rd Annual Meeting, 14-16 October. SPE 1411-G.
33. G. G. Bernard, (1967). *"Effect of Floodwater Salinity on Recovery of Oil from Cores Containing Clays"*. 38th Annual California Regional Meeting of the Society of Petroleum Engineers of A.I.M.E in Los Angeles, Calif. 26-27 October. SPE 1725.
34. P. P. Jadhunandan and N. R. Morrow, (1991). *"Spontaneous Imbibition of Water by Crude Oil/Brine/Rock Systems"*. Petroleum Recovery Research Center, New Mexico inst. of Mining and Technology, Socorro, NM (US).(15(4)): p. 319-345.
35. P. P. Jadhunandan and N. R. Morrow, (1995). *"Effect of Wettability on Waterfloods Recovery for Crude-Oil/Brine/Rock Systems"*. SPE, New Mexico Petroleum Recovery Research Center.
36. H. O. Yildiz and N. R. Morrow, (1996). *"Effect of Brine Composition on Recovery of Moutary Crude Oil by Waterflooding"*. Journal of petroleum Science and Engineering,

- New Mexico Petroleum Recovery Research Center, New Mexico and Western Research Institute, University of Wyoming. **14**: p. 159-168.
37. G. Q. Tang and N. R. Morrow, (1997). "*Salinity, Temperature, Oil Composition, and Oil Recovery by Waterflooding*". University of Wyoming. SPE 36680.
 38. N. R. Morrow, et al., (1998). "*Prospects of Improved Oil Recovery Related to Wettability and Brine Composition*". Journal of petroleum Science and Engineering 20 (1998). Department of Chemical and Petroleum Engineering, University of Wyoming, Laramie, WY 82071, USA: p. 267-276.
 39. G. Q. Tang and N. R. Morrow, (1999). "*Influence of Brine Composition and Fines Migration on Crude Oil/Brine/Rock Interactions and Oil Recovery*". Journal of Petroleum Science and Engineering 24 (1999). Department of Chemical and Petroleum Engineering, University of Wyoming, P.O. Box 3295, Laramie, WY 82071, USA.: p. 99-111.
 40. M. M. Sharma and P. R. Filoco, (2000). "*Effect of Brine Salinity and Crude-Oil Properties on Oil Recovery and Residual Saturation*". SPE Journal, University of Texas. SPE 65402. **5**.
 41. Y. Zang and N. R. Morrow, (2006). "*Comparison of Secondary and Tertiary Recovery With Change in Injection Brine Composition for Crude Oil/Sandstone Combinations*". University of Wyoming. Paper SPE 99757 presented at the SPE/DOE Symposium on Improved Oil Recovery, Tulsa, Oklahoma, 22-26 April.
 42. Y. Zhang, X. Xie, and N. R. Morrow, (2007). "*Waterflood Performance by Injection of Brine With Different Salinity for Reservoir Cores*". Paper was prepared for presentation at the 2007 SPE Annual Technical Conference and Exhibition held in Anaheim, California, U.S.A, 11-14 November 2007. SPE 109849, University of Wyoming. .
 43. K. J. Webb, C. J. J. Black, and H. AL-Ajeel, (2004). "*Low Salinity Oil Recovery - Log-Inject-Log*". Presented at the SPE/DOE Symposium on Improved Oil Recovery, Tulsa, Oklahoma, 17-21 April, SPE 89379.
 44. R. Gupta, et al., (2011). "*Enhanced Waterflood for Middle East Carbonate Cores - Impact of Injection Water Composition*". Presentation at the SPE Middle East Oil and Gas show and Conferenced held in Manama, Bahrain, 25-28 Sep. 2011. .
 45. J. Seccombe, et al., (2010). "*Demonstration of Low-Salinity EOR at Interwell Scale, Endicott Field, Alaska*". Presented for presentation at the 2010 SPE Improved Oil Recovery Symposium held in Tulsa, Oklahoma, USA, 24-28 April 2010.
 46. A. Skauge and B. Ottesen, (2002). "*A Summary of Experimentally Derived Relative Permeability and Residual Saturation on North Sea Reservoir Cores*". Paper SCA 2002-12 presented at the International Symposium of the Society of Vore Analysts, Monterey, California, USA, 22-25 september.
 47. J. C. Seccombe, et al., (2008). "*Designing a Tertiary Low Salinity EOR Waterflood for the Endicott Field*". Presented at the SPE IOR Symposium Tulsa, OK, 19-23 April. SPE 113480.
 48. P. L. McGuire, et al., (2005). "*Low Salinity Oil Recovery: An Exciting New EOR Opportunity for Alaska's North Slope*". Presented for presentation at the 2005 SPE Western Regional Meeting held in Irvine, CA. U.S.A., 30 March - 1 April 2005.
 49. K. Skettingland, et al., (2011). "*Snorre Low-Salinity-Water Injection-Coreflooding Experiments and Single-Well Field Pilot.*". Paper accepted for presentation at the SPE Improved Oil Recovery Symposium, Tulsa, 24-28 April 2010. SPE 129877.
 50. K. Webb, A. Lager, and C. Black, (2008). "*Comparison of High/Low Salinity Water/Oil Relative Permeability*". Paper prepared for presentation at the International Symposium of the Society of Core Analysts held in Abu Dhabi, UAE 29 October- 2 November, 2008.

51. A. Lager, et al., (2006). *"Low Salinity Oil Recovery - An Experimental Investigation"*. Presented at the International Symposium to the Society of Core Analysts, Trondheim Norway, September 12-16, 2006. Paper SCA2006-35.
52. N. R. Morrow and J. S. Buckley, (2011). *"Improved Oil Recovery by Low-Salinity Waterflooding"*. May 2011. SPE 129421.
53. E. C. Donaldson, R. D. Thomas, and P. B. Lorenz, (1969). *"Wettability Determination and Its Effect on Recovery Efficiency"*. SPE 2338.
54. R. N. Morrow, (1990). *"Wettability and Its effect on Oil Recovery"*. December 1990.
55. G. J. Hirasaki, (1991). *"Wettability: Fundamentals and Surface Forces"*. SPE, June 1991.
56. K. Sandengen, (2011). *"Experimental Evidence of Low Salinity Water Flooding Yielding a More Oil-Wet Behaviour"*. Paper presented at The International Symposium of the Society of Core Analysts held in Austin, Texas, USA 18-21 September, 2011.
57. A. Ashraf, et al., (2010). *"Laboratory Investigation of Low Salinity Waterflooding as Secondary Recovery Process: Effect of Wettability."*. Paper presented for presentation at the SPE Oil and Gas India Conference and Exhibition held in Mumbai, India, 20-22 January 2010.
58. T. Austad, A. RezaeiDoust, and T. Puntervold, (2010). *"Chemical Mechanism of Low Salinity Water Flooding in Sandstone Reservoir."*. Paper was presented for presentation at the 2010 SPE Improved Oil Recovery Symposium held in Tulsa, Oklahoma, USA, 24-28 April 2010.
59. R. Ehrlich and R. J. Wygal, (1997). *"Interrelation of Crude Oil and Rock Properties With the Recovery of Oil by Caustic Waterflooding."*. SPE Journal, vol. 17, no. 4, p. 263-270.
60. G. R. Jerauld, et al., (2006). *"Modeling Low-Salinity Waterflooding."*. Paper accepted for presentation at 2006 SPE Annual Technical Conference and Exhibition, San Antonio, Texas, 24-27 September. SPE 102239.
61. A. J. Valocchi, R. I. Street, and P. V. Roberts, (1981). *"Transport of Ion Exchanging Solutes in Ground Water: Chromatography Theory and Field Simulation."*. Vol. 17, no. 5, p. 1517-1527.
62. T. Amarson and R. G. Keil, (2000). *"Mechanisms of Pore Water Organic Matter Adsorption to Montmorillonite."*. *Marine Chemistry*, Vol. 71, p. 309-320.
63. G. Sposito, (1989). *"The Chemistry of Soils"*. Oxford University Press, Oxford, 275 pp.
64. J. S. Solbakken, (2010). *"An Experimental Study of Low Salinity Surfactant Flooding in Low Permeability Berea Sandstone."*. Master Thesis. University of Bergen.
65. D. J. Ligthelm, et al., (2009). *"Novel Waterflooding Strategy by Manipulation of Injection Brine Composition."*. Paper presented for presentation at the 2009 SPE EUROPEC/EAGE Annual Conference and Exhibition held in Amsterdam, The Netherlands, 8-11 June 2009. SPE 119835.
66. V. H. Olphen, (1963). *"An Introduction to Clay Colloid Chemistry."*. Interscience Publishers, John Wiley and Sons, New York.
67. H. G. Rueslatten, O. Hjelmeland, and O. M. Selle, (1994). *"Wettability of Reservoir Rocks and the Influence of Organo-Metallic Compounds."*. *North Sea Oil and Gas Reservoir*, Vol. 3, p. 317-324.
68. D. M. Clementz, (1982). *"Alteration of Rock Properties by Adsorption of Petroleum Heavy Ends."*. Implications of Enhanced Oil Recovery, April 1982. SPE/DOE 10683.
69. M. K. Li and H. S. Fogler, (1978). *"Acoustic Emulsification. Part 2: Breakup of the Large Primary Oil Droplets in a Water Medium."*. *Journal of Fluid Mechanics*. **88**: p. 513-528.

70. Daniel C. Harris, (2010). *"Quantitative Chemical Analysis."* Eighth Edition. . Clancy Marshall.
71. J. D. Cutnell and K. W. Johnson, (2010). *"Introduction to Physics."*, ed. t. Edition. John Wiley & Sons (Asia) Pte Ltd.
72. W. D. Harkins and F. E. Brown, (1919). *"Determination of Surface Tension (Free Surface Energy) and the Weight of Falling Drops: The surface Tension of Water and Benzene by the Capillary Height Method."* J. AM. Chem. Soc, (41): p. 499.
73. M. C. Wilkinson, (1972). *"Extended Use of, and Comments on, the Drop-Weight (Drop-Volume) Technique for the Determination of Surface and Interfacial Tension"*. Journal of Colloid and Interfaces Science. **40**(1): p. 14-25.
74. J. C. Earnshaw, et al., (1996). *"The Drop Volume Method for Interfacial Tension Determination: An Error Analysis"*. Journal of Colloid and Interface Science, (0015): p. 150-155.
75. Harley Y. Jennings, (1967). *"The Effect of Temperature and Pressure on the Interfacial Tension of Benzene-Water and Normal Decane-Water"*. Journal of Colloid and Interface Science. **24**: p. 323-329.
76. Z. Susana, R. Jhosgre, and A. L. López de Ramos, (2001). *"Interfacial Tension of Alane + Water Systems"*. J. Chem. Eng. . **46**(5): p. 1086-1088.
77. A. E. Nymark, (2010). *"Wetting Properties of Quartz Surfaces in Systems With Crude Oil, Water and Enzyme."*. Master Thesis. University of Bergen.
78. W. G. Anderson, (1986). *"Wettability Literature Survey- Part 2: Wettability Measurement."*. Society of Petroleum Engineers.
79. W. A. Derungs, (1956). *"Naphthenic Acid Corrosion - an Old Enemy of Petroleum Industry."*. Corrosion 12: p. 41-46.
80. Y. Bian, (2009). *"Non-Aqueous Phase Titration for Total Acid Number of Crude Oil."* Rice University, Texas, Houston, 08.10.2009.
81. H. M. Weiss, et al., (2000). *"The Norwegian Industry Guide to Organic Geochemical Analyses."*. Edition 4.0, 30. may 2000. Published by Norsk Hydro, Statoil, Geolab Nor, SINTEF and Norwegian Petroleum Directorate.
82. Linda K. Moen, (1996). *"Effects of the Reaction Environment on the Formation and Decomposition of Organic Acids in Oil."*. Master Thesis. University of Bergen.: p. 40.
83. J. Kaliyugarasan, (2013). *"Surface Chemistry Study of Low Salinity waterflood."*. Master Thesis. University of Bergen.
84. G. Tang and R. Morrow, (2002). *"Injection of Dilute Brine and Crude Oil/Brine/rock Interactions."*. American Geophysical Union.
85. A. Skauge, et al., (1999). *"Effects of Organic Acids and Bases and Oil Composition on Wettability."*. Society of Petroleum Engineering Inc.
86. J. S. Buckley and T. Fan, (2005). *"Crude Oil/Brine Interfacial Tension."*. Paper prepared for presentation at the International Symposium of the Society of Core Anlysts held in Toronto, Canada, 21-25 August.
87. C. S. Vijapurapu and D. N. Rao, (2003). *"Effect of Brine Dilution and Surfactant Concentration on Spreading and Wettability."*. Society of Petroleum Engineering Inc.

Appendix

This appendix presents all data used to calculate the results obtain in the experimental work.

All results presented in this thesis are given with a standard deviation or relative uncertainty.

Standard deviation is a measurement of how closely the data are clustered about the mean and is calculated by equation A.1.1 [70].

$$Error = \sqrt{\frac{\sum_i^n (x_i - \bar{x})^2}{N - 1}} \quad (\text{A.1.1})$$

Were N is the number of parallels, x_i is the value of parallel i , and \bar{x} is the average of the parallels.

To calculate the propagation of uncertainty when finding the mean value of parallels, equation A.1.2 was used.

$$e = \sqrt{\sum_i^n e_i^2} \quad (\text{A.1.2})$$

Were e_i is the i 'te standard deviation of parallel i .

A.1 Brines

This sub-chapter in appendix lists all recipes of the brines used and their concentrations.

Table A.1.1 lists all the information of the synthetic seawater, table A.1.2 for the high salinity water, table A.1.3 for low salinity water and table A.1.4 for the brines containing individually ions.

Table A.1.1 Composition, ionic concentrations and ionic strength in SSW.

Salt	Amount [mg]				
NaCl	24890.0				
KCl	670.0				
MgCl ₂ ·6H ₂ O	11130.0				
CaCl ₂ ·2H ₂ O	1725.0				
Na ₂ SO ₄	4055.0				
NaHCO ₃	195.0				
Total TDS	42665.0				
Ion	Concentration [mg/L]	Cations		Anions	
		mmole/L	meq/L	mmole/L	meq/L
Na ⁺	11071.0	481.56	481.56		
K ⁺	410.0	10.49	410.00		
Mg ²⁺	1329.0	54.67	109.34		
Ca ²⁺	475.0	11.85	23.70		
CO ₃ ²⁻	0.0			0.00	0.00
HCO ₃ ⁻	145.0			2.38	2.38
Cl ⁻	20288.0			572.30	572.30
SO ₄ ²⁻	2778.0			28.92	57.83
Total	36496.0		1024.60		632.51
Percent divalent ions:		12.99 %		9.14 %	
Ionic strength of the solution [mmole/L]: 724.25					

Table A.1.2 Composition, ionic concentrations and ionic strength in HS water.

Salt	Amount [mg]				
NaCl	27513.0				
KCl	744.0				
MgCl ₂ ·6H ₂ O	2166.0				
CaCl ₂ ·2H ₂ O	7942.0				
NaHCO ₃	0.0				
Total TDS	35267.0				
Ion	Concentration [mg/L]	Cations		Anions	
		mmole/L	meq/L	mmole/L	meq/L
Na ⁺	10822.9	470.77	470.77		
K ⁺	390.2	9.98	9.98		
Mg ²⁺	258.9	10.65	21.31		
Ca ²⁺	2165.1	54,02	108,04		
CO ₃ ²⁻	0,0			0,00	0,00
HCO ₃ ⁻	0,0			0,00	0,00
Cl ⁻	21629,8			610,10	610,10
SO ₄ ²⁻	0,0			0,00	0,00
Total	35267,0		610,10		610,10
Percent divalent ions:		21.20 %		-	
Ionic strength of the solution [mmole/L]: 674.8					

Table A.1.3 Composition, ionic concentrations and ionic strength in LS water.

Salt	Amount [mg]	
NaCl	2970.00	
Total TDS	2970.00	
Ion	[ppm]	[mmol/L]
Na ⁺	1169	50.85
Cl ⁻	1833	51.71
Total	3002	
Ionic Strength [mmole/L]: 51.28		

Table A.1.4 Amount of salt mixed to make the brines containing individual ions, and the ionic concentration.

Salt	Ion	Amount Salt [g]	Amount ion [g]	Ppm [mg/Kg]
CaCl ₂ ·2H ₂ O	Ca ²⁺	0.0184	0.0050	10.03
		0.0916	0.0250	49.96
		0.1834	0.0500	100.02
MgCl ₂ ·6H ₂ O	Mg ²⁺	0.0416	0.0050	9.95
		0.2087	0.0250	49.93
		0.4179	0.0500	99.99
K ₂ CO ₃	CO ₃ ²⁻	0.0057	0.0025	9.90
		0.0288	0.0125	50.02
		0.0575	0.0250	99.86
Na ₂ SO ₄	SO ₄ ²⁻	0.0037	0.0025	10.01
		0.0185	0.0125	50.00
		0.0371	0.0251	100.36
Na ₃ PO ₄ ·12H ₂ O	PO ₄ ³⁻	0.0100	0.0025	10.00
		0.0500	0.0125	50.00
		0.1000	0.0250	100.00
Na ₂ B ₄ O ₇ ·10H ₂ O	B ₄ O ₇ ²⁻	0.0063	0.0026	10.256
		0.0308	0.0125	50.140
		0.0615	0.0250	100.117

A.2 Density Data

This sub-chapter provides all density measurements obtained which were needed in the IFT calculations. The standard deviation was estimated based on variation in the measured data.

Table A.2.1 shows the density of the two different oils used in the IFT measurements.

Table A.2.1 Density measured for crude oil A-12 and Exp-12_{x&i}. Density of decane is also listed.

Oil Phase	Density ρ [g/mL]			Average Density ρ [g/mL]
	Parallel 1	Parallel 2	Parallel 3	
A-12	0.9203	0.9204	0.9202	0.9203\pm0.0001
Exp-12 _{x&i}	0.9629	0.9625	0.9628	0.9627\pm0.0002
Decane ¹				0.7300

¹Density vale decane is listed in encyclopedia.

Table A.2.2 presents the density measurements obtained for SSW, HS and LS water and the corresponding dilutions.

Table A.2.2 Density for SSW, HS and LS water and the corresponding dilutions. Density of deionized water is also listed.

Brine	[Vol %]	Density ρ [g/mL]		Average Density ρ [g/mL]
		Parallel 1	Parallel 2	
SSW	100	1.0150	1.0150	1.0150±0.0000
	50	1.0013	1.0017	1.0015±0.0003
	10	0.9909	0.9907	0.9908±0.0001
	6.67	0.9899	0.9899	0.9899±0.0000
	4.55	0.9892	0.9894	0.9893±0.0001
HS	100	1.0143	1.0141	1.0142±0.0001
	75	1.0111	1.0111	1.0111±0.0000
	50	1.0009	1.0013	1.0011±0.0003
	30	0.9977	0.9975	0.9976±0.0001
	10	0.9914	0.9910	0.9912±0.0003
	6.67	0.9900	0.9906	0.9903±0.0004
	4.55	0.9899	0.9897	0.9898±0.0001
LS		0.9984	0.9982	0.9983±0.0001
Deionized water ¹				0.9975

¹Density value for deionized water is listed in encyclopedia.

Table A.2.3 shows all density measurements for brines containing 10, 50 or 100 ppm Ca^{2+} , CO_3^{2-} , Mg^{2+} , SO_4^{2-} , PO_4^{3-} , $\text{B}_4\text{O}_7^{2-}$.

Table A.2.3 Density for brines containing 10, 50 or 100 ppm Ca²⁺, CO₃²⁻, Mg²⁺, SO₄²⁻, PO₄³⁻, B₄O₇²⁻.

Ion	Ppm [mg/Kg]	Density, ρ [g/mL]		Density, ρ [g/mL]
		Parallel 1	Parallel 2	
Ca ²⁺	10.03	1.0001	0.9998	0.9999±0.0002
	49.96	1.0002	1.0002	1.0002±0.0000
	100.02	1.0004	1.0002	1.0003±0.0001
Mg ²⁺	9.95	1.0042	1.0046	1.0044±0.0003
	49.93	1.0049	1.0047	1.0048±0.0001
	99.99	1.0056	1.0056	1.0056±0.0000
CO ₃ ²⁻	9.90	0.9994	0.9990	0.9992±0.0003
	50.02	0.9990	0.9996	0.9993±0.0004
	99.86	0.9995	0.9993	0.9994±0.0001
SO ₄ ²⁻	10.01	0.9990	0.9992	0.9991±0.0001
	50.00	0.9989	0.9989	0.9989±0.0000
	100.36	0.9990	0.9994	0.9992±0.0003
PO ₄ ³⁻	10.00	0.9988	0.9990	0.9989±0.0001
	50.00	0.9989	0.9991	0.9990±0.0001
	100.00	0.9994	0.9987	0.9991±0.0005
B ₄ O ₇ ²⁻	10.256	1.0022	1.0020	1.0021±0.0001
	50.140	1.0036	1.0032	1.0034±0.0003
	100.12	1.0063	1.0060	1.0062±0.0002

A.3 SARA-Analyses and TAN

All the data needed to calculate the total acid number and SARA-content in the oils are provided in this sub-chapter.

A.3.1 Saturated, Aromatic and Resins Content

Table A.3.1 provides the densities of the different solvents used to separate the constituents in the oils by chromatography. Densities were needed to calculate the amount of saturate, aromatic and resin content in the oils.

Table A.3.1 Density of solvents at ambient temperature.

Solvent	Density ρ [g/mL]
Hexane	0.6548
DCM ¹ /Hexane (10:90)	0.7223
DCM/MeOH (50:50)	1.0609

¹DCM= dichloromethane

Table A.3.2 summarizes the amount of eluate collected from the chromatography. Each solvent contains their corresponding dissolved crude oil constituent.

Table A.3.2 Amount of eluate stored from chromatography.

Weight of solvent [g]			
Solvent	A-12	Exp-12 _{x&i}	Exp-12
Hexane	1.6755	1.3938	1.7051
DCM/Hexane (10:90)	0.9855	1.5411	1.1606
DCM/MeOH (50:50)	2.2928	0.9677	0.7532
Solvent [mL]			
Solvent	A-12	Exp-12 _{x&i}	Exp-12
Hexane	2.5588	2.1286	2.6040
DCM/Hexane (10:90)	1.3644	2.1336	1.6068
DCM/MeOH (50:50)	2.1612	0.9122	0.7100

Table A.3.3 lists the measured amount of saturate, aromatic and resin content in the oils.

Table A.3.3 Fraction of aliphatic, aromatic and polar content in the oils.

Oil A-12				
Constituent	Parallell 1 [mg]	Parallell 2 [mg]	Mean [mg]	SD
Aliphatic	0.1408	0.1426	0.1417	0.0013
Aromatic	0.0408	0.0427	0.0418	0.0013
Polar	0.0312	0.034	0.0326	0.0020
Exp-12 _{x&i}				
Constituent	Parallell 1 [mg]	Parallell 2 [mg]	Mean [mg]	SD
Aliphatic	0.1391	0.1432	0.1412	0.0029
Aromatic	0.0182	0.0197	0.0190	0.0011
Polar	0.0401	0.0408	0.0405	0.0005
Exp-12				
Constituent	Parallell 1 [mg]	Parallell 2 [mg]	Mean [mg]	SD
Aliphatic	0.1399	0.1346	0.1373	0.0037
Aromatic	0.0366	0.0378	0.0372	0.0008
Polar	0.0482	0.0500	0.0491	0.0013

A.3.2 Asphaltene Precipitation

Table A.3.4 shows the results of each weighted parallel of asphaltenes.

Table A.3.4 Amount of asphaltene weighted in the centrifuge tubes.

Oil	Parallel 1 [g]	Parallel 2 [g]	Parallel 3 [g]
A-12	N/A	0.0173	0.0160
Exp-12 _{x&i}	0.0202	0.0186	N/A
Exp-12	0.0333	0.0346	N/A

Table A.3.5 lists the weighted amount of asphaltene in the oils.

Table A.3.5 Amount of asphaltene in the oils.

Oil	Parallel 1 [mg/g]	Parallel 2 [mg/g]	Parallel 3 [mg/g]	Mean [mg/g]	SD
A-12	N/A	34.42	31.96	33.19	1.74
Exp-12 _{x&i}	39.87	37.17	N/A	38.52	1.91
Exp-12	66.08	68.97	N/A	67.53	2.04

A.3.3 Total Acid Number

Table A.3.6 summarizes the concentration of KOH in iso-propanol (titrant), molecular weight of KOH and the molarity of the blank. These properties are needed in the calculation of TAN.

Table A.3.6 Property of the titrant.

Property	A-12	Exp-12 _{x&i}	Exp-12
Titrant: KOH in iso-propanol [mol/L]	0.0411	0.0411	0.0411
Mm (KOH) [g/mol]	56.103	56.106	56.106
Blank [mmol]	0.0058	0.0058	0.0058

Figure A.3.1 illustrates the equivalence point for crude oil A-12 measured by base titration.

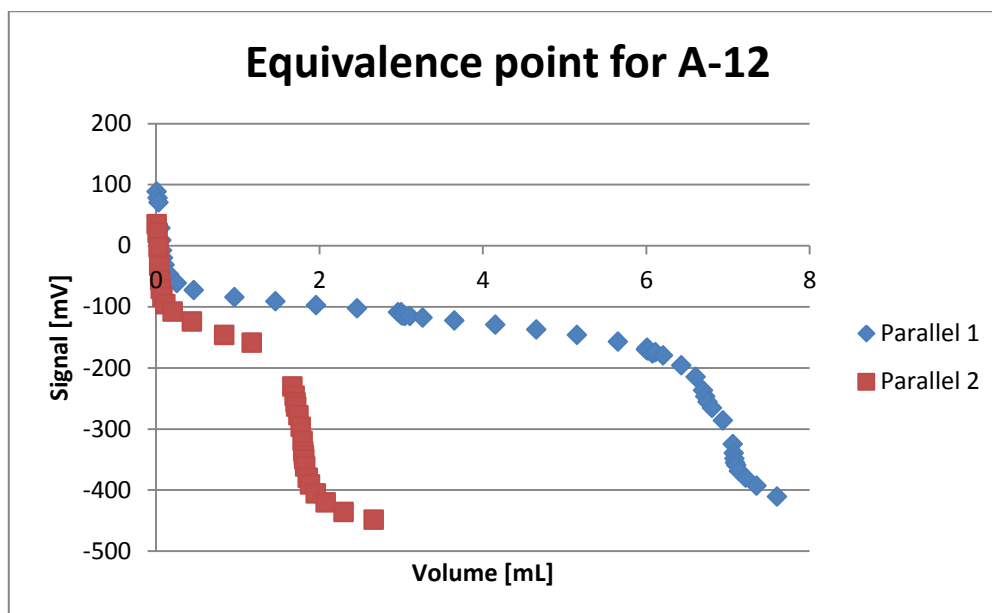


Figure A.3.1 Graph showing the equivalence point for crude oil A-12. The equivalence points are listed in table A.3.7.

Table A.3.7 lists the amount of crude oil A-12 sample used, volume titrant needed for neutralization, concentration of acid components and the resulting total acid number.

Table A.3.7 Total acid number obtained for crude oil A-12.

Parallel	Crude oil A-12 [g]		Volume titrant [mL]	Molality [mmol]	TAN [mg KOH/g]
1	4.1225	EQP 1	6.7011	0.2751	3.66 ¹
		EQP 2	7.0744	0.2904	3.87
2	1.0104	EQP	1.8086	0.0742	3.80
Average					3.84±0.05

¹This value was not used in the calculation of average EQP.

Figure A.3.2 illustrates the equivalence point for crude oil Exp-12_{x&i} measured by base titration.

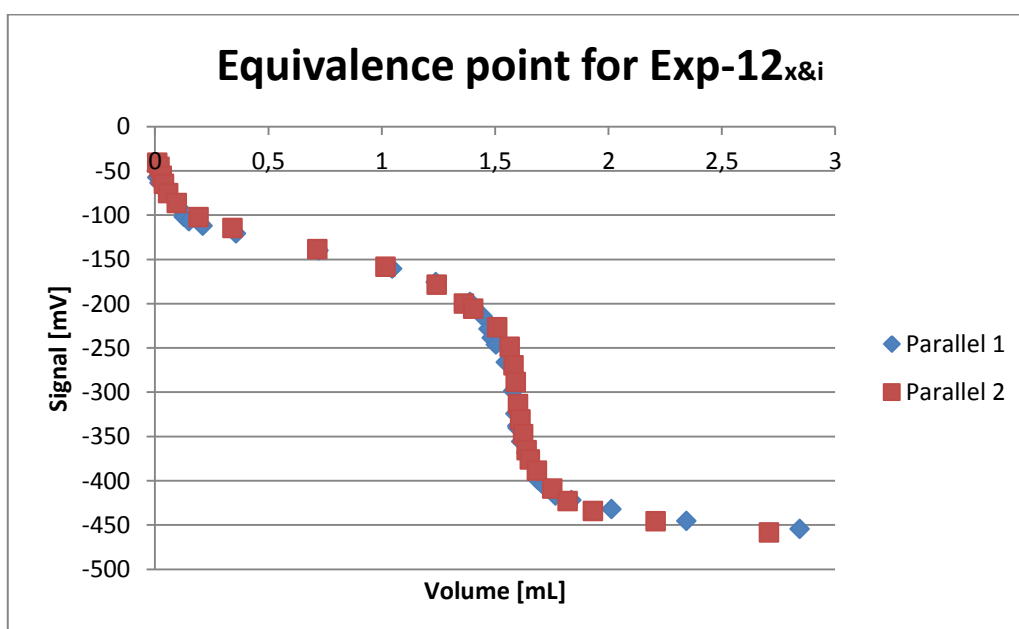


Figure A.3.2 Graph showing the equivalence point for crude oil Exp-12_{x&i}. The equivalence points are listed in table A.3.8.

Table A.3.8 lists the amount of crude oil Exp-12_{x&i} sample used, volume titrant needed for neutralization, concentration of acid components and the resulting total acid number.

Table A.3.8 Total acid number obtained for crude Exp-12_{x&i}

Parallel	Oil [g]	Volume titrant [mL]	Molarity [mmol]	TAN [mg KOH/g]
1	1.9989	EQP	1.598	1.68
2	2.0104	EQP	1.611	1.68
Average				1.68±0.01

Figure A.3.3 illustrates the equivalence point for crude oil Exp-12 measured by base titration.

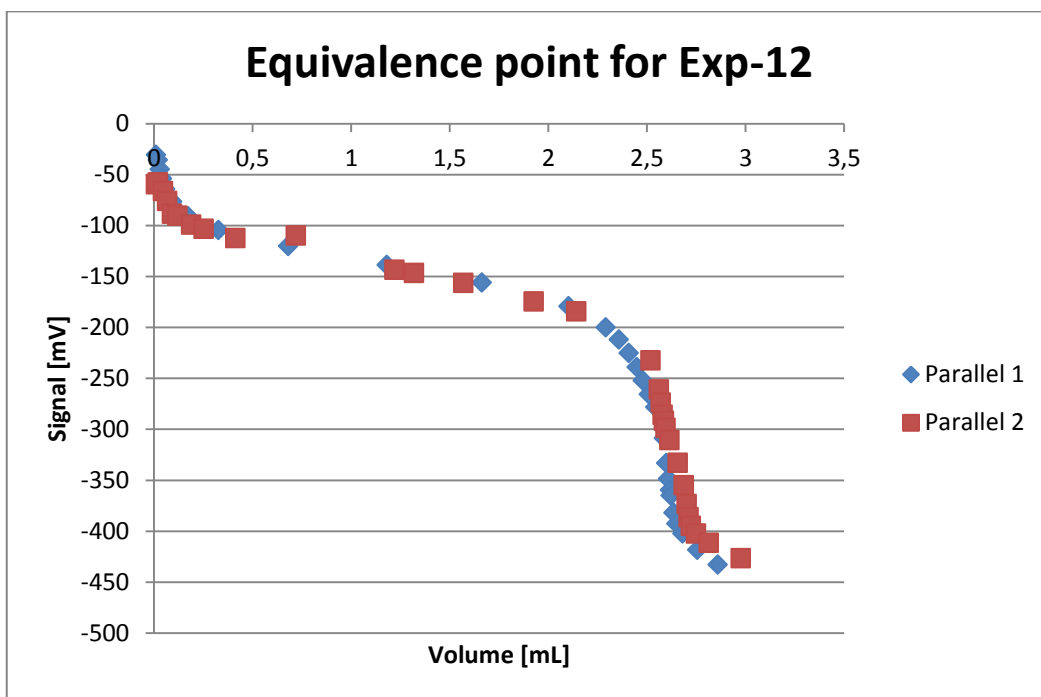


Figure A.3.3 Graph showing the equivalence point for crude oil Exp-12. The equivalence points are listed in table A.3.9.

Table A.3.9 lists the amount of crude oil Exp-12 sample used, volume titrant needed for neutralization, concentration of acid components and the resulting total acid number.

Table A.3.9 Total acid number obtained for crude Exp-12.

Parallel	Oil [g]		Volume titrant [mL]	Molarity [mmol]	TAN [mg KOH/g]
1	2.0009	EQP	2.617	0.1074	2.85
2	2.0064	EQP	2.586	0.1062	2.81
Average					2.83±0.03

A.4 Zeta-Potential and Electrophoretic Mobility

Measurements

This chapter provides all the data generated from the measured electrophoretic mobility and zeta-potential between the crude oils and brine emulsions.

Crude oil A-12 and Exp-12_{x&i} contained acidic and basic components. The change in pH of the aqueous phase after adding one drop of oil is presented after the measurements in each sub-chapter.

A.4.1 Crude Oil A-12/Brine Emulsions

Table A.4.1 lists the electrophoretic mobility and table A.4.2 lists the zeta-potential obtained for crude oil A-12/brine emulsion at the given pH. The emulsion consisted of 5 μ L oil dispersed in 10 mL $\frac{1}{2}$ LS water, $\frac{1}{44}$ SSW and $\frac{1}{44}$ HS water. Table A.4.3 shows the change in pH of the brine phase when one drop of oil is mixed.

Table A.4.1 Electrophoretic mobility for crude oil A-12/brine emulsion at the given pH. pH-meter uncertainty ± 0.01 .

1/44 SSW - [$\mu\text{mcm/Vs}$]				
pH	Parallel 1	Parallel 2	Parallel 3	Mean
2.10	-2.67 \pm 0.1	-2.55 \pm 0.2	-	-2.61 \pm 0.2
3.87	-2.96 \pm 0.09	-2.73 \pm 0.2	-	-2.85 \pm 0.2
6.18	-3.62 \pm 0.2	-3.75 \pm 0.08	-	-3.68 \pm 0.2
7.06	-3.99 \pm 0.1	-3.87 \pm 0.09	-	-3.93 \pm 0.1
8.49	-3.98 \pm 0.09	-4.17 \pm 0.08	-	-4.08 \pm 0.1
9.36	-3.87 \pm 0.06	-3.69 \pm 0.07	-	-3.78 \pm 0.09
1/44 HS - [$\mu\text{mcm/Vs}$]				
pH	Parallel 1	Parallel 2	Parallel 3	Mean
2.02	-1.05 \pm 0.09	-0.73 \pm 0.07	-	-0.89 \pm 0.1
3.89	-1.56 \pm 0.2	-1.35 \pm 0.2	-	-1.46 \pm 0.3
5.88	-2.86 \pm 0.2	-2.98 \pm 0.08	-	-2.92 \pm 0.2
6.91	-3.14 \pm 0.08	-3.19 \pm 0.3	-	-3.17 \pm 0.3
8.83	-3.38 \pm 0.08	-3.27 \pm 0.09	-	-3.33 \pm 0.1
10.96	-3.21 \pm 0.05	-3.47 \pm 0.1	-	-3.34 \pm 0.1
1/2 LS - [$\mu\text{mcm/Vs}$]				
pH	Parallel 1	Parallel 2	Parallel 3	Mean
2.16	-3.43 \pm 0.1	-4.14 \pm 0.1	-4.52 \pm 0.06	-4.03 \pm 0.2
4.01	-4.91 \pm 0.2	-4.27 \pm 0.1	-	-4.59 \pm 0.3
5.93	-5.22 \pm 0.3	-5.87 \pm 0.2	-	-5.55 \pm 0.4
6.78	-5.48 \pm 0.2	-4.91 \pm 0.3	-	-5.19 \pm 0.4
8.03	-6.00 \pm 0.2	-6.99 \pm 0.2	-5.42 \pm 0.3	-6.14 \pm 0.4
10.86	-7.41 \pm 0.2	-7.03 \pm 0.1	-	-7.22 \pm 0.2

Table A.4.2 Zeta-potential for crude oil A-12/brine emulsion at the given pH. pH-meter uncertainty ± 0.01 .

1/44 SSW - [mV]				
pH	Parallel 1	Parallel 2	Parallel 3	Mean
2,10	-34.1 \pm 1	-32.5 \pm 2	-	-33.3 \pm 3
3,87	-37.7 \pm 1	-34.8 \pm 2	-	-36.3 \pm 2
6,18	-46.1 \pm 3	-47.9 \pm 1	-	-47.0 \pm 3
7,06	-50.8 \pm 1	-49.3 \pm 1	-	-50.1 \pm 2
8,49	-50.8 \pm 1	-53.2 \pm 1	-	-52.0 \pm 2
9,36	-49.9 \pm 0.8	-47.1 \pm 0.9	-	-48.5 \pm 1
1/44 HS - [mV]				
pH	Parallel 1	Parallel 2	Parallel 3	Mean
2,02	-13.4 \pm 1	-9.3 \pm 0.9	-	-11.4 \pm 1
3,89	-19.9 \pm 3	-17.3 \pm 2	-	-18.6 \pm 4
5,88	-36.4 \pm 3	-38.0 \pm 1	-	-37.2 \pm 3
6,91	-40.1 \pm 1	-40.8 \pm 4	-	-40.5 \pm 4
8,83	-43.1 \pm 1	-41.8 \pm 1	-	-42.5 \pm 2
10,96	-40.9 \pm 0.6	-44.3 \pm 2	-	-42.6 \pm 2
1/2 LS -[mV]				
pH	Parallel 1	Parallel 2	Parallel 3	Mean
2,16	-43.8 \pm 2	-52.8 \pm 1	-57.6 \pm 0.8	-51.4 \pm 2
4,01	-62.6 \pm 3	-54.4 \pm 4	-	-58.5 \pm 5
5,93	-66.6 \pm 4	-74.8 \pm 3	-	-70.7 \pm 5
6,78	-69.9 \pm 3	-62.6 \pm 4	-	-66.3 \pm 5
8,03	-76.5 \pm 23	-89.2 \pm 2	-69.1 \pm 4	-78.3 \pm 5
10,86	-94.6 \pm 3	-89.7 \pm 2	-	-92.2 \pm 3

Figure A.4.1 displays the electrophoretic mobility between crude oil A-12 and 2.3% SSW, 2.3% HS water and 50% LS water. Further, figures A.4.2, A.4.3 and A.4.4 show individually the electrophoretic mobility as a function of pH. These figures are added as an example of the generated electrophoretic mobility between emulsions which had been set in the ultrasonic bath immediately after crude oil had been added to the brine and shaken, see section 5.4.2.

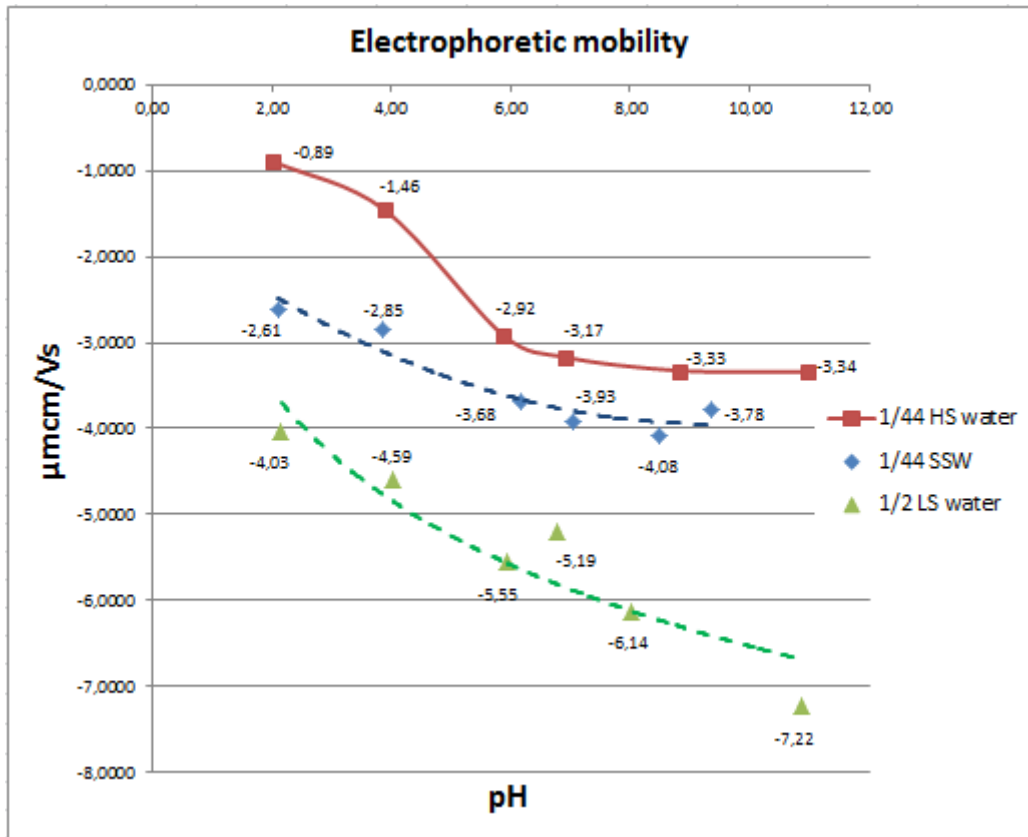


Figure A.4.1 Electrophoretic mobility of crude oil A-12 dispersed in 2.3% diluted SSW and 2.3% HS water, and 50% LS water. The pH was varied from 2.00-11.00. pH-meter uncertainty ± 0.01 .

Table A.4.3 Change in pH (brine phase) by generating an emulsion of 5 μL crude oil A-12 in 10.0 mL Brine. pH-meter uncertainty ± 0.01 .

1/2 LS			1/44 SSW			1/44 HS		
pH initial	pH w/ oil	ΔpH	pH initial	pH w/ oil	ΔpH	pH initial	pH w/ oil	ΔpH
2.18	2.16	-0.02	2.12	2.1	-0.02	2.04	2.02	-0.02
4.16	4.01	-0.15	3.98	3.87	-0.11	3.95	3.89	-0.06
6.12	5.93	-0.19	6.22	6.18	-0.04	6.04	5.88	-0.16
7.54	6.78	-0.76	7.46	7.06	-0.40	7.53	6.91	-0.62
9.13	8.03	-1.10	9.06	8.49	-0.57	9.14	8.83	-0.31
11.12	10.86	-0.26	9.68	9.36	-0.32	11.16	10.96	-0.20

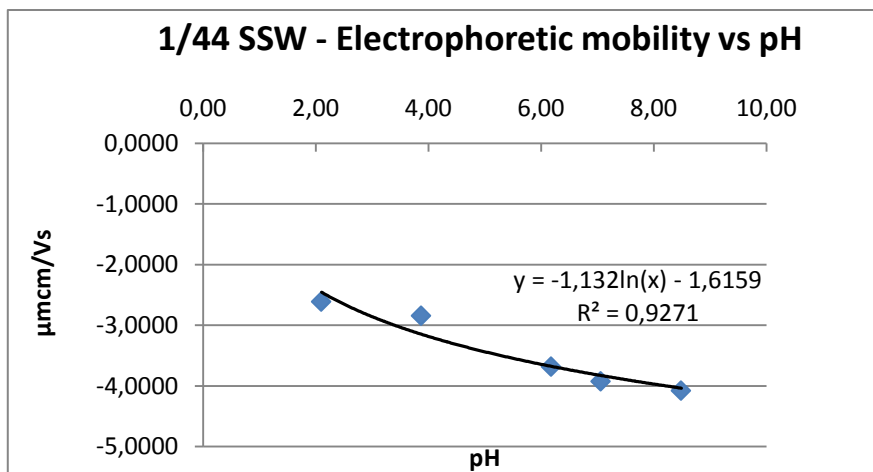


Figure A.4.2 The electrophoretic mobility of crude oil A-12 dispersed in 2.3% SSW as a function of pH. pH-meter uncertainty ± 0.01 .

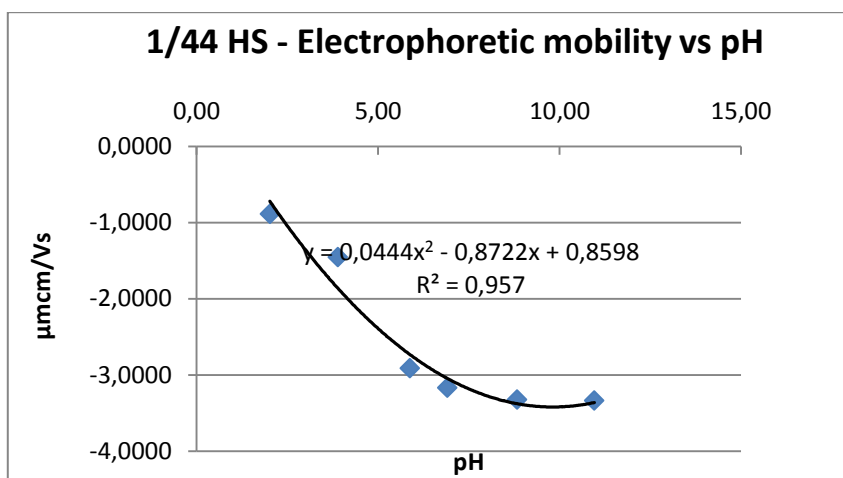


Figure A.4.3 The electrophoretic mobility of crude oil A-12 dispersed in 2.3% HS water as a function of pH. pH-meter uncertainty ± 0.01 .

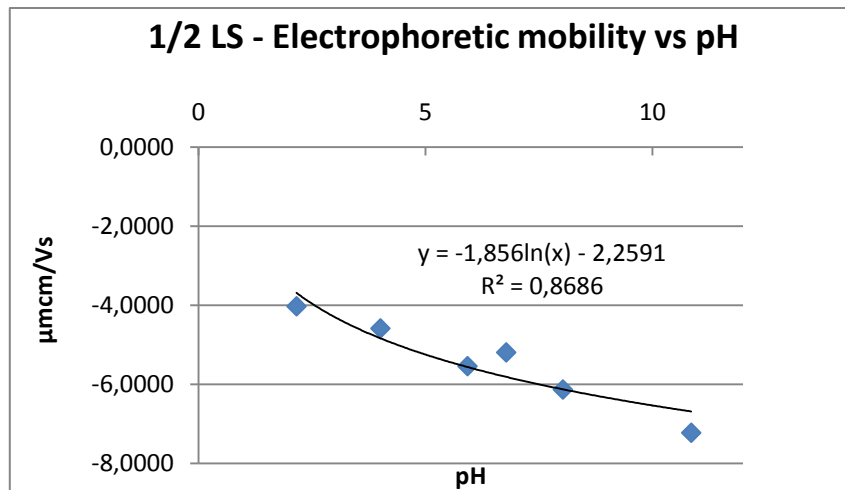


Figure A.4.4 The electrophoretic mobility of crude oil A-12 dispersed in 50% LS water as a function of pH. pH-meter uncertainty ± 0.01 .

A.4.2 Crude Oil Exp-12_{x&i}/Brine Emulsions

Table A.4.4 lists the electrophoretic mobility and table A.4.5 lists the zeta-potential obtained for crude oil Exp-12_{x&i}/brine emulsion at the solutions genuine pH, but changed as crude oil was added. The emulsion consisted of 5 µL oil dispersed in 10 mL LS water containing 10, 50 or 100 ppm Ca²⁺, Mg²⁺, CO₃²⁻, SO₄²⁻, PO₄³⁻, B₄O₇²⁻. Table A.4.6 shows the change in pH of the brine phase when one drop of oil is mixed. Figure A.4.5 shows the electrophoretic mobility between 5 µL crude oil Exp-12_{x&i} in 10 mL LS water containing 10, 50 or 100 ppm Ca²⁺, Mg²⁺, CO₃²⁻, SO₄²⁻, B₄O₇²⁻ or PO₄³⁻.

Table A.4.4 Electrophoretic mobility for crude oil Exp-12_{x&i} dispersed in brine at the given pH. pH-meter uncertainty ± 0.01 .

LS + Ca²⁺ - [$\mu\text{mcm/Vs}$]					
pH	ppm	Parallel 1	Parallel 2	Parallel 3	Mean
5.88	10	-3.74 \pm 0.07	-3.41 \pm 0.07	-	-3.58 \pm 0.09
5.94	50	-2.99 \pm 0.1	-2.76 \pm 0.04	-3.01 \pm 0.1	-2.92 \pm 0.2
5.97	100	-2.34 \pm 0.08	-2.35 \pm 0.1	-2.24 \pm 0.1	-2.31 \pm 0.2
LS + Mg²⁺ - [$\mu\text{mcm/Vs}$]					
pH	ppm	Parallel 1	Parallel 2	Parallel 3	Mean
6.58	10	-4.33 \pm 0.1	-4.18 \pm 0.1	-	-4.26 \pm 0.1
6.33	50	-2.76 \pm 0.04	-3.01 \pm 0.1	-2.54 \pm 0.1	-2.77 \pm 0.2
5.99	100	-2.24 \pm 0.1	-2.37 \pm 0.09	-2.35 \pm 0.1	-2.32 \pm 0.2
LS + SO₄²⁻ - [$\mu\text{mcm/Vs}$]					
pH	ppm	Parallel 1	Parallel 2	Parallel 3	Mean
7.23	10	-3.48 \pm 0.09	-3.27 \pm 0.1	-3.31 \pm 0.1	-3.35 \pm 0.2
6.80	50	-3.16 \pm 0.1	-3.08 \pm 0.1	-	-3.12 \pm 0.2
6.49	100	-2.79 \pm 0.1	-2.58 \pm 0.1	-	-2.69 \pm 0.2
LS + CO₃²⁻ - [$\mu\text{mcm/Vs}$]					
pH	ppm	Parallel 1	Parallel 2	Parallel 3	Mean
8.87	10	-6.02 \pm 0.09	-5.77 \pm 0.09	-	-5.89 \pm 0.1
9.85	50	-5.89 \pm 0.2	-5.65 \pm 0.1	-6.02 \pm 0.2	-5.85 \pm 0.3
9.93	100	-5.84 \pm 0.2	-5.71 \pm 0.1	-	-5.77 \pm 0.2
LS + PO₄³⁻ - [$\mu\text{mcm/Vs}$]					
pH	ppm	Parallel 1	Parallel 2	Parallel 3	Mean
8.85	10	-4.92 \pm 0.2	-4.89 \pm 0.1	-	-4.90 \pm 0.2
10.36	50	-5.32 \pm 0.08	-5.56 \pm 0.1	-	-5.44 \pm 0.2
10.61	100	-5.42 \pm 0.08	-5.42 \pm 0.2	-	-5.42 \pm 0.2
LS + B₄O₇²⁻ - [$\mu\text{mcm/Vs}$]					
pH	ppm	Parallel 1	Parallel 2	Parallel 3	Mean
8.29	10	-4.55 \pm 0.2	-4.43 \pm 0.1	-5.09 \pm 0.2	-4.49 \pm 0.3
8.84	50	-5.12 \pm 0.2	-5.27 \pm 0.2	-	-5.20 \pm 0.2
8.96	100	-5.32 \pm 0.3	-5.85 \pm 0.09	-6.07 \pm 0.2	-5.75 \pm 0.3
LS - [$\mu\text{mcm/Vs}$]					
pH		Parallel 1	Parallel 2	Parallel 3	Mean
7.85		-3.93 \pm 0.2	-4.27 \pm 0.1	-3.47 \pm 0.1	-3.89 \pm 0.2

Table A.4.5 Zeta-potential for crude oil Exp-12_{x&i} dispersed in brine at the given pH. pH-meter uncertainty ± 0.01 .

LS + Ca²⁺ - [mV]					
pH	ppm	Parallel 1	Parallel 2	Parallel 3	Mean
5.88	10	-47.7 \pm 0.8	-43.5 \pm 0.8	-	-45.6 \pm 1
5.94	50	-38.2 \pm 2	-35.2 \pm 0.5	-38.4 \pm 1	-37.3 \pm 2
5.97	100	-29.9 \pm 1	-30.0 \pm 1	-28.6 \pm 2	-29.5 \pm 2
LS + Mg²⁺ - [mV]					
pH	ppm	Parallel 1	Parallel 2	Parallel 3	Mean
6.58	10	-55.2 \pm 1	-53.3 \pm 1	-	-54.3 \pm 2
6.33	50	-35.2 \pm 0.5	-38.4 \pm 1	-32.4 \pm 1	-35.3 \pm 2
5.99	100	-28.6 \pm 2	-30.2 \pm 1	-30.0 \pm 1	-29.6 \pm 2
LS + SO₄²⁻ - [mV]					
pH	ppm	Parallel 1	Parallel 2	Parallel 3	Mean
7.23	10	-44.4 \pm 1	-41.7 \pm 2	-42.2 \pm 2	-42.3 \pm 3
6.80	50	-40.3 \pm 2	-39.2 \pm 2	-	-39.8 \pm 3
6.49	100	-35.6 \pm 2	-33.0 \pm 2	-	-34.3 \pm 2
LS + CO₃²⁻ - [mV]					
pH	ppm	Parallel 1	Parallel 2	Parallel 3	Mean
8.87	10	-76.7 \pm 1	-73.6 \pm 1	-	-75.2 \pm 3
9.85	50	-75.2 \pm 3	-72.1 \pm 2	-76.7 \pm 2	-74.7 \pm 4
9.93	100	-74.4 \pm 2	-72.9 \pm 2	-	-73.7 \pm 3
LS + PO₄³⁻ - [mV]					
pH	ppm	Parallel 1	Parallel 2	Parallel 3	Mean
8.85	10	-62.7 \pm 2	-62.5 \pm 2	-	-62.6 \pm 2
10.36	50	-67.9 \pm 1	-70.9 \pm 2	-	-69.4 \pm 2
10.61	100	-69.1 \pm 1	-69.1 \pm 2	-	-69.1 \pm 2
LS + B₄O₇²⁻ - [mV]					
pH	ppm	Parallel 1	Parallel 2	Parallel 3	Mean
8.29	10	-58.0 \pm 3	-56.5 \pm 2	-64.9 \pm 2	-57.3 \pm 4
8.84	50	-65.3 \pm 2	-67.3 \pm 2	-	-66.3 \pm 3
8.96	100	-67.9 \pm 3	-74.6 \pm 1	-77.4 \pm 2	-73.3 \pm 4
LS - [mV]					
pH		Parallel 1	Parallel 2	Parallel 3	Mean
7.85		-50.1 \pm 2	-54.5 \pm 2	-44.2 \pm 1	-49.6 \pm 3

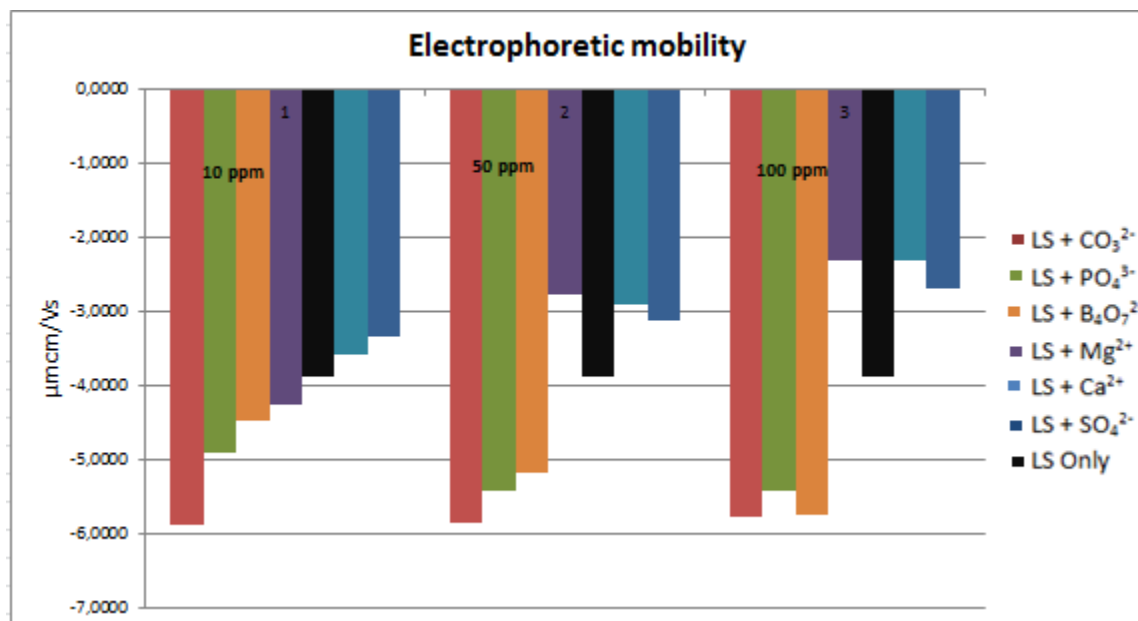


Figure A.4.5 Electrophoretic measurements of 5 μL crude oil Exp-12_{x&i} in 10 mL LS water containing 10, 50 or 100 ppm Ca²⁺, Mg²⁺, CO₃²⁻, SO₄²⁻, B₄O₇²⁻ or PO₄³⁻.

Table A.4.6 Change in pH (brine phase) by generating an emulsion of 5 μL Exp-12_{x&i} and 10.0 mL brine. pH-meter uncertainty ± 0.01 .

Ca²⁺				Mg²⁺			
Ppm	pH initial	pH o/w system	ΔpH	Ppm	pH initial	pH o/w system	ΔpH
10	6.05	5.88	-0.17	10	7.52	6.58	-0.94
50	6.04	5.94	-0.10	50	6.19	6.33	0.14
100	6.00	5.97	-0.03	100	5.95	5.99	0.04
CO₃²⁻				PO₄³⁻			
Ppm	pH initial	pH o/w system	ΔpH	Ppm	pH initial	pH o/w system	ΔpH
10	9.47	8.87	-0.60	10	9.53	8.85	-0.68
50	10.08	9.85	-0.23	50	10.42	10.36	-0.06
100	10.34	9.93	-0.41	100	10.76	10.61	-0.15
SO₄²⁻				LS			
Ppm	pH initial	pH o/w system	ΔpH	pH initial	pH o/w system	ΔpH	
10	6.00	7.23	1.23	6.24	7.85	1.61	
50	6.03	6.80	0.77				
100	6.02	6.49	0.47				
B₄O₇²⁻							
Ppm	pH initial	pH o/w system	ΔpH				
10	8.69	8.29	-0.40				
50	8.96	8.84	-0.12				
100	9.02	8.96	-0.06				

A.4.3 Crude Oil Exp-12_{x&i}/Brine Emulsions at Constant Brine Molality

Table A.4.7 lists the electrophoretic mobility and table A.4.8 lists the zeta-potential obtained for crude oil Exp-12_{x&i}/brine emulsion. The pH of the solutions was adjusted to 4 and 9 but as crude oil was added, the pH changed. The emulsions consisted of 5 μL oil dispersed in 6 mL LS water containing 10, 50 or 100 ppm Ca²⁺, Mg²⁺, CO₃²⁻, SO₄²⁻, PO₄³⁻, B₄O₇²⁻.

The molality of the brines was held constant at 6.61E^{-8} mole/Kg.

Figure A.4.6 summarizes electrophoretic mobility results.

Table A.4.7 Electrophoretic mobility of crude oil Exp-12_{x&i}/brine emulsion at the given pH. pH-meter uncertainty ± 0.01 .

LS + Mg²⁺ - [$\mu\text{mcm/Vs}$]			
pH	Parallel 1	Parallel 2	Mean
4.02	-1.03 \pm 0.01	-1.21 \pm 0.08	-1.12 \pm 0.08
8.99	-4.06 \pm 0.1	-3.94 \pm 0.06	-4.00 \pm 0.1
LS + Ca²⁺ - [$\mu\text{mcm/Vs}$]			
pH	Parallel 1	Parallel 2	Mean
3.99	-0.36 \pm 0.04	-0.67 \pm 0.02	-0.51 \pm 0.04
8.98	-3.18 \pm 0.09	-3.07 \pm 0.1	-3.12 \pm 0.2
LS + SO₄²⁻ - [$\mu\text{mcm/Vs}$]			
pH	Parallel 1	Parallel 2	Mean
4.08	-1.72 \pm 0.07	-1.99 \pm 0.04	-1.86 \pm 0.08
8.95	-4.32 \pm 0.06	-4.36 \pm 0.05	-4.34 \pm 0.08
LS + CO₃²⁻ - [$\mu\text{mcm/Vs}$]			
pH	Parallel 1	Parallel 2	Mean
3.97	-1.83 \pm 0.06	-2.03 \pm 0.04	-1.94 \pm 0.08
8.95	-4.23 \pm 0.07	-4.20 \pm 0.1	-4.22 \pm 0.1
LS + PO₄³⁻ - [$\mu\text{mcm/Vs}$]			
pH	Parallel 1	Parallel 2	Mean
3.97	-0.93 \pm 0.03	-0.66 \pm 0.02	-0.80 \pm 0.07
9.01	-4.42 \pm 0.1	-4.19 \pm 0.07	-4.30 \pm 0.1
LS + B₄O₇²⁻ - [$\mu\text{mcm/Vs}$]			
pH	Parallel 1	Parallel 2	Mean
3.98	-1.14 \pm 0.04	-1.16 \pm 0.06	-1.15 \pm 0.07
8.95	-4.53 \pm 0.1	-4.44 \pm 0.08	-4.48 \pm 0.1
LS - [$\mu\text{mcm/Vs}$]			
pH	Parallel 1	Parallel 2	Mean
4.01	-0.69 \pm 0.05	-0.86 \pm 0.04	-0.77 \pm 0.06
9.06	-5.03 \pm 0.04	-5.02 \pm 0.04	-5.03 \pm 0.06

Table A.4.8 Zeta-potential of crude oil Exp-12_{x&i}/brine emulsion at the given pH. pH-meter uncertainty ± 0.01 .

LS + Mg²⁺ - [mV]			
pH	Parallel 1	Parallel 2	Mean
4.02	-13.1 \pm 0.1	-15.5 \pm 0.2	-14.3 \pm 0.3
8.99	-51.7 \pm 2	-50.3 \pm 0.8	-51.0 \pm 2
LS + Ca²⁺ - [mV]			
pH	Parallel 1	Parallel 2	Mean
3.99	-4.6 \pm 0.5	-8.5 \pm 0.2	-6.6 \pm 0.5
8.98	-40.5 \pm 1	-39.2 \pm 2	-39.9 \pm 2
LS + SO₄²⁻ - [mV]			
pH	Parallel 1	Parallel 2	Mean
4.08	-22.0 \pm 0.9	-25.4 \pm 0.5	-23.7 \pm 1
8.95	-55.0 \pm 0.8	-55.7 \pm 0.7	-55.4 \pm 1
LS + CO₃²⁻ - [mV]			
pH	Parallel 1	Parallel 2	Mean
3.97	-23.4 \pm 0.9	-25.9 \pm 0.5	-24.7 \pm 1
8.95	-53.9 \pm 0.8	-53.6 \pm 1	-53.8 \pm 2
LS + PO₄³⁻ - [mV]			
pH	Parallel 1	Parallel 2	Mean
3.97	-11.9 \pm 0.3	-8.5 \pm 0.2	-10.2 \pm 0.4
9.01	-56.3 \pm 2	-53.4 \pm 0.9	-54.9 \pm 2
LS + B₄O₇²⁻ - [mV]			
pH	Parallel 1	Parallel 2	Mean
3.98	-14.5 \pm 0.5	-14.8 \pm 0.8	-14.7 \pm 0.9
8.95	-57.7 \pm 1	-56.6 \pm 1	-57.2 \pm 2
LS - [mV]			
pH	Parallel 1	Parallel 2	Mean
4.01	-8.8 \pm 0.6	-10.9 \pm 0.5	-9.9 \pm 0.8
9.06	-64.1 \pm 0.5	-64.1 \pm 0.6	-64.1 \pm 0.7

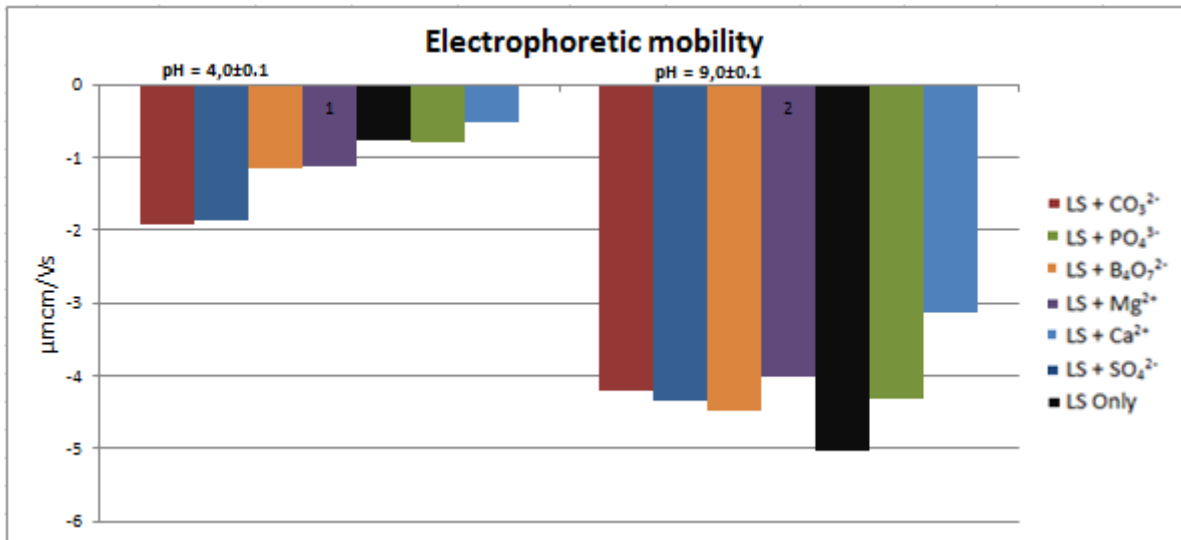


Figure A.4.6 Zeta-potential for 5 μL crude oil Exp-12_{x&i} in 6 mL LS water containing constant ionic molality of Ca^{2+} , Mg^{2+} , CO_3^{2-} , SO_4^{2-} , $\text{B}_4\text{O}_7^{2-}$ or PO_4^{3-} . pH was maintained at 4.00 ± 0.1 and 9.00 ± 0.1 .

A.5 Interfacial Tension Measurements

All the IFT measurements are presented with an uncertainty based on equation A.1.3.

$$\left(\frac{\sigma_{\sigma}}{\sigma}\right)^2 = \left(\frac{\sigma_V}{V}\right)^2 + \left(\frac{\sigma_{\Delta\rho}}{\rho}\right)^2 + \left(\frac{\sigma_r}{r}\right)^2 + \left(\frac{\sigma_{F_c}}{F_c}\right)^2 \quad (\text{A.1.3})$$

Since the uncertainty in the measured volume is significant higher than the measured densities, radius of the needle tip and the correlation factor, F_c , equation A.1.3 was reduced to equation A.1.4.

$$\frac{\sigma_{\sigma}}{\sigma} \approx \frac{\sigma_V}{V} \quad (\text{A.1.4})$$

A.5.1 IFT between Crude Oil A-12 and SSW, HS Water and LS Water

Table A.5.1 lists the parameters obtained to calculate the interfacial tension between crude oil A-12 and SSW, HS and LS water (see equation 5.4). The interfacial tensions are also listed.

Table A.5.1 Interfacial tension results for crude oil A-12 in SSW, HS, LS water and the corresponding dilutions.
The relative uncertainty of the IFT results is ±5%.

Aqueous phase	%-Solution	V [m³/drop]	F	σ [mN/m]
HS	100.00	1.24E-07	0.8176	28
	75.00	1.20E-07	0.8168	26.2
	50.00	1.27E-07	0.8182	24.7
	30.00	1.39E-07	0.8206	25.8
	10.00	1.69E-07	0.8254	28.6
	6.67	1.75E-07	0.8263	29.2
	4.55	1.90E-07	0.8282	31.4
SSW	100.00	7.46E-08	0.8033	17.3
	50.00	1.09E-07	0.8141	21.4
	10.00	1.52E-07	0.8229	25.7
	6.67	1.57E-07	0.8236	26.1
	4.55	1.62E-07	0.8244	26.7
LS		1.66E-07	0.8250	30.9
Deionized water		1.90E-07	0.8282	34.9

A.5.2 IFT between Crude Oil Exp-12_{x&i} and LS Water Containing Different Ions

In the following, tables A.5.2, A.5.3 and A.5.4 list the parameters obtained to calculate the interfacial tension between crude oil Exp-12_{x&i} and 3000 ppm NaCl solution containing 10, 50 or 100 ppm Ca²⁺, Mg²⁺, CO₃²⁻, SO₄²⁻, PO₄³⁻ or B₄O₇²⁻. Table A.5.5 lists the parameters and calculated IFT between Exp-12_{x&i} and LS water. All tables also present the interfacial tension obtained with uncertainty.

Table A.5.2 Interfacial tension results between crude oil Exp-12_{x&i} and 3000 ppm NaCl solution containing 10, 50 and 100 ppm Ca²⁺ to the left and Mg²⁺ to the right.
 pH ranged from 2.00 – 9.60. pH-meter uncertainty ±0.01.
 The relative uncertainty of the IFT results is ±5%.

10 ppm Ca²⁺			
pH	V [m³/drop]	F	σ [mN/m]
2.05	1.45E-07	0.8569	23.4
4.02	1.47E-07	0.8571	23.7
6.06	1.45E-07	0.8569	23.4
7.92	1.42E-07	0.8565	22.9
9.47	1.13E-07	0.8531	18.4
50 ppm Ca²⁺			
pH	V [m³/drop]	F	σ [mN/m]
2.05	1.35E-07	0.8558	22.0
4.02	1.54E-07	0.8577	25.0
6.06	1.46E-07	0.8570	23.8
7.92	1.40E-07	0.8563	22.7
9.47	1.06E-07	0.8519	17.3
100 ppm Ca²⁺			
pH	V [m³/drop]	F	σ [mN/m]
2.05	1.34E-07	0.8557	21.9
4.02	1.52E-07	0.8576	24.8
6.06	1.41E-07	0.8565	23.0
7.92	1.37E-07	0.8560	22.3
9.47	1.11E-07	0.8528	18.2

10 ppm Mg²⁺			
pH	V [m³/drop]	F	σ [mN/m]
2.04	1.36E-07	0.8559	24.5
3.93	1.54E-07	0.8577	27.8
6.10	1.51E-07	0.8575	27.3
8.05	1.46E-07	0.8570	26.4
9.45	1.24E-07	0.8544	22.4
50 ppm Mg²⁺			
pH	V [m³/drop]	F	σ [mN/m]
2.02	1.35E-07	0.8557	24.6
4.05	1.51E-07	0.8575	27.6
5.92	1.47E-07	0.8570	26.7
8.18	1.41E-07	0.8564	25.7
9.52	1.08E-07	0.8523	19.8
100 ppm Mg²⁺			
pH	V [m³/drop]	F	σ [mN/m]
2.00	1.33E-07	0.8556	24.8
4.04	1.49E-07	0.8572	27.6
6.11	1.46E-07	0.8570	27.2
8.00	1.34E-07	0.8557	25.0
9.53	9.33E-08	0.8498	17.5

Table A.5.3 Interfacial tension results between crude oil Exp-12_{x&i} and 3000 ppm NaCl solution containing 10, 50 and 100 ppm CO₃²⁻ to the left and SO₄²⁻ to the right. pH ranged from 2.00 – 10.00. pH-meter uncertainty ±0.01. The relative uncertainty of the IFT results is ±5%.

10 ppm CO ₃ ²⁻				10 ppm SO ₄ ²⁻			
pH	V [m ³ /drop]	F	σ [mN/m]	pH	V [m ³ /drop]	F	σ [mN/m]
2.08	1.38E-07	0.8561	21.8	2.05	1.33E-07	0.8556	21.1
4.05	1.54E-07	0.8578	24.4	4.03	1.53E-07	0.8576	24.1
6.01	1.50E-07	0.8574	23.8	5.99	1.48E-07	0.8572	23.3
7.99	1.46E-07	0.8570	23.1	8.15	1.40E-07	0.8563	22.1
9.55	1.12E-07	0.8529	17.8	9.50	1.21E-07	0.8541	19.2
50 ppm CO ₃ ²⁻				50 ppm SO ₄ ²⁻			
pH	V [m ³ /drop]	F	σ [mN/m]	pH	V [m ³ /drop]	F	σ [mN/m]
2.04	1.40E-07	0.8563	22.2	2.06	1.34E-07	0.8557	21.1
4.06	1.56E-07	0.8579	24.6	4.06	1.46E-07	0.8569	22.9
5.97	1.46E-07	0.8570	23.1	6.00	1.43E-07	0.8566	22.4
8.10	1.42E-07	0.8565	22.9	8.09	1.38E-07	0.8561	21.7
9.90	4.59E-08	0.8364	7.5	9.46	1.24E-07	0.8545	19.6
100 ppm CO ₃ ²⁻				100 ppm SO ₄ ²⁻			
pH	V [m ³ /drop]	F	σ [mN/m]	pH	V [m ³ /drop]	F	σ [mN/m]
2.06	1.32E-07	0.8554	21.0	2.04	1.33E-07	0.8556	21.1
3.98	1.49E-07	0.8573	23.7	4.09	1.50E-07	0.8573	23.7
6.09	1.40E-07	0.8564	22.3	6.03	1.47E-07	0.8571	23.3
8.00	1.30E-07	0.8553	20.8	7.99	1.40E-07	0.8563	22.1
9.96	1.57E-08	0.8101	2.6	9.53	1.23E-07	0.8544	19.6

Table A.5.4 Interfacial tension results between crude oil Exp-12_{x&i} and 3000 ppm NaCl solution containing 10, 50 and 100 ppm $B_4O_7^{2-}$ to the left and PO_4^{3-} to the right. pH ranged from 2.00 – 9.60. pH-meter uncertainty ± 0.01 . The relative uncertainty of the IFT results is $\pm 5\%$.

10 ppm $B_4O_7^{2-}$			
pH	V [m³/drop]	F	σ [mN/m]
2.07	1.29E-07	0.8551	22.1
4.03	1.45E-07	0.8569	24.8
6.09	1.43E-07	0.8566	24.4
7.98	1.39E-07	0.8562	23.7
9.45	8.33E-08	0.8479	14.4
50 ppm $B_4O_7^{2-}$			
pH	V [m³/drop]	F	σ [mN/m]
2.06	1.35E-07	0.8557	23.8
4.06	1.44E-07	0.8568	25.5
6.03	1.44E-07	0.8568	25.4
8.06	1.31E-07	0.8553	23.1
9.55	4.59E-08	0.8364	8.3
100 ppm $B_4O_7^{2-}$			
pH	V [m³/drop]	F	σ [mN/m]
2.05	1.31E-07	0.8553	24.7
4.01	1.46E-07	0.8570	27.6
6.02	1.42E-07	0.8565	26.7
7.96	1.19E-07	0.8539	22.6
9.58	3.16E-08	0.8282	6.2

10 ppm PO_4^{3-}			
pH	V [m³/drop]	F	σ [mN/m]
2.05	1.28E-07	0.8550	20.1
4.03	1.43E-07	0.8567	22.5
5.95	1.41E-07	0.8564	22.1
8.09	1.29E-07	0.8551	20.3
9.47	9.21E-08	0.8496	14.6
50 ppm PO_4^{3-}			
pH	V [m³/drop]	F	σ [mN/m]
2.06	1.29E-07	0.8551	20.4
4.06	1.47E-07	0.8571	23.2
6.01	1.43E-07	0.8567	22.5
7.95	1.25E-07	0.8546	19.7
9.45	1.03E-07	0.8515	16.3
100 ppm PO_4^{3-}			
pH	V [m³/drop]	F	σ [mN/m]
2.04	1.30E-07	0.8552	20.5
3.98	1.52E-07	0.8575	23.9
6.07	1.47E-07	0.8571	23.2
8.02	1.15E-07	0.8533	18.2
9.44	8.80E-08	0.8488	14.0

Table A.5.5 Interfacial tension results between crude oil Exp-12_{x&i} and 3000 ppm NaCl solution. pH ranged from 2.00 – 9.50. pH-meter uncertainty ± 0.01 . The relative uncertainty of the IFT results is $\pm 5\%$.

3000 ppm NaCl			
pH	V [m³/drop]	F	σ [mN/m]
2.07	1.34E-07	0.8557	20.7
4.03	1.51E-07	0.8574	23.2
6.03	1.43E-07	0.8566	22.0
7.94	1.42E-07	0.8565	21.9
9.46	1.21E-07	0.8540	18.7

A.5.3 IFT as a Function of Time in Contact between Crude Oil Exp-12_{x&i} and Brines

The tables presented in this sub-chapter show the parameters obtained to calculate the interfacial tension between crude oil Exp-12_{x&i} and 3000 ppm NaCl solution containing 10, 50 and 100 ppm Mg²⁺, B₄O₇²⁻. The aqueous phase and the crude oil had been in contact for some days to reach equilibrium. Table A.5.6 shows the IFT measurements were the aqueous phase contained magnesium which had been equilibrated for 11 days and borate for 14 days. Table A.5.7 shows the IFT measurements were the aqueous phase was only LS water with no additional electrolyte added and the equilibration time was also 14 days.

Table A.5.8 lists the difference in IFT between first contact and after equilibrium. In addition, the average in IFT in the pH region from 2-8 is displayed.

Table A.5.6 Interfacial tension results between crude oil Exp-12_{x&i} and LS water containing 10, 50 and 100 ppm Mg²⁺ after 11 days in equilibrium to the left and B₄O₇²⁻ with 14 days equalization time to the right. pH ranged from 2.00 – 9.60. pH-meter uncertainty ±0.01. The relative uncertainty of the IFT results is ±5%.

10 ppm Mg ²⁺			
pH	V [m ³ /drop]	F	σ [mN/m]
2.03	1.21E-07	0.8541	21.9
4.08	1.37E-07	0.8560	24.7
5.94	1.29E-07	0.8551	23.3
8.01	1.27E-07	0.8549	23.1
9.54	1.23E-07	0.8543	22.2
50 ppm Mg ²⁺			
pH	V [m ³ /drop]	F	σ [mN/m]
2.05	8.77E-08	0.8488	16.2
3.97	9.94E-08	0.8509	18.3
5.96	9.71E-08	0.8505	17.9
8.10	9.43E-08	0.8500	17.4
9.58	7.89E-08	0.8469	14.6
100 ppm Mg ²⁺			
pH	V [m ³ /drop]	F	σ [mN/m]
2.02	8.59E-08	0.8484	16.1
4.05	9.55E-08	0.8502	17.9
6.05	9.59E-08	0.8503	18.0
8.09	9.22E-08	0.8496	17.3
9.44	7.98E-08	0.8471	15.0
10 ppm B ₄ O ₇ ²⁻			
pH	V [m ³ /drop]	F	σ [mN/m]
2.05	8.56E-08	0.8484	14.8
4.02	9.74E-08	0.8506	16.8
6.05	9.59E-08	0.8503	16.5
8.01	9.20E-08	0.8496	15.8
9.47	7.21E-08	0.8453	12.5
50 ppm B ₄ O ₇ ²⁻			
pH	V [m ³ /drop]	F	σ [mN/m]
2.08	8.77E-08	0.8488	15.6
3.97	9.85E-08	0.8508	17.5
6.00	9.74E-08	0.8506	17.3
7.93	8.89E-08	0.8490	15.8
9.44	4.27E-08	0.8349	7.7
100 ppm B ₄ O ₇ ²⁻			
pH	V [m ³ /drop]	F	σ [mN/m]
2.06	8.65E-08	0.8485	16.5
4.00	9.73E-08	0.8506	18.4
6.05	9.36E-08	0.8499	17.8
7.95	7.39E-08	0.8457	14.1
9.45	2.54E-08	0.8229	5.0

Table A.4.7 Interfacial tension results between crude oil Exp-12_{x&i} and 3000 ppm NaCl solution after 14 days in equilibrium. pH ranged from 2.00 – 9.60. pH-meter uncertainty ± 0.01 .
The relative uncertainty of the IFT results is $\pm 5\%$.

3000 ppm NaCl			
pH	V [m³/drop]	F	σ [mN/m]
2.08	8.60E-08	0.8484	13.4
4.08	9.47E-08	0.8501	14.7
5.99	9.37E-08	0.8499	14.6
8.07	9.11E-08	0.8495	14.2
9.49	8.19E-08	0.8476	12.8

Table A.5.8 Difference in the IFT measurements between first contact and after equilibration. In addition, the average IFT in the pH region from 2-8 is displayed.

	pH	Mg²⁺	B₄O₇²⁻	LS water
		σ [mN/m]	σ [mN/m]	σ [mN/m]
10 ppm	2	2,7	7,3	7,3
	4	3,0	8,1	8,5
	6	4,0	7,8	7,5
	8	3,3	7,8	7,7
Average		3,2	7,8	7,7
50 ppm	2	8,5	7,3	
	4	9,3	8,1	
	6	8,9	7,8	
	8	8,3	7,8	
Average		8,7	7,8	
100 ppm	2	8,7	7,3	
	4	9,7	8,1	
	6	9,2	7,8	
	8	7,7	7,8	
Average		8,8	7,8	

A.6 Diverging pH in the Aqueous Phase

This chapter presents the measured data which confirms that the pH in the brine phase diverged from the time it was made to three days after. The change in pH of the low salinity water after adding each individual ion is also listed. This is shown in table A.6.1.

Table A.6.1 List of pH changes.

Solvent; 3000 ppm NaCl, pH = 6.24		pH of the brine after selected ion was added	Δ pH After adding the selected ion	pH of the solution after three days in equilibrium	Δ pH After three days in equilibrium
Ion in solution	ppm				
Ca ²⁺	10	5.92	-0.32	6.05	0.13
	50	5.81	-0.43	6.04	0.23
	100	5.75	-0.49	6.00	0.25
Mg ²⁺	10	6.30	0.06	7.52	1.22
	50	5.81	-0.43	6.19	0.38
	100	5.68	-0.56	5.95	0.27
SO ₄ ²⁻	10	6.05	-0.19	6.00	-0.05
	50	6.02	-0.22	6.03	0.01
	100	5.97	-0.27	6.02	0.05
CO ₃ ²⁻	10	9.72	3.48	9.47	-0.25
	50	10.27	4.03	10.08	-0.19
	100	10.46	4.22	10.34	-0.12
PO ₄ ³⁻	10	9.43	3.19	9.53	0.1
	50	10.31	4.07	10.42	0.11
	100	10.77	4.53	10.76	-0.01
B ₄ O ₇ ²⁻	10	8.83	2.59	8.69	-0.14
	50	9.02	2.78	8.96	-0.06
	100	9.05	2.81	9.02	-0.03